CUTTING METHODS AND MACHINE TOOL ISSUES IN DIE AND MOLD MACHINING

BY

LIANGJI XU

A DISSERTATION PRESENTED TO THE GRADUATE SCHOOL
OF THE UNIVERSITY OF FLORIDA IN PARTIAL FULFILLMENT
OF THE REQUIREMENTS FOR THE DEGREE OF
DOCTOR OF PHILOSOPHY

UNIVERSITY OF FLORIDA

1996

To Limin

ACKNOWLEDGMENTS

The author would like to express his sincere gratitude to Dr. John K. Schueller and Dr. Jiri Tlusty for their guidance and generous support during this research. The author also thanks Dr. Scott Smith, Dr. John Ziegert and Dr. Sherman Bai for serving on his committee, and for their continuous support and inspiration.

The author would also like to thank all the members in the Machine Tool Research Center who have been of great assistance to him. Special thanks go to Dr. Bob Winfough, Mr. David Smith, Mr. Steve Nelson, Mr. Tarek Al-Hawari, Mr. David Bernhard and Dr. Sinan Badrawy.

Portions of this research were financially sponsored by the National Science Foundation.

TABLE OF CONTENTS

APPENDICES

NOMENCLATURE

a_a	Path increment in axial direction
a_{low}	Lower boundary of the effective depth of cut
a_c	Critical radial increment
a_d	Critical step over size on the removed material surface
a_e	Effective depth of cut
a_h	Distance for calculating maximum depth of cut
a_i	Tool immersion at the boundary of previous path
a_m	Maximum depth of cut
a_o	Tool immersion at the outer boundary
a_r	Path increment in radial direction
a_s	Step over size
a_{up}	Upper boundary of the effective depth of cut
a_v	Exact maximum depth of cut
a_w	Distance for calculating maximum depth of cut
b_{lim}	Depth of cut at the stability limit
f_t	Feed per tooth
e	Offset of the "off-centered" ball end mill
K_s	Cutting stiffness of work piece material
l_c	Offset of previous path ellipse to the cutting edge
l_e	Major axis of the previous path ellipse
r	Ball nose end mill insert radius
r_c	Arc radius on the removed surface
r_e	Cutter radius at the effective depth of cut
r_f	Distance for calculating r_e at inclined ball end milling
r_g	Distance for calculating r_e at inclined ball end milling
r_i	Cutter radius at the boundary of previous path
r_o	Cutter radius at the outer boundary
r_p	Distance for calculating r_e at inclined ball end milling
r_q	Distance for calculating r_e at inclined ball end milling
r_s	Distance for calculating r_e at inclined ball end milling
r_t	Cutter radius at the thickness of removed material layer
r_v	Offset to symmetric center
r_w	Distance for calculating r_e at inclined ball end milling

R	Cutter radius
$Re[G]_{min}$	Minimum value of the real part of the system transfer function
t	Thickness of removed material layer
t_a	Critical thickness
t_c	Thickness limit for depth of cut smaller than cutter radius
t_0	Critical thickness for relieving ball nose mill tip from cutting
u	Horizontal axis in u-v coordinate system
v	Vertical axis in u-v coordinate system
v_e	Cutting velocity at the effective depth of cut
ε	Cutter axis inclined angle
ϕ	Cutting edge position angle
ϕ_e	Cutting edge position angle at the effective depth of cut
ϕ_i	Cutting edge position angle at the boundary of previous path
ϕ_o	Cutting edge position angle at the outer boundary
ϕ_p	Cutting edge position angle boundary
ϕ_q	Cutting edge position angle boundary
ϕ_r	Cutting edge position angle when depth of cut equals r in slotting
ψ	Path increment angle
ω	Rotational speed of the milling cutter

Abstract of Dissertation Presented to the Graduate School
of the University of Florida in Partial Fulfillment of the
Requirements for the Degree of Doctor of Philosophy

CUTTING METHODS AND MACHINE TOOL ISSUES
IN DIE AND MOLD MACHINING

By

LIANGJI XU

December 1996

Chairman: Dr. John K. Schueller
Cochairman: Dr. Jiri Tlusty
Major Department: Mechanical Engineering

The objective of this research project was to develop a technique for the direct machining of dies and molds in their hardened state. The technique was applied to the milling of hardened dies with ball end mills. The cutting geometry of the multi-path ball end milling and inclined ball end milling was identified and the mathematical expressions for the instant depth of cut were derived. It was found that the "step-up" path increment mode and inclined ball end milling create the best cutting conditions. The poor cutting condition of "zero speed zone" could be avoided by applying those methods. Experimental data showed that the cutting force was decreased by using those methods. Finite element analyses were conducted on the SETCO high speed spindle with different ball end mills. The results showed that for the insert type cutter with high stiffness, the major vibration mode was the spindle mode, while for the solid cutter with low stiffness, the tool mode dominated. The cutting experiments supported the judgement concluded from the finite element model. An open

architecture NC controller was developed and installed in a three-axis milling machine. A user interface software for the controller was developed. The controller and the user interface software create a user-friendly operation environment for machining dies and molds. A high pressure coolant system has been built and the effect of the coolant in hardened steel machining was investigated. The high pressure coolant greatly reduced the temperature in the cutting area. It was also observed that the cutting force was decreased by using coolant. The disadvantage of using coolant in the machining of hardened die and mold steel was the increasing of tool wear due to chipping.

This research indicates that the direct machining of die and mold steel in the hardened state is feasible. High stiffness of the machine tool, particularly of the tool-tool holder-spindle system, promotes successful machining of hardened dies and molds. For a three-axis milling machine, "step-up" increment mode is recommended, while if five-axis machining ability is available, an inclined tool will create the best cutting condition in ball end milling. An open architecture NC controller will benefit the machining of dies and molds by allowing such enhancements as tool breakage detection and chatter recognition to be easily added. The high pressure coolant was effective to reduce the cutting temperature and decrease the cutting force, but attention needs to be paid to tool wear.

CHAPTER ONE
INTRODUCTION

Background of Die and Mold Machining

Die and mold manufacturing is an important segment of modern industry. The shipments of the die and mold industry in the United States are more than nine billion dollars annually in the 1990s, besides the dies and molds produced and used in the same companies (Department of Commerce, 1993). The conventional process of die and mold manufacturing is shown in Figure 1.1.

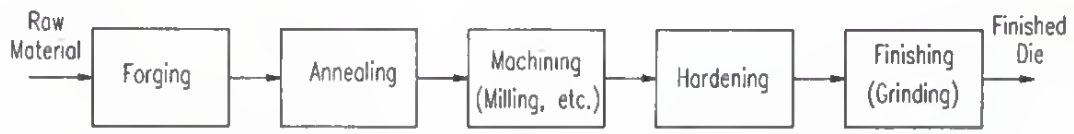

Figure 1.1 Traditional die and mold manufacturing procedure.

Dies and molds are generally formed close to the desired shape by hot forging. In order to accommodate the following machining, dies and molds are usually annealed. After rough machining, dies and molds are sent to be heat treated again, usually quenching and tempering, to obtain the desired hardness and other mechanical properties. In the hardened state, dies and molds are sent back to the machine shop for finishing, usually grinding, to improve the surface qualities and reach the final dimension. The primary complaint about the traditional method is the lengthy production time and high energy consumption, which

unavoidably result in a high production cost. Another problem is that after rough machining, the heat treatment failures often occur on the dies and molds due to stress concentration and thermal distortion, particularly on sharp corners and thin walls. Besides producing new dies and molds, the reconditioning of worn dies and molds also needs to follow the same procedures from annealing to finish grinding. Researchers have been looking for alternative methods to reduce the time and cost of the traditional die and mold manufacturing procedure. Along with the developments of metal cutting technologies, a new manufacturing procedure for hardened material was proposed by Koenig et al. (1984) and other researchers. With the proposed procedure, the heat treatment for hardening is directly conducted after forging. The whole machining procedure is completed on hardened material. In addition, the finishing is done by cutting, rather than grinding. If this method is introduced to die and mold manufacturing, as shown in Figure 1.2, substantial benefits will accede to the die and mold industries.

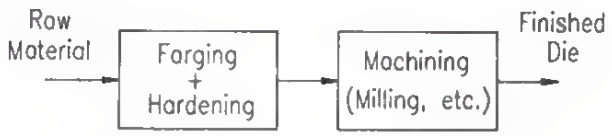

Figure 1.2 Proposed die and mold manufacturing procedure.

First, the annealing procedure is eliminated, thus saving substantive time and energy. If the hardening of the material is conducted right after the forging, more savings can be expected. In addition, the repeated transportation between heat treatment and machining is reduced to only one trip. Since finish grinding is replaced by cutting, the finishing metal removal rate can be increased several times. Moreover, since rough machining and finishing

are all conducted by cutting, it becomes possible to complete the production of a die or a mold in one machine tool. The reductions of machining time and cost can be significant. Another advantage of the proposed procedure is that the distortion and fracture during heat treatment are minimized. Since the hardening procedure is conducted on unmachined material (raw or forged), no specific protection measurements generally used for machined dies and molds are needed. Not only does the hardening procedure become simpler, but also high heat treatment qualities are ensured. Therefore, with the new method, the savings on the production time, production cost, energy consumption, and investment can be significant. The quality improvement is also consequential.

To facilitate this procedure of die and mold manufacturing, some relating topics need to be investigated. They include the theories and practices of hardened metal cutting, the tool geometry and its role in the machining, the application of the coolant, and finally, the requirement for the machine tool as well as its controller.

Objective and Approaches

The objective of this research project was to develop a technique for the direct machining of dies and molds in the hardened state.

To approach this objective, the cutting geometry of ball end milling will be discussed. The mathematical expressions of the instant depth of cut in multi-path ball end milling will be derived. The cutting geometry of the "inclined ball end milling" will be discussed. Ball end milling tests on pre-hardened H13 die steel have been conducted. During the experiments, the cutting force and the cutting sound signal have been recorded. Post-

processing and analysis have been conducted. A finite element analysis of a tool-tool holder-spindle system has been conducted. The vibration modes of the system have been calculated. A high pressure coolant system has been built and cutting tests with the system have been conducted. To facilitate the application of advanced techniques such as chatter recognition and tool breakage detection developed in the Machine Tool Research Center at the University of Florida (MTRC) into die and mold machining, an open architecture NC controller and user interface software have been developed.

Literature Review

Machining of Hard Material

Koenig et al (1984) applied "combination" and "elimination" methods of the process sequence optimization theory on hard material machining. They proposed eliminating the annealing procedure and direct machining of hardened material, and combining the rough machining and finishing in one procedure to make it possible to complete the machining in one machine tool. Koenig et al successfully applied the new procedure on the turning of a bearing ring (HRC 65), skive hobbing of gear teeth (HRC 60), face milling of a slide way (HRC 56), as well as some drilling, boring and broaching experiments.

Cutting Tools for Hard Material

The most important component of the machining system for hard metal cutting is probably the cutting tools. Koenig et al (1984) proposed some necessary conditions for cutting edges while machining of the hardened ferrous materials. The cutting edge used for this purpose needs to have high hardness (>HV 1600), high transverse rupture strength (>350

N/mm^2), high fracture toughness (>5 MPa-$m^{1/2}$), and high temperature resistance (>800 ° C). For intermittent cutting like milling, high thermal conductivity is also required. In order to increase cutting stability, Koenig et al proposed using a negative rake angle with chamfer on the cutting edge. Koenig et al also investigated various cutting edge materials and finally concluded that CBN was the most proper cutting edge material for cutting ferrous materials in their hardened state. In some cases, to reduce the cost, carbide tools could also be used in milling operations and the best results could be obtained with micro grain carbide (Koenig et al, 1990). Due to their lower traverse rupture strength and lower fracture toughness, ceramic tools were considered unsuitable for use in intermittent cutting like milling (Koenig et al, 1984).

Machine Tools

Machine tools also play an critical role in the hard material cutting process. Due to the dramatic increasing of the cutting force for hardened material, higher power machine tools are needed. Since the final finishing is also conducted with cutting instead of additional grinding, the precision of the machine tool also becomes critical. The high hardness cutting tools are needed for hard material cutting. Therefore, the tools are generally brittle and prone to chipping. To avoid chipping, special attention needs to be paid to the rigidity of the machine tool. On this issue, Koenig et al (1984) pointed out "Although this fact has been generally recognized, stringent requirements have not been implemented except in special cases. Consequently, whenever machining of hardened work material was unsuccessful, poor tool performance has been attributed to the failure rather than to the lack of adequate rigidity of the machine tool system used."

Ball End Mills

Ball end mills are widely used in die and mold manufacturing due to their unique advantage in easily cutting sculptured surfaces. Work has been done to improve the performance of ball end mills by many researchers. Hosoi (Hosoi and Hoshi, 1977) invented a ball end mill with unique cutting edge, the "Hosoi ball nose mill". Instead of the conventional flat cutting edge, Hosoi designed a spiral curved cutting edge. The tool engagement with workpiece starts from the center of the cutter and gradually propagates to the outer edge. Since cutting forces increase gradually, the chipping of the cutting edge due to the cutting force impact at the beginning of the engagement is reduced. The cutting forces are also lower than those of conventional ball end cutters.

Electrical-Discharge Machining

Another method of machining of metallic material besides cutting is electrical-discharge machining (EDM). The electrical conductive workpiece material is eroded to the desired shape by electrical spark discharges during the machining process. It has been developed since 1940 and is especially successful on producing small diameter holes, narrow slots and intricate shapes like turbine blades. It has also been adopted by die manufacturers to produce die cavities. The main shortcoming of EDM is its low metal removal rate, ranging from 0.1 to 25 cm^3/hour (Kalpakjian, 1992). If the time used for machining the EDM electrode is included, the total machining time becomes even longer. Another problem with EDM is the recast structure left on the workpiece surface by EDM procedure, which has low fatigue properties. For some alloys, EDMed surfaces can reach only half or less of the fatigue property left on milled surfaces. Therefore, sometimes the finishing grinding is still needed.

Finally, the disposal of the dielectric fluid used in EDM procedure is becoming a major environment concern. Hence, despite the widespread use of EDM, there is interest in returning to milling.

CHAPTER TWO
ANALYTICAL SOLUTION OF THE DEPTH OF CUT IN MULTI-PATH BALL END MILLING

The cutting geometry of ball end milling is more complicated than that of flat end milling. Despite the industrial importance of ball end milling, there have been only a limited number of studies of the cutting geometry. Yang and Park (1991) assumed that the orthogonal cutting theory is still valid in ball end milling. They applied the cutting force equations from orthogonal cutting to infinitismal elements on the ball end cutting edge. The coefficients in the equations were obtained from the orthogonal turning tests. The total cutting force was then derived through the integration of the force elements. Sim and Yang (1993) extended this method to include the effect of the cutter deflection.

Yucesan and Altintas (1993) questioned the assumptions and the method used by Yang and Park (1991). Yucesan and Altintas (1993) pointed out that the assumption of the colinearity of the chip movement direction and the friction force direction are not necessarily true for all materials. They also believed that the neglect of the variation of the cutting mechanics parameters (such as cutting speed, shear, friction, pressure and chip flow angle) along the ball end mill with a variable helix angle caused the discrepancy of the experimental results from the mathematical calculations done by Yang and Park (1991). Yucesan and Altintas (1993) introduced the effective cutting force coefficients, which depend on the flute immersion geometry and the feed rate, to take care of the variations of the friction and the

pressure along the ball end mill flute. Those coefficients were obtained experimentally through slot cutting with specially grounded ball end mills. A force model was then built based on the general mechanisms of the chip formation and the contact between tool and the workpiece. The model was classified as a "semi-mechanistic analytical model" by Yucesan and Altintas (1996). Altintas and Lee (1996) developed a software program to predict the cutting force, torque, power, feed marks, dimensional errors, vibration marks, chatter vibrations and stability lobes in milling operations. Examples of the chatter simulation were presented with flat end milling and ball end milling. In the flat end milling case, the stability lobes generated by this program was compared favorably with experimental results.

Feng and Menq (1994) believed that the validity of modeling the complex 3-D cutting such as ball end milling with the 2-D or simple 3-D model used by some researchers has not been well established. They introduced a force model for ball end milling which featured tangential and radial force coefficients and size effect coefficients. The force coefficients were represented by third order polynomials. The numerical value of those coefficients were obtained experimentally for individual tool-workpiece combinations. Tool runout was also considered in their model.

Tlusty (1986) and Smith and Tlusty (1990, 1991, 1992 and 1993) developed a comprehensive cutting force model for milling operations. Besides the static cutting forces, the dynamic forces generated from the system during the cutting process were also considered in the model. The stability limit for a milling process to be stable was expressed as

$$b_{\lim} = -\frac{1}{2\, n_a\, K_s\, \mu\, Re[G]_{\min}} \qquad (2.1)$$

where b_{lim} is the axial depth of cut at the limit of stability, n_a is the average number of engaged teeth on the milling cutter, K_t is the cutting stiffness of the workpiece material, μ is the directional factor depending on the radial immersion of the cutter, and $Re[G]_{min}$ is the minimum value of the real part of the oriented transfer function of the milling system. If the axial depth of cut in a milling process was larger than b_{lim}, the system became unstable. The theory and the model have been successively applied to flat end mills.

In ball end milling, except for very simple cases as shown in Figure 2.1, the axial depth of cut is generally a variable of the tool rotational angle rather than a constant value in flat end milling cases. It causes difficulties to directly extend the above discussed dynamic model into ball end milling. Therefore, in order to analyze the dynamic response of ball end milling, the depth of cut in multi-path cases needs to be investigated. Sufficient discussion of this issue has not been found in the literature.

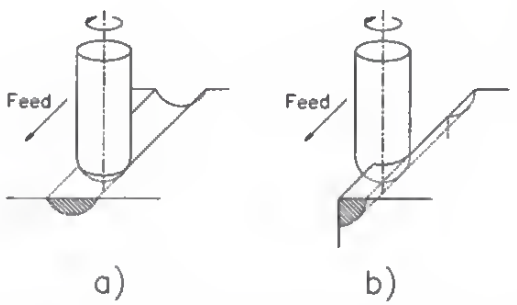

Figure 2.1 Single path ball end milling. a) slotting; b) cornering.

Derivation of General Equations

In a general multi-path milling processing, the milling cutter moves incrementally to another starting position after each cutting path, as shown in Figures 2.2 a) b), c), and d).

The incremental motion can be either in the radial direction or in the axial direction of the cutting tool, as shown in Figure 2.2 a) and b). However, the most popular application of ball end milling is the machining of sculptured surfaces, which often requires path increments in the axial and radial directions simultaneously. Examples are shown in Figures 2.2 c) and d).

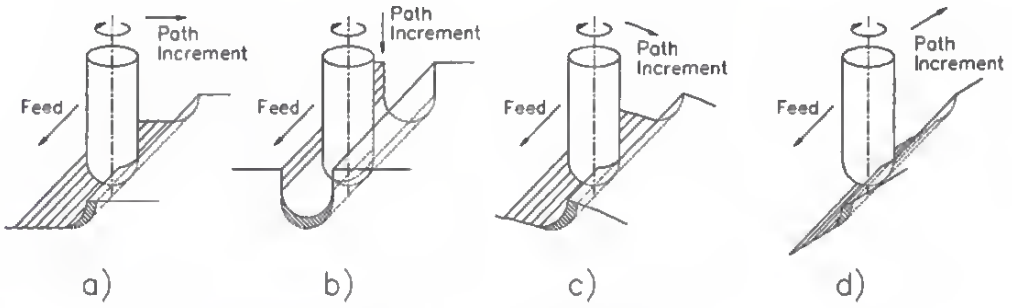

Figure 2.2 Multi-path ball end milling. a) solely radial increment; b) slotting; c) "step-down" increment; d) "step-up" increment.

The basic cutting geometry of the multi-path ball end milling with both axial and radial path increments is shown in Figure 2.3. The shaded area represents the part of the material being removed by the current cutting path. The depth of cut is determined by the vertical distance from the upper boundary of the shaded area to the tip of the ball end mill. It can be seen that the upper boundary is composed of two parts: *a-b* and *b-c*. The part represented by *a-b* is a cylindrical surface formed by the previous cutting path, and the part represented by *b-c* is the surface being removed by the current cutting path. Assuming that the thickness of the removed material layer t is not changed with the path increment, the inclined angle of the surface being removed will be identical to the path increment angle ψ determined by a_r and a_a

$$\tan \psi = \frac{a_a}{a_r} \tag{2.2}$$

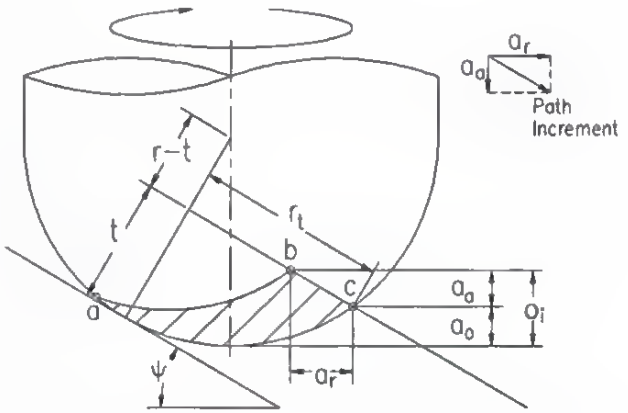

Figure 2.3 Basic cutting geometry in ball end milling.

The geometric analysis of the depth of cut in *a-b* part is shown in Figure 2.4. The upper part of Figure 2.4 a) is a section view of the ball end milling along the axial direction. The solid circle represents the current tool position, and the dotted circle represents the previous tool position one feed per tooth f_t earlier. The lower part of Figure 2.4 a) is a section view A-A, which shows the cutting edge plane in the current tool position. Here a zero axial rake angle is assumed to simplify the analysis. Figure 2.4 b) shows the detail of the A-A section view in the *u-v* coordinate system with its original at the tip of the ball end mill. The shaded area is the cross section view of the undeformed chip. It can be seen that the instant depth of cut a_e in ball end milling at the position angle ϕ is determined by the intersection of the cutting edge *o-p-q* and the cylindrical surface formed by the previous

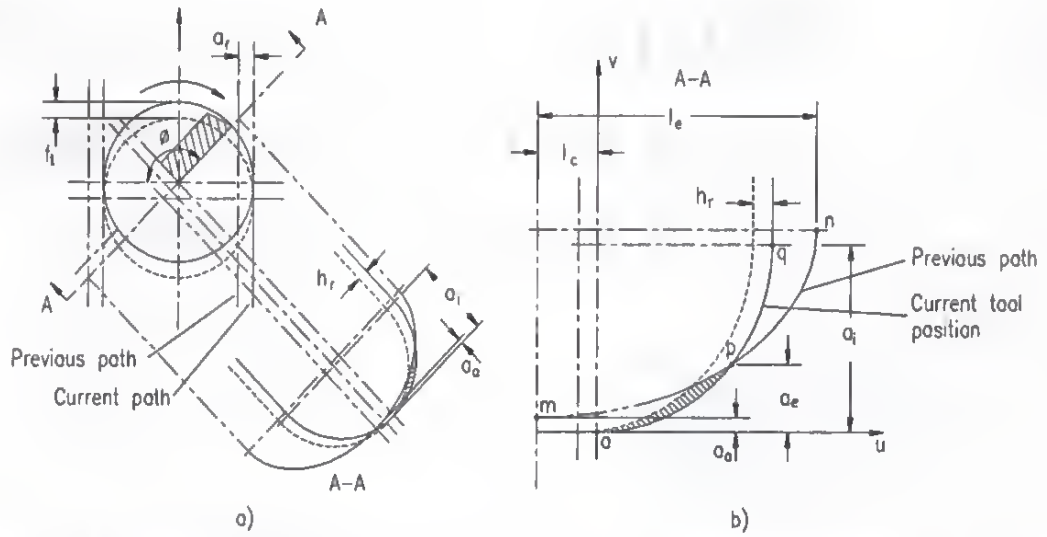

Figure 2.4 Geometric analysis of the effective depth of cut in ball end milling. a) view in axial direction; b) A-A view in detail.

cutting path, which becomes a partial ellipse *m-p-n* in Figure 2.4.b). The equations for the ellipse *m-p-n* and the cutting edge *o-p-q* in the *u-v* coordinate system can be written as

$$\frac{(u + l_c)^2}{l_e^2} + \frac{(v - r - a_a)^2}{r^2} = 1 \qquad (2.3)$$

and

$$u^2 + (v - r)^2 = r^2 \qquad (2.4)$$

respectively. The major axis of the ellipse l_e and the offset l_c can be obtained from

$$l_e = \left| \frac{r}{\cos \phi} \right| \qquad (2.5)$$

and

$$l_c = \left| \frac{a_r}{\cos \phi} \right| \tag{2.6}$$

Substituting for u, l_e, and l_c in Equation (2.3) with Equations (2.4), (2.5) and (2.6), and realizing that a v value which satisfies both Equations (2.3) and (2.4) is actually the instant depth of cut a_e, the general equation for a_e within a-b area can be written as

$$a_e^2 \sin^2\phi - 2a_e(a_a + r\sin^2\phi) + 2a_r\sqrt{2a_f r - a_e^2}\,|\cos\phi| + a_r^2 + a_a^2 + 2a_a r = 0 \quad \text{for } \phi \le \phi_i \tag{2.7}$$

where ϕ_i is the position angle of the cutting edge across the boundary of the cylindrical surface (position b in Figure 2.3). Since at this point the instant depth of cut a_e is equal to the tool immersion at the boundary of previous path a_i, the critical angle ϕ_i, where the cutting edge crosses the previous path boundary, can be derived from Equation (2.7)

$$\phi_i = \cos^{-1}\left(\frac{a_r}{\sqrt{2a_f r - a_i^2}} - \sqrt{1 + \frac{2a_a a_i - 2a_a r - a_a^2}{2a_f r - a_i^2}}\right) \tag{2.8}$$

For calculating the instant depth of cut in b-c area, a detailed view of this area in Figure 2.3 is shown in Figure 2.5 where

$$\begin{aligned} r_i &= \sqrt{r^2 - (r - a_i)^2} \\ r_o &= \sqrt{r^2 - (r - a_o)^2} \\ r_e &= \sqrt{r^2 - (r - a_e)^2} \end{aligned} \tag{2.9}$$

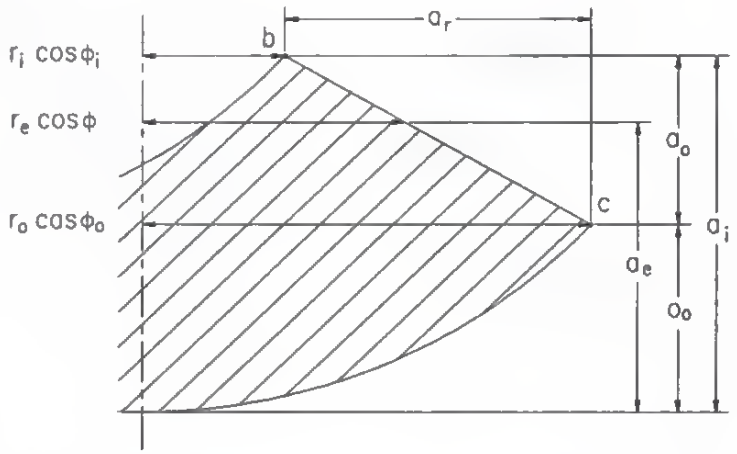

Figure 2.5 Cutting geometry in the area of the removed material layer.

Based on the geometry shown in Figure 2.5, the instant depth of cut in *b-c* can be obtained from

$$a_e + (\sqrt{2a_f r - a_i^2}\cos\phi_i - \sqrt{2a_e r - a_e^2}\cos\phi)\frac{a_a}{a_r} - a_i = 0 \qquad for \quad \phi > \phi_i \quad (2.10)$$

where a_i is the tool immersion at the boundary of previous path, which can be calculated from the radial increment a_a and the tool immersion at the outer boundary of the removed material layer a_o as shown in Figures 2.3 and 2.5. That is

$$a_i = a_o + a_a \qquad (2.11)$$

where

$$a_o = r\,(1-\cos\psi) + t\cos\psi - r_t \sin\psi \qquad (2.12)$$

where r_t is the cutter radius measured along the thickness of the removed material layer as shown in Figure 2.3

$$r_t = \sqrt{2rt - t^2} \tag{2.13}$$

With the aid of the geometric analysis, the general equations for calculating the instant depth of cut a_e have been derived. Equation (2.7) can be used to calculate a_e at the cylindrical surface formed by the previous cutting path, and Equation (2.10) can be used at the surface being removed by the current path. The critical angle at the boundary can be calculated from Equation (2.8). The general equations can be used to solve a_e in various path increment directions as shown in Figure 2.2. Four path increment cases are discussed individually below. Before discussing the general cases of cutting sculptured or oblique surfaces with ball end milling, two special cases with $\psi = 0°$ and $\psi = 90°$ are introduced, where an analytical solution of the instant depth of cut can be easily obtained from the general equations, while numerical methods might be needed in general cases.

Case Studies

Path Increment Angle $\psi = 0°$

In this case, the axial increment a_a becomes zero and the path increment is solely in the radial direction of the cutting tool, as shown in Figure 2.2 a). This is often known as "plane cutting" because a layer of the material perpendicular to the spindle is removed from the workpiece. The calculation of the instant depth of cut in this case becomes simpler. Since $a_a = 0$, Equation (2.7) can be simplified to

$$\left(\frac{a_e^2}{r^2} - 2\frac{a_e}{r}\right)\sin^2\phi + 2\frac{a_r}{r}\sqrt{2\frac{a_e}{r} - \frac{a_e^2}{r^2}}\,|\cos\phi| + \frac{a_r^2}{r^2} = 0 \qquad for\ \phi \le \phi_i \quad (2.14)$$

The instant depth of cut can be readily obtained from

$$a_e = r - \sqrt{r^2 - a_r^2\left(\frac{1+|\cos\phi|}{\sin^2\phi}\right)^2} \qquad for\ \phi \le \phi_i \quad (2.15)$$

Assuming the thickness of the removed material layer t is not changed, the solution for a_e at a position angle larger than ϕ_i becomes fairly simple

$$a_e = t \qquad for\ \phi > \phi_i \quad (2.16)$$

The equation to calculate the critical angle ϕ_i can also be simplified to

$$\phi_i = \cos^{-1}\left(\frac{a_r}{\sqrt{2rt - t^2}} - 1\right) \quad (2.17)$$

Figure 2.6 shows some examples of the instant depth of cut in the cases where $\psi = 0°$. It can be seen that the instant depth of cut in ball end milling gradually increases to its maximum value, which is the thickness of the removed material layer t. In flat end milling, the transition only relies on the helix angle of the cutting tool, which is usually small. Therefore, the force impact and the thermal shock in ball end milling should be lower than those in flat end milling. Figure 2.6 shows three cases with varied radial feed a_r. Since the metal removal rate is limited by the maximum cutting force allowed for a specific tool, the

metal removal rate for all three cases in Figure 2.6 remains unchanged by adjusting the thickness of the removed material layer. If the dynamic stability can be assured, it is preferable to program the cutting path with small radial feed a_r and high removed layer thickness t, to fully utilize the cutting velocity in the ball end milling. If a larger a_r and a smaller t is programed, the cutting process is concentrated on the lower part of the ball end cutter, causing the cutting process to deteriorate due to the lower cutting speed near the tip of the cutter. In addition, the surface finishing becomes worse due to the deep "scallop" tool marks left by the cutting with a large radial increment a_r.

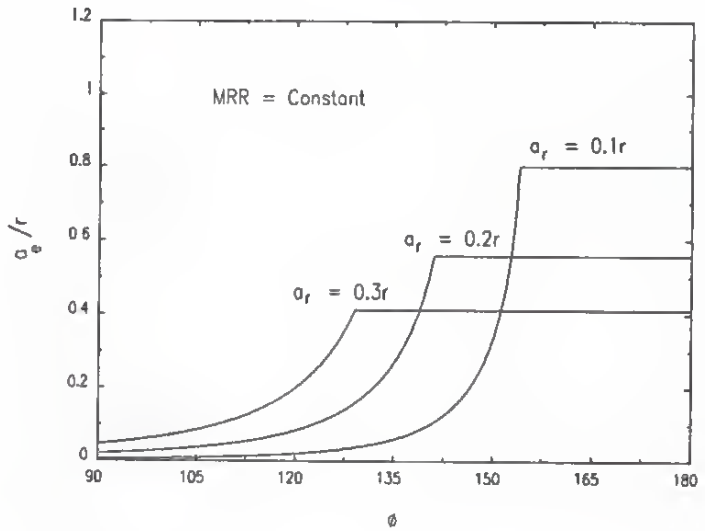

Figure 2.6 Examples of the instant depth of cut in ball end milling with ψ=0. The metal removal rate remains unchanged for all cases.

Path Increment Angle $\psi = 90°$

In this case, the path increment is solely in the tool axial direction as shown in Figure 2.2 b). This cutting strategy is often called "slotting". Since the radial feed a_r is zero in this

case, the calculation of the instant depth of cut can be simplified. In this case, Equation (2.7) becomes

$$a_e^2\sin^2\phi - 2a_e(a_a + r\sin^2\phi)\frac{v}{r} + a_a^2 + 2a_a r = 0 \qquad (2.18)$$

and an analytical solution for the instant depth of cut a_e can be obtained from

$$a_e = r + a_a\csc^2\phi - \sqrt{r^2+a_a^2(\csc^4\phi-\csc^2\phi)} \qquad for\ \phi_r \le \phi \le 180°-\phi_r \quad (2.19)$$

where ϕ_r is the critical angle when the instant depth of cut equals the cutter radius r. The critical angle ϕ_r can be obtained from Equation (2.18) by substituting for a_e with the cutter radius r

$$\phi_r = \sin^{-1}(\frac{a_a}{r}) \qquad (2.20)$$

Figure 2.7 shows some examples of the instant depth of cut in slotting. The portion drawn with dashed lines represent the instant depth of cut a_e when ϕ is smaller than ϕ_r or larger than 180°-ϕ_r. It is assumed in Figure 2.7 that the ball end cutter has a cylindrical shank with cutting radius r. It can be written as

$$u = r \qquad for\ v > r \qquad (2.21)$$

in the u-v coordinate system shown in Figure 2.4. Combining Equation (2.21) with Equation (2.3), the instant depth of cut in $v > r$ with this specific tool can be solved by

$$a_e = a_a + (1 - \sin\phi)\, r \qquad for\ \phi<\phi_r\ or\ \phi>180°-\phi_r \qquad (2.22)$$

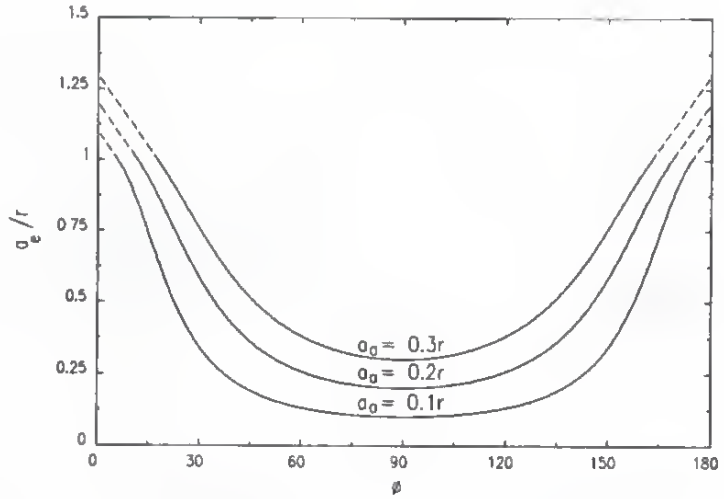

Figure 2.7 Examples of the instant depth of cut in slotting cases.

There is a major difference for the depth of cut in slotting with a ball end mill compared to slotting with a flat end mill. In flat end milling, the maximum depth of cut is equal to the axial increment a_a. However, this is true only at $\phi = 90°$ in ball end milling. Except for that point, the instant depth of cut a_e is always larger than a_a. The instant depth of cut reaches the maximum value when ϕ is at 0 or 180 degrees

$$a_e = r + a_a \qquad for\ \phi = 0°\ or\ 180° \tag{2.23}$$

Therefore, particular caution needs to be taken for slotting with ball end mills. Excessive depth of cut might cause the cutting process to fall into an unstable situation based on Equation (2.1).

Path Increment Angle $0° < \psi < 90°$, "Step-Down"

The derivation of the general equations for the instant depth of cut discussed above was done for the general "step-down" case, of which $\psi = 0°$ and $\psi = 90°$ are two special

cases. It is called "step-down" since the path increment moves both "forward" with a_r and "downward" with a_a at the same time as shown in Figures 2.2 c) and 2.3. In most "step-down" path increment cases, the instant depth of cut can be directly solved using the general equations derived above. Some examples of the depth of cut in the "step-down" path increment are shown in Figure 2.8. As a comparison, the case with $\psi = 0°$ is also shown in Figure 2.8.

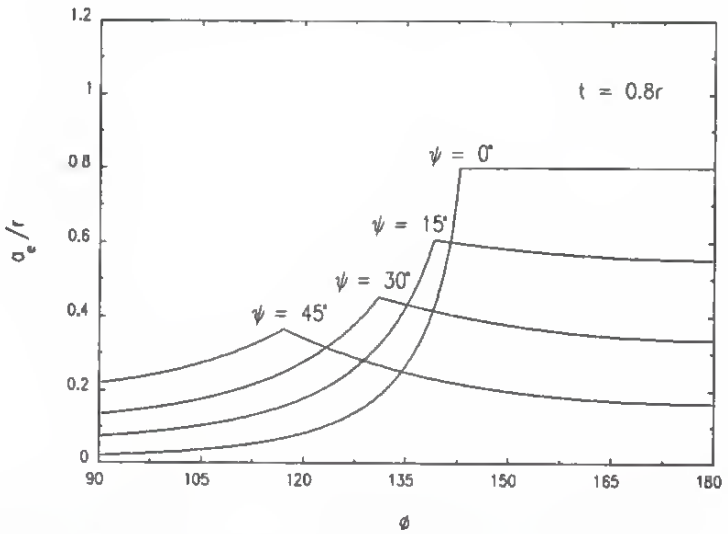

Figure 2.8 Examples of the instant depth of cut in "step-down" path increment cases.

It can be seen that although the thickness of the removed material layer t is the same (arbitrarily set to 80% of the cutter radius) for all cases, the instant depth of cut a_e varies with the path increment angle ψ. With ψ increasing, the engaged cutting area becomes more concentrated on the lower part of the ball end cutter, which is unfavored due to the lower cutting speed at that area. The instant depth of cut varies with both the path increment value as shown in Figure 2.9, and the removed layer thickness as shown in Figure 2.10. It is

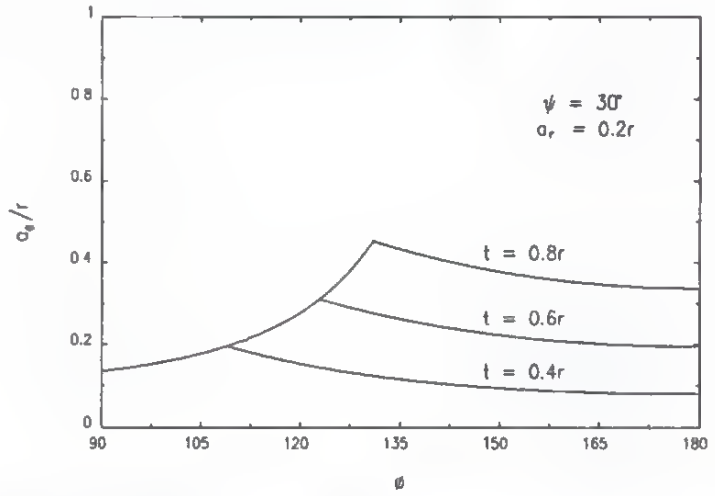

Figure 2.10 Examples of the instant depth of cut in "step-down" path increment with various thickness of the removed material layers.

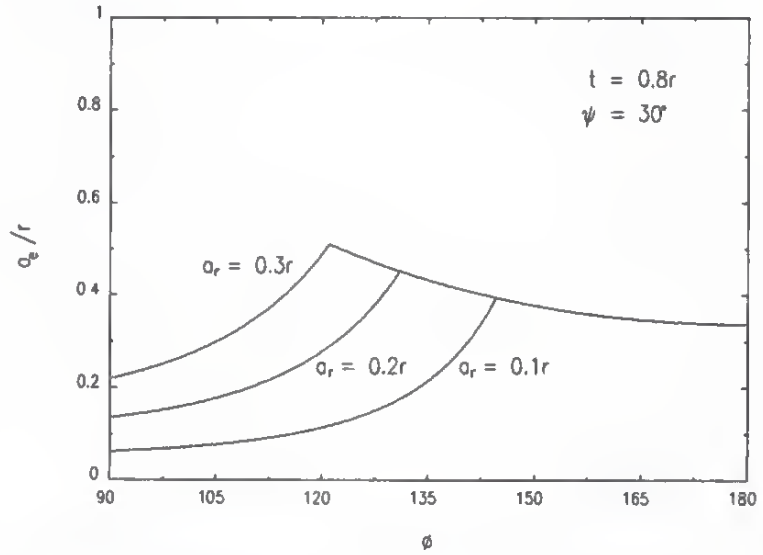

Figure 2.9 Examples of the instant depth of cut in "step-down" path increment with various step sizes.

interesting that if the thickness of the removed material t is further reduced than the examples shown in Figure 2.10, the cutting condition can be improved. As shown in Figure 2.11, if t is smaller than the critical thickness t_0, the tip of the ball end mill is disengaged from cutting.

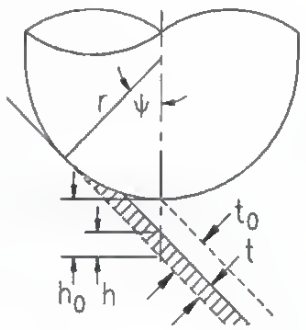

Figure 2.11 Cutting geometry with the thickness of the removed layer smaller than t_0.

The critical thickness t_0 is a function of the path increment angle ψ and proportional to the cutter radius r according to

$$t_0 = (1 - \cos \psi)\, r \tag{2.24}$$

Figure 2.12 shows some examples in this case. In the examples, ψ is arbitrarily set to 45°. Based on Equation (2.24), t_0 equals $0.293r$ when $\psi = 45°$. For $t = 0.3r$, which is larger than t_0, the tip of the ball end mill is still engaged in cutting, and the instant depth of cut a_e can be calculated as before. For $t = 0.2$r and $t = 0.1$r, which are smaller than t_0, the tip of the ball end mill is disengaged. In those cases, the general equations derived above can not be directly applied. The instant depth of cut is determined by the difference between the upper boundary and the lower boundary of the tool engagement as shown in Figure 2.12, which can be expressed as

$$a_e = a_{up} - a_{low} \tag{2.25}$$

where both upper boundary a_{up} and the lower boundary a_{low} can be calculated from the general equations derived above. In the examples shown in Figure 2.12, a_{up} is calculated by Equation (2.7) before ϕ_i and by Equation (2.10) after ϕ_i, while a_{low} is calculated by Equation (2.10). Therefore, by carefully controlling the thickness of the removed material layer to less than t_0, the tip of the ball end mill can be disengaged from cutting in "step-down" mode. However, for small ψ cases, requiring the cutter tip relief might be impractical due to a small t_0 value based on Equation (2.24), causing low metal removal rates.

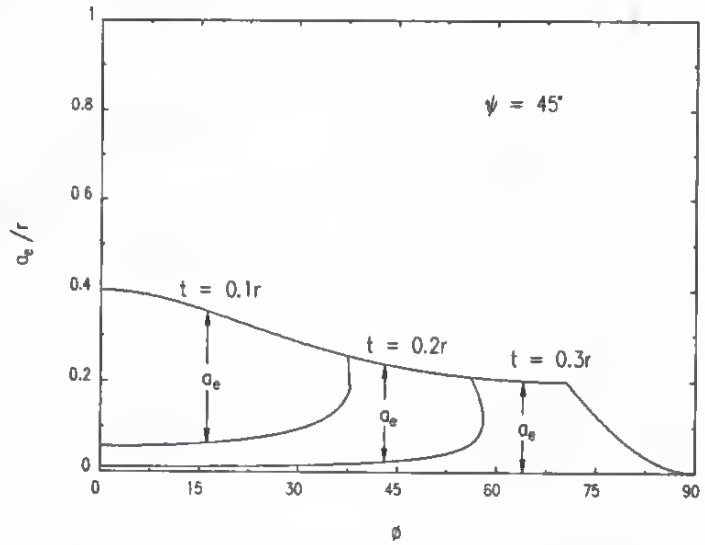

Figure 2.12 Examples of the instant depth of cut in "step-down" path increment with $t < t_0$.

Path Increment Angle -90° > ψ > 0°, "Step-Up"

In the contrast to the "step-down" case, the path increment in "step-up" case moves "upward" in the axial direction at the same time when the path moves "forward" radially, as shown in Figure 2.2 d). The main advantage of "step-up" path increment is its higher cutting velocity. From Figure 2.13 it can be seen that the maximum cutting radius for a given

removed material thickness t is at point b on the cutting edge for "step-up" path increment, while the maximum cutting radius is at point a for "step-down" increment. Larger cutting radius in "step-up" mode brings in a higher cutting velocity in the ball end milling process.

If only the spherical part of the ball end mill is desired to be engaged in the cutting process, as shown in Figure 2.13, the maximum removed layer thickness should be limited to thickness t_c

$$t_c = (1 - \sin |\psi|)\, r \tag{2.26}$$

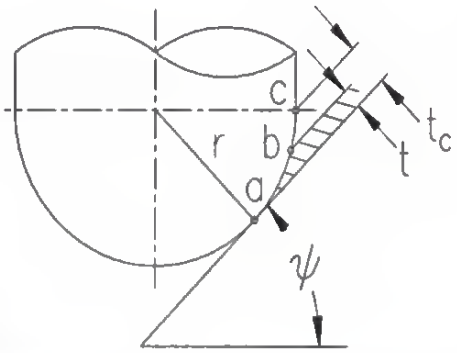

Figure 2.13 Basic cutting geometry in "step-up" path increment.

Similar to the phenomenon discussed in the "step-down" mode, it is found that in the "step-up" case, the tip of the ball end mill can be also relieved from cutting, if the radial feed in the path increment is limited to a certain value. The critical radial feed a_c at which the disengagement starts is a function of the path increment angle

$$\begin{aligned} a_c &= r \sin |2\psi| && \textit{for } |\psi| < 45° \\ a_c &= r && \textit{for } |\psi| \geq 45° \end{aligned} \tag{2.27}$$

The values of a_c and t_c as functions of the inclined angle ψ are shown in Figure 2.14. If a radial feed a_r is smaller than a_c in "step-up" path increment, the tip of the ball end mill will disengage the cutting. As shown in Figure 2.14, this condition is easy to satisfy, particularly when $|\psi|$ is larger than 45°. However, it is also can be seen in Figure 2.14 that the limitation for the removed layer thickness t_c becomes smaller for a larger ψ, if the cutting is required to be limited to the spherical part of the cutter. For solid ball end mills and some insert type ball end mills with cutting ability on the shank, this requirement can be wavered. In this case, the limitation of t_c is not mandatory, and the advantages of relieving the cutter tip from cutting can be fully taken in the cutting process.

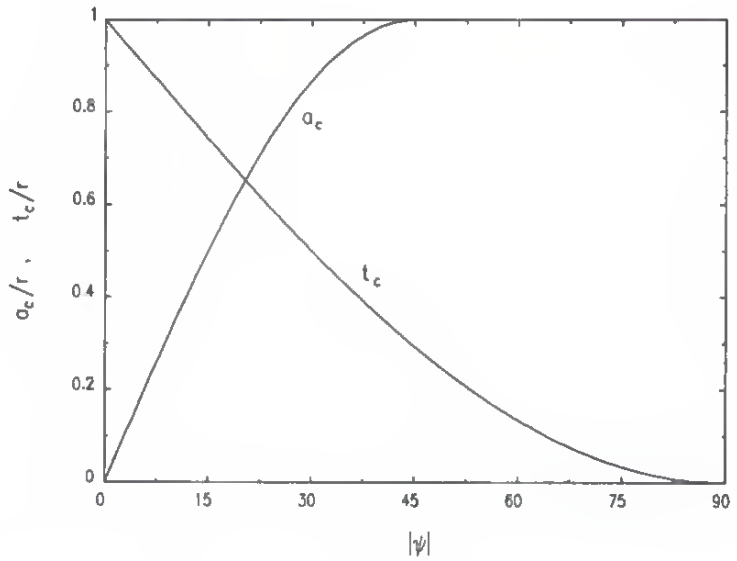

Figure 2.14 Step size and thickness in "step-up" path increment.

The calculation for the instant depth of cut in the "step-up" case is similar to that in the "step-down" case. For the situation where the tip of the ball end mill disengages, the instant depth of cut is also determined by the upper boundary and the lower boundary of the

tool engagement. Equation (2.25) used in "step-down" cases also applies for the "step-up" cases. The only difference is that for "step-up" cases, the upper boundary a_{up} is calculated from Equation (2.10) and the lower boundary a_{low} is calculated from Equation (2.7). Figure 2.15 shows two examples of the cases where the tip of the ball end mill disengages. It can be seen that when the thickness of the removed layer is too high, the depth of cut will exceed the cutter radius r, which is not desired in some circumstances. For the cases where the disengagement of the ball nose cutter tip does not happen, the general equations directly apply. Figure 2.16 shows two examples for those cases. Even in this situation, the "step-up" increment also has advantages compared with the "step-down" mode. The instant depth of cut a_e becomes larger than the removed layer thickness t when ϕ is beyond ϕ_i. The engaged cutting area is then expanded to the higher speed region on the ball end cutter.

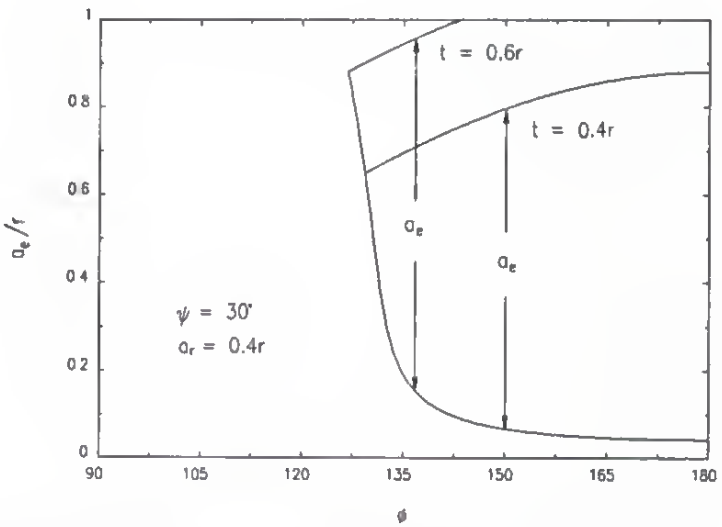

Figure 2.15 Examples of the instant depth of cut in "Step-up" case with $a_r < a_e$.

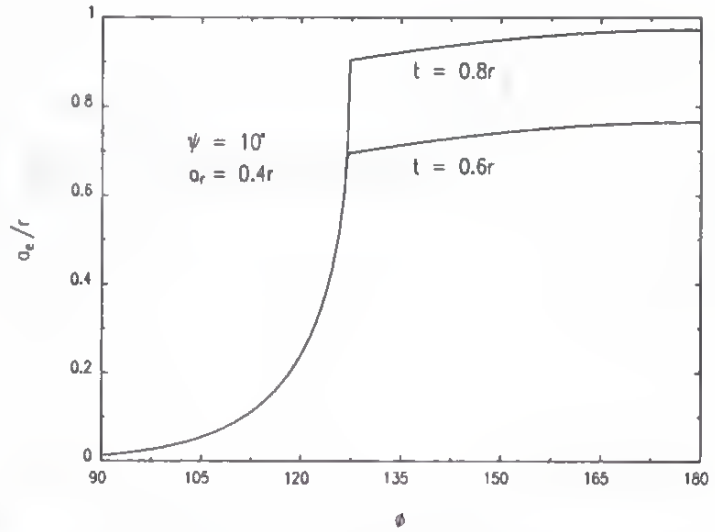

Figure 2.16 Examples of the instant depth of cut in "Step-up" case with $a_r > a_c$.

Based on the discussion on four individual cutting path increment modes, it can be concluded that the "step-up" mode creates the most favorable cutting condition for ball end milling. Due to the expanded cutting area in the higher speed region and the readiness of relieving the cutter tip from engaging, higher cutting efficiency, longer tool life and smoother surface finishing can be expected. The experimental results, which will be shown in Chapter Three, also indicate that the cutting force can be reduced by using "step-up" mode due the improved cutting condition.

Maximum Depth of Cut

As discussed in the beginning of this chapter, the stability limit b_{lim} gives a criterion to evaluate whether a milling process is dynamically stable. Since the instant depth of cut in ball end milling is a function of the cutter rotational angle, it is difficult to directly apply the

stability limit in the ball end milling. As a simple solution, it can be practiced to use the maximum depth of cut in the ball end milling as an "apparent" value to compare with the stability limit. The accuracy of this method is understandably low since only at a particular tool rotational angle the cutting reaches the maximum depth of cut. At the other angles, the depth of cut is always lower than that value. However, since this method is conservative, it can be used as an approximate estimate for ball end milling.

It is instructive to examine the maximum depth of cut in ball end milling in multi-path circumstance for the above discussed four path increment modes. It will be seen that the maximum depth of cut a_m is a function of the thickness of the removed layer t, the step over distance a_s on the removed layer surface plane, and the path increment angle ψ.

$\psi = 0°$, "Plane Cutting"

For this simple case

$$a_m = t \qquad for \quad \psi = 0° \tag{2.28}$$

$\psi = 90°$, "Slotting"

It needs to be aware that in this case

$$a_m = r + t \qquad for \quad \psi = 90° \tag{2.29}$$

$0° < \psi < 90°$, "Step-Down"

Three cases need to be considered when the maximum depth of cut is calculated in the "step-down" increment situation, as shown in Figure 2.17.

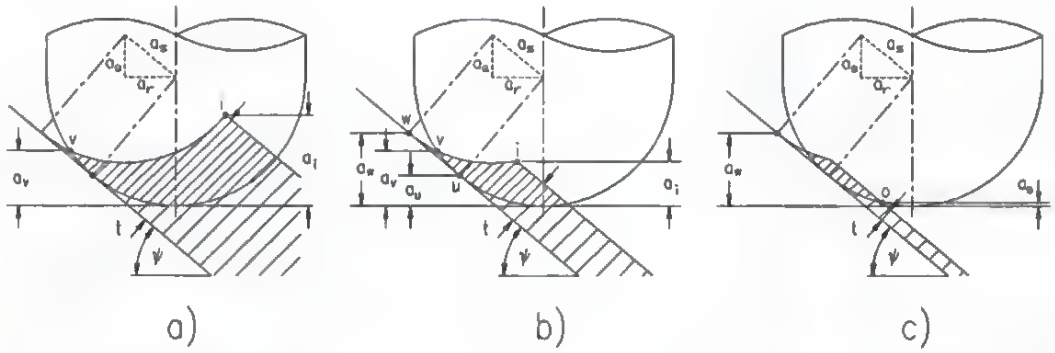

Figure 2.17 Geometry of the maximum depth of cut in "step-down" increment cases. a) $t > t_a$; b) $t_a > t > t_0$; c) $t < t_0$.

If the thickness of the removed layer is large, as shown in Figure 2.17 a), the maximum depth of cut is the vertical distance from point *I* to the tip of the ball nose cutter. Therefore

$$a_m = a_i \tag{2.30}$$

from Equations (2.11), (2.12) and (2.13), the maximum depth of cut can be obtained as

$$a_m = r - (r-t)\cos\psi - (\sqrt{2rt - t} - a_s)\sin\psi \qquad for\ t > t_a \tag{2.31}$$

where a_s is the step distance

$$a_s = \sqrt{a_a^2 + a_r^2} \tag{2.32}$$

and t_a is the critical thickness of the removed layer, which will be expressed later in Equation (2.37).

If the thickness of the removed layer t is smaller than the previous case, while it is still larger than the critical value t_0 to relieve the tip of the tool, as shown in Figure 2.17 b), the maximum depth of cut is determined by point *v*, which is the intersection point of the current

cutting path and the previous path

$$a_m = a_v \tag{2.33}$$

where a_v is the distance from the intersection point v to the tip of the ball nose tool. The value of a_v can be calculated from Equation (2.7), the general equation for the instant depth of cut. The maximum depth of cut is calculated as

$$a_m = \sqrt{(a_s\sin\psi+2r(\sin^2\psi-\cos^2\psi)^2-a_s^2-4r^2\sin\psi-4ra_s\sin\psi)} \\ -a_s\sin\psi-2r(\sin^2\psi-\cos^2\psi) \tag{2.34}$$

Instead of using the exact form of the maximum depth of cut derived from a_v, an approximate form of a_m can be derived based on the distance from point w to the tip of the ball end mill. As shown in Figure 2.17 b), point w is the normal intersection point of the previous cutting path and the machined surface plane. Based on the geometry shown in Figure 2.17 b), the distance from point w to the tip of the ball nose cutter a_w can be written as

$$a_w = r\ (1\ -\ \cos\psi)\ +\ a_s\sin\psi \tag{2.35}$$

Since a_w is always larger than a_v, it is conservative to use

$$a_m = a_w \qquad for\ t_a > t > t_0 \tag{2.36}$$

The criterion whether to use Equation (2.31) based on a_v, or Equation (2.36) based on a_w, depends on the thickness of the removed layer t and the surface inclined angle ψ. The critical thickness t_a can be calculated from

$$t_a = 2\ r\ \sin^2\psi \tag{2.37}$$

If t is larger than t_a, Equation (2.31) should be used. Otherwise, Equation (2.36) should be applied.

For the situation where t is smaller than the critical value t_0, the tip of the ball end mill disengages. In this case, the maximum depth of cut should be represented as

$$a_m = a_w - a_o \tag{2.38}$$

where a_o is the distance from point o to the tip of the ball nose cutter as shown in Figure 2.17 c). Then a_o can be solved by Equation (2.12). The maximum depth of cut can be written as

$$a_m = (a_s + \sqrt{2rt - t^2})\ \sin\psi - t\ \cos\psi \qquad for\ t < t_0 \tag{2.39}$$

It can be seen that if a t is smaller than t_0, it must be smaller than t_a, since

$$\frac{t_0}{t_a} = \frac{1}{2\ (1 + \cos\psi)} < 1 \qquad for\ 0° < \psi < 90° \tag{2.40}$$

<u>$-90° < \psi < 0°$, "Step-Up"</u>

Similar to the "step-down" increment case, the tip of the ball end cutter will be also relieved from cutting in certain circumstances in the "step-up" case. The critical value is the step size between each cutting path. The critical step size can be refer to the radial step increment as a_e shown in Equation (2.27) or to the step size on the removed material surface plane as a_d

$$a_d = 2\ r \sin|\psi| \qquad for\ |\psi| < 45°$$
$$a_d = 1.414\ r \qquad for\ |\psi| \geq 45° \tag{2.41}$$

Figure 2.18 shows geometry for the maximum depth of cut in two situations. In Figure 2.18 a), where a_s is larger than a_d, the maximum depth of cut is simply equal to a_o. Based on Equation (2.12)

$$a_m = r\ (1-\cos\psi) + t\ \cos\psi + \sqrt{2rt - t^2}\ \sin|\psi| \qquad for\ a_s \geq a_d \tag{2.42}$$

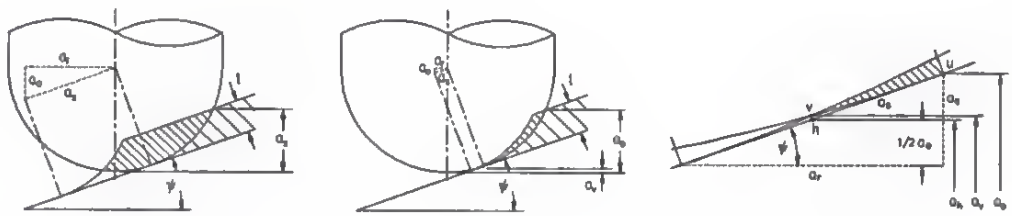

Figure 2.18 Geometry of the maximum depth of cut in "step-up" increment mode. a) $a_s > a_d$; b) $a_s < a_d$; c) detailed view of b).

If a_s is smaller than a_d, the tip of the ball end mill will be relieved. As shown in Figure 2.18 b), the maximum depth of cut in this case should be

$$a_m = a_o - a_v \qquad for\ a_s < a_d \tag{2.43}$$

where a_v is the distance from the intersection of the current cutting path and the previous one to the tip of the ball nose cutter. Then a_v can be calculated from Equation (2.7), the general equation for the instant depth of cut in ball end milling as

$$a_v = \sqrt{(a_s\sin|\psi|+2r(\sin^2\psi-\cos^2\psi)^2-a_s^2-4r^2\sin|\psi|-4ra_s\sin|\psi|)} - a_s\sin|\psi| - 2r(\sin^2\psi-\cos^2\psi) \quad (2.44)$$

To avoid the complicated calculation for a_v, an approximate solution can be used to calculate a_m from a_h instead of a_v as shown in Figure 2.18 c). The value of a_h is the distance from the point h to the tip of the ball nose cutter. Point h is obtained from the intersection of line v-h and the machined surface plane. Line v-h is perpendicular to the machined surface and reaches the intersection point of the current path and the previous one. Then the maximum depth of cut can be obtained from

$$a_m = a_o - a_h \qquad for\ a_s < a_d \quad (2.45)$$

where a_h is calculated from

$$a_h = r\ (1 - \cos\psi) - \frac{1}{2}\ a_s\ \sin\psi \quad (2.46)$$

For a positive a_h, Equation (2.45) can be written as

$$a_m = t\ \cos\psi + \sqrt{2rt - t^2}\ \sin|\psi| + \frac{1}{2}\ a_s\ \sin|\psi| \qquad for\ a_s \geq a_d\ and\ a_h > 0 \quad (2.47)$$

If a_h is less than or equal to zero, Equation (2.42) should be applied.

Equations (2.28) through (2.47) give the equations for calculating the maximum depth of cut in multi-path ball end milling. The maximum depth of cut can be used as a conservative approximate estimate to determine the stability of a milling system.

CHAPTER THREE
CUTTING FORCE AND INCLINED BALL END MILLING

"Zero Speed Zone" and Off-centered Tool

The cutting velocity in ball end milling is proportional to the cutting radius along the cutting edge. At the area near the tip of the ball end mill, the cutting velocity drops to near zero due to the small radius. This area can be called the "zero speed zone" in ball end milling. Due to the extreme low cutting velocity in this area, the workpiece material is often either plowed or indented into the deep layer, instead of becoming chips sheared off from the workpiece material during the milling operation. The cutting efficiency, the heat dissipation, and the surface finishing degrade significantly in cutting with the "zero speed zone".

In order to solve the problems resulted by the "zero speed zone", one approach is the use of the "off-centered" ball end mill. Figure 3.1 shows two Valenite "off-centered" ball end mills used in the cutting experiments. The circular insert is installed off-centered with an offset e from the cutter rotational center, and the nominal cutter radius R is no longer identical to the insert radius r, instead,

$$R = r + e \tag{3.1}$$

Although a non-zero minimum velocity can be achieved, the cutting velocity at the tip of the ball end mill is still trivial due to the limited offset. For example, if the cutting velocity at the

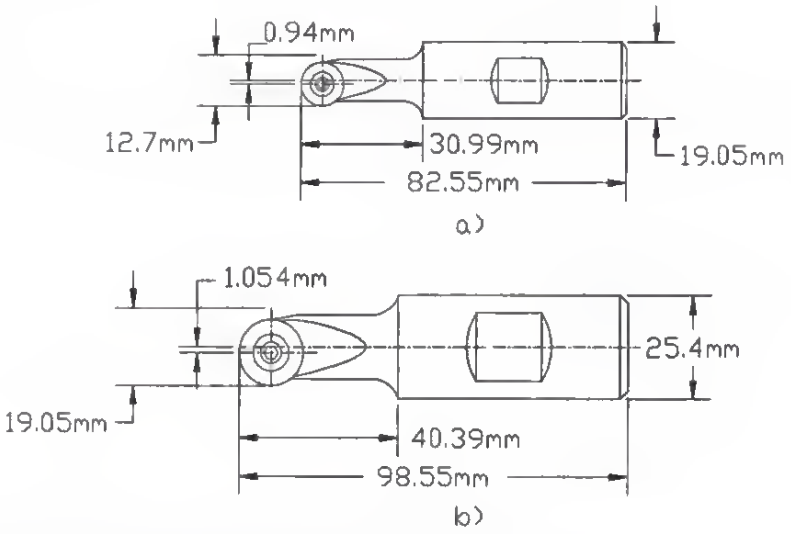

Figure 3.1 "Off-centered" ball end mills. a) Valenite 50K1R10W3; b) Valenite 75K1R12W4.

nominal cutter radius reaches 150 m/min (500 ft/min) for tool 50K1R10W3, the cutting velocity at the tip of the ball end mill is only 22 m/min (74 ft/min). The experiments results also show that the improvement is not obvious on the surface finishing and the tool life by using those off-centered tools. The cutting velocity at the tip of the cutter can be further increased by extending the offset *e*. For the same inserts, it means that larger tool diameter is needed based on Equation (3.1). The tool then becomes so called "bull nose" cutter. The "bull nose" cutter might not be suitable for some die and mold machining tasks such as spherical concavities, which require ball end milling. Therefore, using off-centered tools may not be an elegant way to solve the "zero speed zone" problem in ball end milling.

Cutting Geometry of Inclined Ball End Milling

From the discussion in Chapter Two "Analytical Solution of the Depth of Cut in Multi-path Ball End Milling", it can been seen that the "zero speed zone" is always engaged

in cutting in $\psi = 0°$, $\psi = 90°$ and most practical "step-down" cases. Only in "step-up" cases, as shown in Figure 3.2 a), can cutting with the "zero speed zone" be easily avoided. The condition for relieving the "zero speed zone" is that the radial increment a_r must be smaller than the criterion a_c. However, a small redial increment a_r may cause a lower metal removal rate and a longer machining time. In milling operations, the feed per tooth is generally set to a small value to limit the cutting force. If the feed direction is aligned with the surface inclined angle, as shown in Figure 3.2 b), then the relief of the "zero speed zone" can be always realized due to a small feed per tooth value. On a three-axis machining center, it can be only achieved in certain inclined surfaces. While in a five-axis machining center, the specific angle, which can be called tool inclined angle ε, can be readily programmed by either rotating the workpiece or rotating the spindle as shown in Figure 3.2 c).

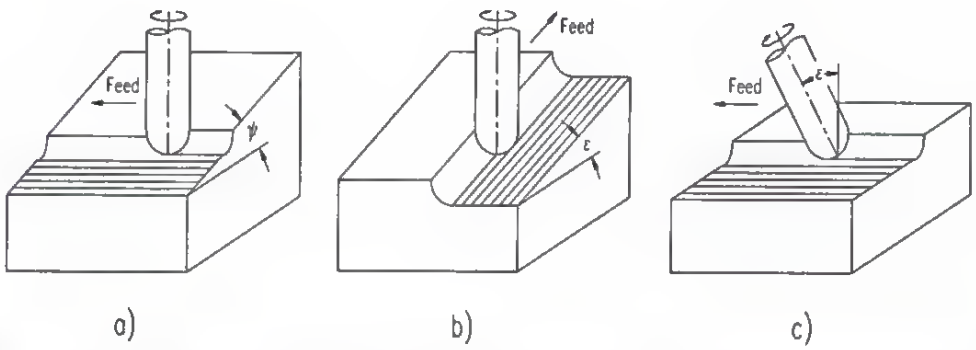

Figure 3.2 "Step-up" and inclined ball end milling. a) "Step-up"; b) Inclined ball end milling in a three-axis machine; c) Inclined ball end milling in a five-axis machine.

The cutting geometry of ball end milling with an inclined cutter is slightly different than the geometry discussed in Chapter Two. Figure 3.3 shows a detailed view of the cutting geometry of a inclined ball end milling in a simple slotting case. The ball end mill with

nominal radius r is inclined with an angle ε towards the radial feed direction. The thickness of the removed layer is t.

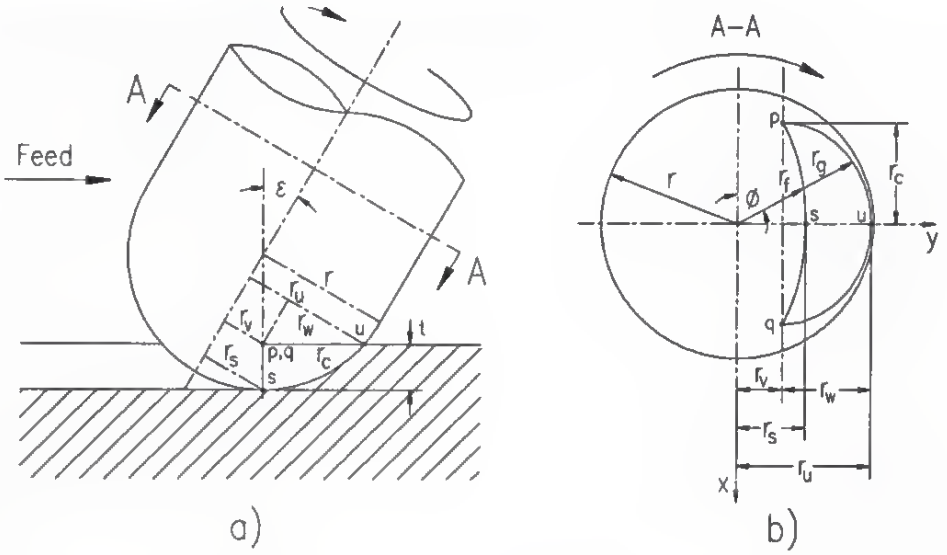

Figure 3.3 Cutting geometry of the inclined ball end milling in simple slotting. a) Side view; b) Section view *A-A*.

A section view from the tool axial direction, view *A-A*, is shown in Figure 3.3 b). The cutter starts engaging at point p. Then the engaged cutting zone on the cutting edge expands up and down at the same time. The instant cutting radius on the lower part and upper part of the cutting edge are represented by r_f and r_g. The engagement is completed at point q. Since the tip of the ball end mill is not engaged in the cutting, the instant depth of cut a_e also takes the form of Equation (2.5), which is repeated in Equation (3.2)

$$a_e = a_{up} - a_{low} \tag{3.2}$$

where a_{up} and a_{low} are the upper and lower boundary of the engaged cutting edge, which can be obtained from Equation (3.3) and (3.4) if r_f and r_g are known.

$$a_{up} = r - \sqrt{r^2 - r_g^2} \tag{3.3}$$

$$a_{low} = r - \sqrt{r^2 - r_f^2} \tag{3.4}$$

The loci of r_g and r_f as functions of the cutter position angle ϕ are recorded by curves *p-u-q* and *p-s-q* respectively. In *A-A* view in Figure 3.3 b), both *p-u-q* and *p-s-q* are ellipse curves. The equation for curve *p-u-q* in the coordinate system shown in Figure 3.3 b) can be written as

$$\frac{x^2}{r_c^2} + \frac{(y - r_v)^2}{r_w^2} = 1 \tag{3.5}$$

where r_c is the arc radius formed by the ball end mill on the removed material surface layer

$$r_c = \sqrt{2rt - t^2} \tag{3.6}$$

r_v is the offset of straight line *p-q* to the symmetric center of the cutter

$$r_v = (r - t) \sin \varepsilon \tag{3.7}$$

and r_w is the distance between point *u* and straight line *p-q*

$$r_w = \sqrt{2rt - t^2} \cos \varepsilon \tag{3.8}$$

In order to obtain r_g as a function of the cutter position angle ϕ, the following coordinate system conversion is made

$$\begin{cases} x = r_g \cos \phi \\ y = r_g \sin \phi \end{cases} \qquad for\ \phi_p \le \phi \le \phi_q \qquad (3.9)$$

where ϕ_p and ϕ_q are the angles when r_g reaches points p and q respectively. Substituting Equations (3.6), (3.7), (3.8) and (3.9) into Equation (3.5), the instant cutter radius r_g can be obtained from

$$r_g = \frac{(r-t)\sin\varepsilon\sin\phi+\cos\varepsilon\sqrt{r^2(\cos^2\varepsilon\cos^2\phi+\sin^2\phi)-(r-t)^2}}{\cos^2\varepsilon\cos^2\phi+\sin^2\phi} \qquad for\ \phi_p\le\phi\le\phi_q \quad (3.10)$$

If r_g is known, the upper boundary of the engaged cutting edge a_{up} is readily obtained from Equation (3.3).

Similarly, the locus of r_f can be written as

$$\frac{x^2}{r^2} + \frac{y^2}{r_s^2} = 1 \qquad (3.11)$$

where r_s is cutter radius when r_f reaches point s, which is also the minimum cutting radius.

$$r_s = r \sin \varepsilon \qquad (3.12)$$

Similar to Equation (3.9)

$$\begin{cases} x = r_f \cos \phi \\ y = r_f \sin \phi \end{cases} \qquad for\ \phi_p \le \phi \le \phi_q \tag{3.13}$$

Substituting Equations (3.12) and (3.13) into Equation (3.11), the instant cutting radius on the curve *p-s-q* can be calculated from

$$r_f = \frac{r \sin \varepsilon}{\sqrt{\cos^2\phi \sin^2\varepsilon + \sin^2\phi}} \qquad for\ \phi_p \le \phi \le \phi_q \tag{3.14}$$

The lower boundary of the engaged cutting edge a_{low} can be obtained from Equation (3.4).

At the point *p* and *q*

$$r_f = r_g = r_p = r_q = \sqrt{r^2 - (r-t)^2 \cos^2\varepsilon} \tag{3.15}$$

The cutter rotational angle at point *p* is

$$\phi_p = \tan^{-1} \frac{(r-t) \sin \varepsilon}{\sqrt{2rt - t^2}} \tag{3.16}$$

and the angle at point *q* is

$$\phi_q = 180° - \phi_p \tag{3.17}$$

For some ball end mills the axial immersion should not be larger than the cutter radius, such as the tools shown in Figure 3.1. In those cases, the thickness *t* needs to be limited to

$$t < r\ (1-\sin\ \varepsilon) \qquad \textbf{(3.18)}$$

Some examples are shown in Figure 3.4, where the thickness of the removed layer is the same for all cases (arbitrarily set to 20 percent of the cutter radius). It can be seen that the engaged cutting area moves away from the "zero speed zone" and into a higher speed region with the increasing of the tool inclined angle ε,. Therefore, by using inclined ball end milling, the "zero speed zone" can be completely avoided from the engaging of cutting. A higher cutting efficiency and better surface finishes can be expected.

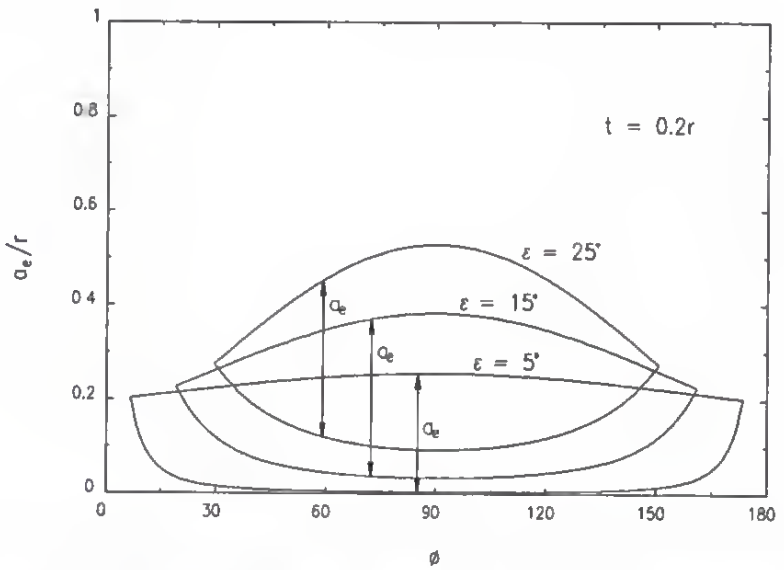

Figure 3.4 Examples of the instant depth of cut with inclined ball end milling.

The equation for the maximum depth of cut for the inclined ball end milling in simple slotting cases can be derived from the cutting geometry shown in Figure 3.3 as

$$a_m = t \cos \varepsilon + \sqrt{2rt - t^2} \sin \varepsilon \qquad for\ t \le r\ (1-\sin\ \varepsilon) \qquad \textbf{(3.19)}$$

A similar equation, Equation (2.47), was derived in Chapter Two. Since the feed per tooth is usually small compared with the tool diameter, the effect of the feed per tooth on the maximum depth of cut is neglected in Equation (3.19).

The relation between the maximum depth of cut and the inclined angle is shown in Figure 3.5. It can be seen that for a given removed layer thickness t, the maximum depth of cut is always larger than t itself, and with the inclined angle increasing, the maximum depth of cut also increases.

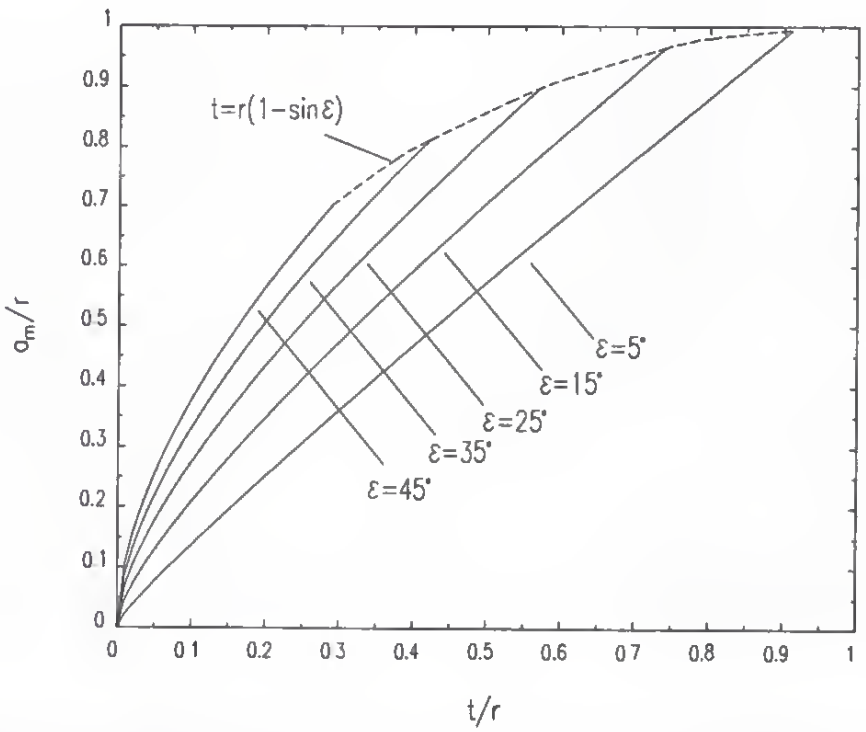

Figure 3.5 The maximum depth of cut in the inclined ball end milling.

It should be noted that Equation (3.19) is only valid for the cases where the maximum axial immersion is less than the cutter radius, which is described in Equation (3.18). For the

cases where the axial immersion is larger than the cutter radius, the maximum depth of cut should be calculated from

$$a_m = \frac{t + r \sin \varepsilon (1 - \sin \varepsilon)}{\cos \varepsilon} \qquad for\ t > r\ (1 - \sin \varepsilon) \tag{3.20}$$

Cutting Force in Ball End Milling

Due to its unique cutting geometry, the cutting force in ball end milling is also different than that in the flat end milling. A major difference is that there is a significant axial force in the ball end milling. The force in the ball end milling at a small element on the cutting edge is shown in Figure 3.6. When this element is engaged in cutting, there is a tangential force ΔF_t on the tool rotational direction and a normal force ΔF_n perpendicular to the cutting edge. The normal force ΔF_n can be further decomposed into the radial force ΔF_r and the axial force ΔF_n as shown in Equation (3.21).

$$\begin{aligned} F_r &= F_n \cos \sigma \\ F_a &= F_n \sin \sigma \end{aligned} \tag{3.21}$$

The direction angle σ varies depending on the position of the element

$$\sigma = \sin^{-1} (1 - \frac{z}{r}) \tag{3.22}$$

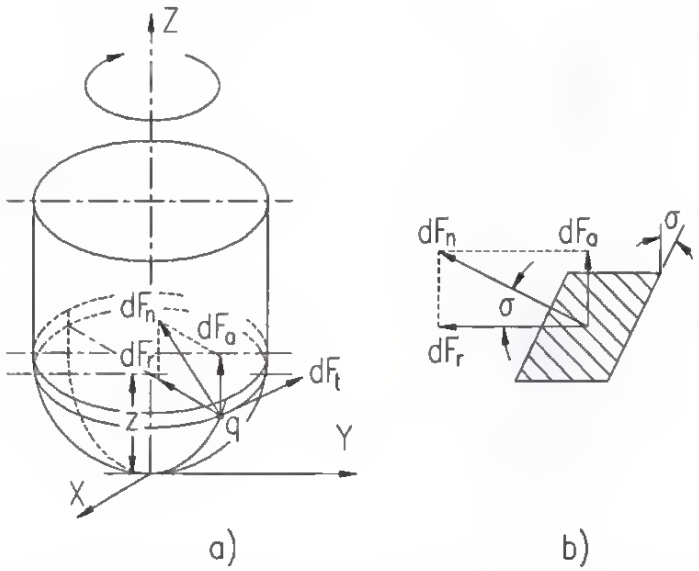

Figure 3.6 Cutting force on the ball end mill. a) Force direction; b) Force in an element.

where z is the vertical position of the element to the tip of the ball end mill as shown in Figure 3.6 a) and r is the nominal cutter radius. It can be seen that at the region near the tip of the ball end mill, z becomes much smaller than r, and the direction angle σ is approaching 90 degrees. The axial force becomes significant in this region.

The axial force was observed in the cutting experiments. Figure 3.7 shows some experimental results of the cutting force in ball end milling. It can be seen that there is a significant axial force F_a existing during the cutting process. This axial force may cause dynamic problems if the system stiffness on the axial direction is not sufficient. Especially in some high speed spindle designs, the preload on the axial direction may be purposely reduced to decrease the bearing temperature. In addition to the cutting geometry, tool condition is also an important factor causing excessive axial force. In the hardened material cutting experiments done by Nelson (1996), a SETCO Phase I high speed spindle with low preload

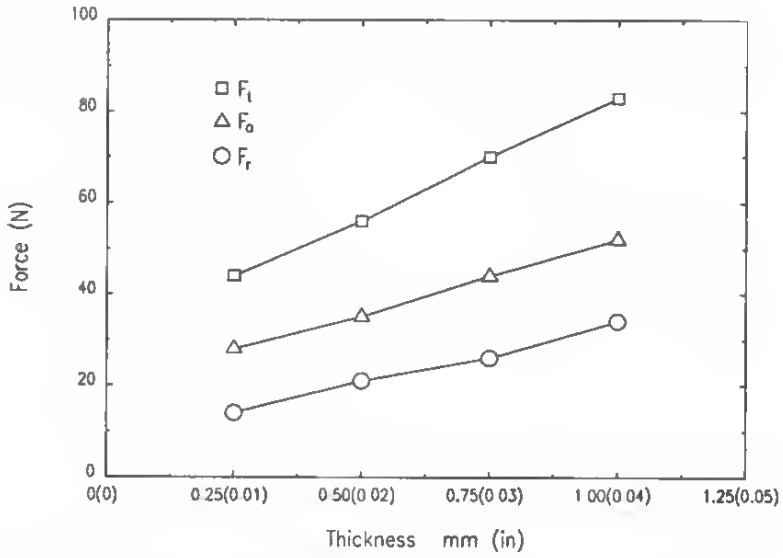

Figure 3.7 Cutting force in ball end milling (plane cutting, 5000 rpm, 50 ipm).

was used. The cutting is stable with new inserts, while a significant vibration was observed when tool wear increased. A comparison cutting test were made on the White-Sundstrand milling machine with two groups of inserts under same cutting parameters. One group is new inserts and the other is "used inserts". The "used inserts" were those used in the previous cutting tests with SETCO high speed spindle, and eliminated due to excessive tool wear (flank wear 0.25 to 0.35 mm (0.010 to 0.014 in)). The axial cutting force were measured and the average value of each group is shown in Figure 3.8. It can be seen that the axial force generated by used inserts is three times higher than that by new inserts. Since the White-Sundstrand spindle is a low speed spindle and designed to accommodate drilling tasks, the preload and consequently the stiffness on the axial direction is high. The used inserts were still able to stably perform the cutting tasks on the SundStrand spindle, while they has caused severe vibration on the SETCO high speed spindle.

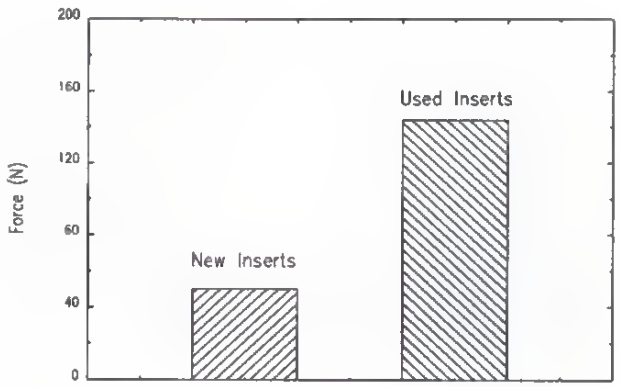

Figure 3.8 Cutting force with new and used inserts (slotting, 5000 rpm, 50 ipm, 0.50 mm (0.02 in) deep)

Cutting Force in "Step-up" Increment Mode

In Chapter Two "Analytical Solution of the Depth of Cut in Multi-path Ball End Milling", it is found that if the "step-up" increment strategy is used, the cutting zone can move up to a larger cutter radius area and the cutting speed will be increased. In addition, if the step size satisfies the critical condition as shown in Equation (2.27), the "zero speed zone" can be avoided. Both factors can improve the cutting condition and reduce the cutting force, particularly the axial force. Figure 3.9 shows the cutting forces measured in the experiments with the "step-up" increment angle $\psi = 25°$.

Comparing the cutting forces in Figure 3.7 and in Figure 3.9, it can be seen that the cutting force on all three directions F_a, F_r and F_t are decreased in the "step-up" mode. That is mainly due to the "ill cutting condition" such as plowing or indenting with the "zero speed zone" is avoided, and a larger cutting radius and higher cutting speed is introduced by shifting

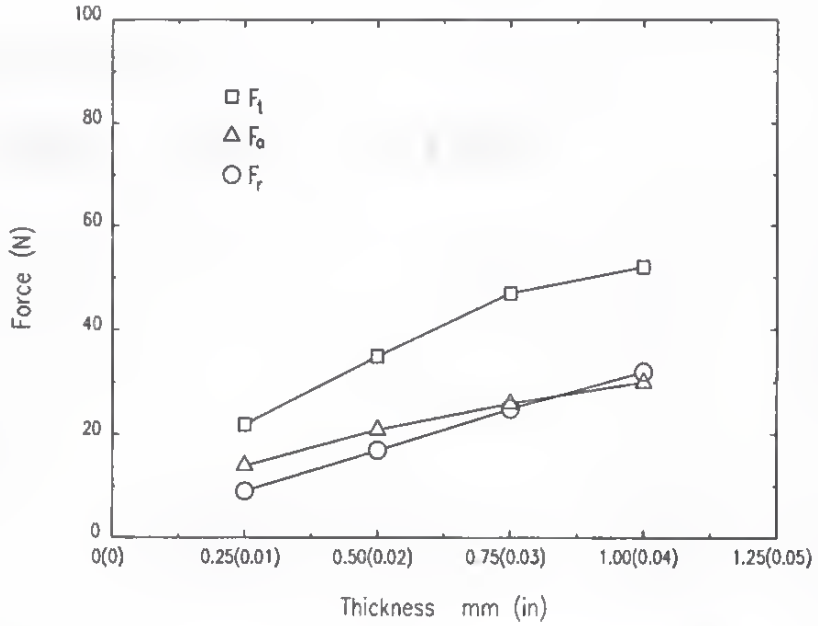

Figure 3.9 Cutting force in "step-up" increment mode (plane cutting, 5000 rpm, 50 ipm, $\psi = 25°$).

the cutting zone. Especially, the decreasing of the axial force reduces the requirement on the axial stiffness, so that the high speed machining can be realized without special requirements on the high speed spindle. In addition to the geometrical analysis in Chapter Two, the experimental results shown here also indicate that "step-up" increment mode can improve the cutting condition in ball end milling.

Cutting Force with Inclined Ball End Milling

Based on the previous discussion, it is known that the inclined ball end milling can completely avoid the "ill cutting condition" with the "zero speed zone", and shift the cutting zone to the larger cutting radius and higher cutting speed area. Therefore the inclined ball end milling can reduce the axial force if five-axis machining ability is available. The axial force

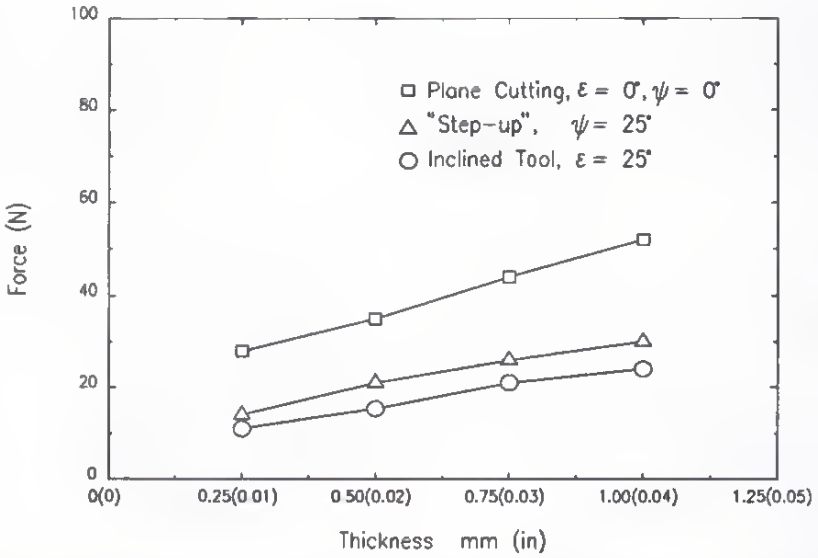

Figure 3.10 Axial force on various cutting condition: plane cutting, "step-up" and inclined tool (5000 rpm, 50 ipm, 0.5mm (0.02in) step over).

was measured in the experiments with the tool inclined 25 degrees. A comparison is made in Figure 3.10. The cutting parameters such as the removed layer thickness, the spindle speed and the feed rate are identical for all three cases in Figure 3.10. The cutting with the inclined tool has the minimum axial force, which is slightly lower than that with the "step-up" increment mode. The reason for this can be explained in the comparison of Equations (2.47) and (3.19). The comparison is also shown in Figure 3.11.

Since the feet per tooth is usually small, its contribution to the depth of cut can be neglected as shown in Equation (3.19) and Figure 3.11 a). While in the "step-up" case, the step size has its contribution to the depth of cut as shown in Equation (2.47) and Figure 3.11 b). Consequently, the depth of cut in the inclined ball end milling is usually lower than that in the "step-up" case. Since the additional depth is located at the lower boundary of the

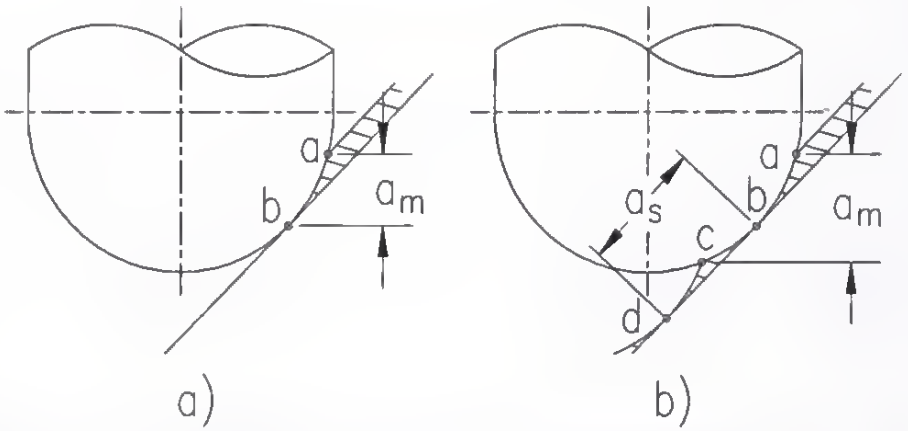

Figure 3.11 Maximum depth of cut in the inclined ball end milling and "step-up" mode. a) inclined ball end milling; b) "step-up".

engaged cutting area on the cutting edge, shown as *b-c* in Figure 3.11 b), it increases the axial cutting force. Therefore, to minimize the harmful axial force to the spindle, the inclined ball end milling is the best solution. In addition, with the improved cutting condition and the increased cutting speed introduced by the inclined ball end milling, higher cutting efficiency, better surface finish and longer tool life can be expected.

Chatter in Ball End Milling

Chatter is an important issue for metal cutting processes. Chatter might damage the workpiece by excessive chatter marks on the surface. It also might cause potential damage to the spindle. The dynamic analysis of a milling system was conducted in order to effectively avoid chatter during the die and mold machining.

The criteria for a given milling system to be stable was given in Equation (2.1) in Chapter Two, "Analytical Solution of the Depth of Cut in Multi-path Ball End Milling", which is repeated here as Equation (3.23)

$$b_{\lim} = -\frac{1}{2\, n_a\, K_s\, \mu\, Re[G]_{\min}} \tag{3.23}$$

The axial depth of cut of a milling process should be smaller than the stability limitation b_{lim}, or chatter will occur. The milling system used in the analysis includes: the McMaster milling machine, the SETCO Phase I high speed spindle, an HDT 9005470 tool holder, and a Valenite 50K1R10W3 single insert ball end mill with cutting diameter 12.7 mm (0.5 in) as shown in Figure 3.1 a). It is assumed that the tool-tool holder-spindle system is the most flexible part in the entire system. The flexibility of the workpiece and the machine tool structure is neglected. The transfer function of the tool-tool holder-spindle system was measured with an Accumeasure ASP-2 Capacitive probe pointed to the tip of the ball end mill in the radial direction of the tool. An Accumeasure System 1000 amplifier was used to convert the probe signal to the voltage signal. A PCB 086C80 instrumented hammer was used as a force impulse source. Figure 3.12 shows the transfer function of the tool-tool holder-spindle system in the tool radial direction. It can be seen that the most dominant mode is at about 7650 Hz. The minimum value of the real part of the transfer function $Re[G]_{min}$ is measured as -9.127×10^{-8} m/N. Considering the slotting is the worst situation for the stability and a single cutting edge is used on the ball end tool, n_a is 0.5 and μ is 0.342 (cos 70°). The workpiece material used in the cutting experiments is AISI H13 tool steel hardened to HRC 47-49. The cutting stiffness of the material is assumed to be approximately 4000 N/mm^2. Then the stability limit b_{lim} for the tool-tool holder-spindle system can be calculated from Equation (3.23)

$$b_{lim} = -\frac{1}{2\times0.5\times4000(N/mm^2)\times0.342\times(-9.127\times10^{-5})(mm/N)} \qquad (3.24)$$
$$= 8\ mm\ (0.32\ in)$$

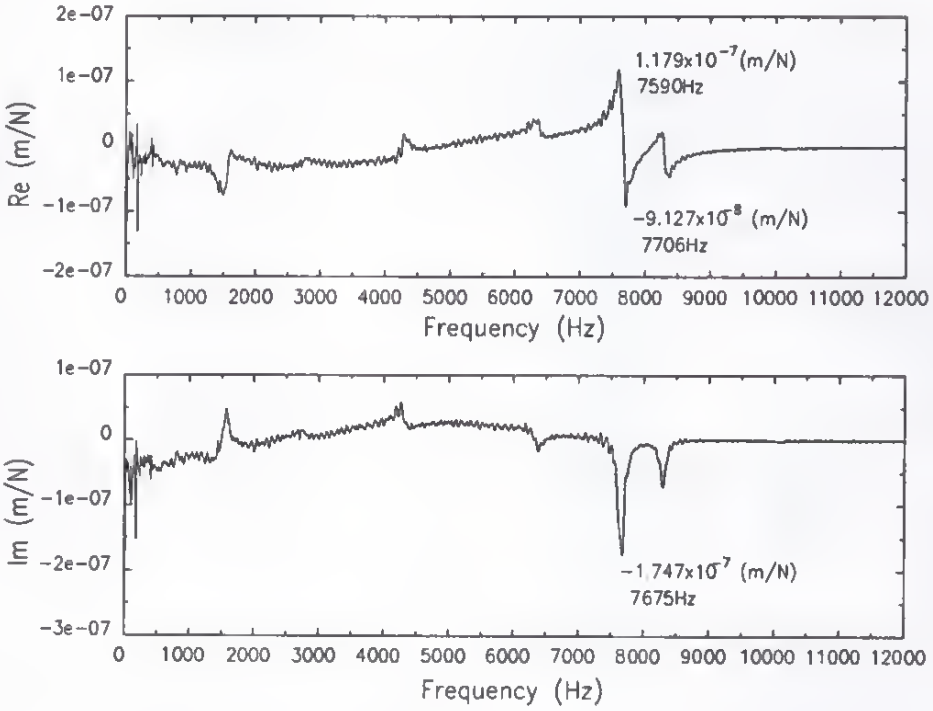

Figure 3.12 Transfer function of the tool-tool holder-spindle system.

The high stability limit is due to the high stiffness of the selected tool and the tool holder. With such a stability limit, the system is stable in normal cutting process, and the strength of the carbide insert becomes the primary concern while machining hardened die and mold steel. Experimental results showed that the carbide insert was broken when the depth of cut of slotting was increased to 3 mm (0.12 in) on machining pre-hardened H13 steel. The sound signal was recorded before the insert was broken. The spectrum of the sound record is shown in Figure 3.13. It can be seen that all the sound energy in the spectrum is concentrated in the

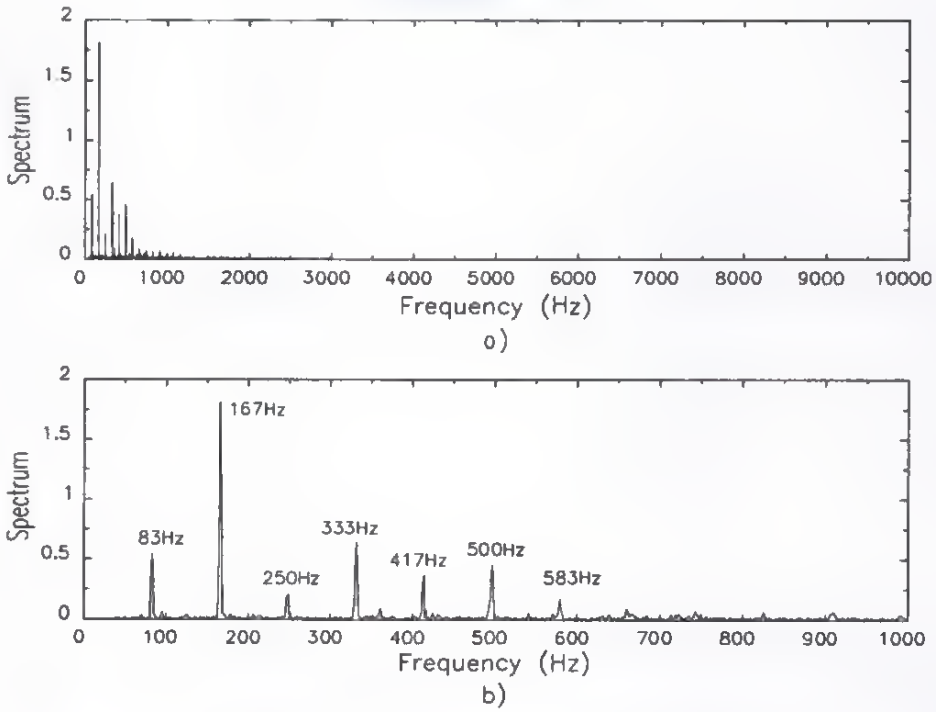

Figure 3.13 Spectrum of the sound record in milling operation (5000 rpm, 50 ipm, 3mm depth). a) Spectrum to 10000Hz; b) Zoomed in 1000Hz.

lower frequency range. No sound energy was detected between 7000Hz to 9000Hz, where the system natural frequency is. The detailed view, Figure 3.13 b), shows that all the energy peaks are located at the run-out frequency (83 Hz) and its harmonics. No chatter signal was observed in the spectrum. Moreover, most insert type ball end mills specify their maximum depths of cut to be equal to their insert radius, including the ball end mill used in the experiments, since there is no cutting ability on the cylindrical shank of the tool. Therefore for the tool used in the experiment, the maximum depth of cut should not exceed 5.4mm (0.213 in). Therefore, the system should be stable for the regular cutting tasks with the workpiece material H13 steel or other materials with less hardness. Since the natural frequency of the system is high (7650 Hz), the cutting process would be more stable for lower

spindle speeds. In this situation, the processing damping would play an important role to minimize the chatter and stabilize the cutting process.

In order to further investigate the dynamic performance of the tool-tool holder-spindle system, a specially designed software SPA (Spindle Analysis), developed by the Manufactory Laboratories, Inc., was used to conduct a finite element analysis on the tool-tool holder-spindle system. The parameters of the Valenite 50K1R10W3 single insert ball end mill and the HDT 9005470 were input into the program together with the SETCO spindle parameters. The calculation results of the system are listed in Table 3.1 and the first three and the seventh mode shapes are shown in Figure 3.14.

Table 3.1 Calculation results of the tool-tool holder-spindle system (Valenite 50K1R10W3 ball end mill, SETCO high speed spindle).

Natural Frequency (Hz)	Modal Stiffness (N/m)	Modal Mass (Kg)	Modal Damping Coefficient (%)	
786.94	.28606E+09	.11701E+02	.750	
1412.23	.95836E+08	.12172E+01	.750	
2157.36	.12270E+10	.66776E+01	.750	
2489.15	.44212E+12	.18075E+04	.750	
3780.43	.92440E+09	.16384E+01	.750	
5343.62	.60415E+09	.53594E+00	.750	
7076.10	.98636E+08	.49899E-01	.750	
7770.72	.41815E+08	.17541E-01	.750	(Tool Mode)
9135.27	.62976E+09	.19115E+00	.750	

From Table 3.1 it can be seen that although the tool mode has the lowest stiffness, the natural frequency of the mode is high compare with most of the spindle modes. Figure 3.14 shows

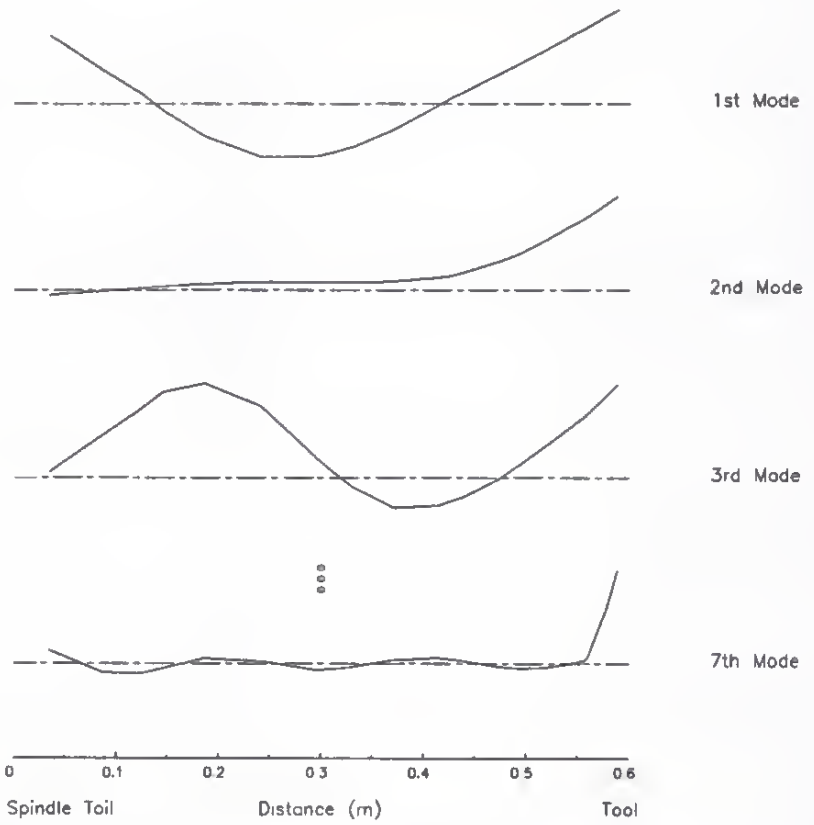

Figure 3.14 Vibration mode shapes of the tool-tool holder-spindle system (Valenite 50K1R10W3 ball end mill, SETCO high speed spindle).

that in the lower frequency range, from the first mode to the sixth mode, the spindle mode dominates the dynamic performance of the system. The tool mode does not rise until the seventh mode which is above 7000 Hz. The results indicate that for the Valenite 50K1R10W3 ball end mill, which has high stiffness, the primary concern for the dynamic performance of the tool-tool holder-spindle system should be on the spindle. With a sufficient spindle stiffness, the process should be stable for normal cutting tasks.

However, if a tool with lower stiffness is used, the system might fall into unstable situation. A SGS SER3LB1/2 two flutes solid carbide ball end mill was tested in the

experiments. The dimensions of the tool are shown in Figure 3.15. The transfer function was measured with an Accumeasure ASP-2 Capacitive probe. A PCB 086C80 instrument hammer was used as the impulse source. Figure 3.16 shows the transfer function in the radial

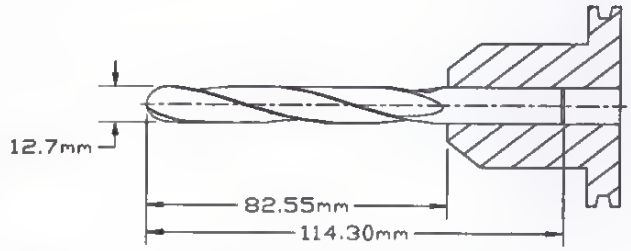

Figure 3.15 SGS SER3LB1/2 solid end mill.

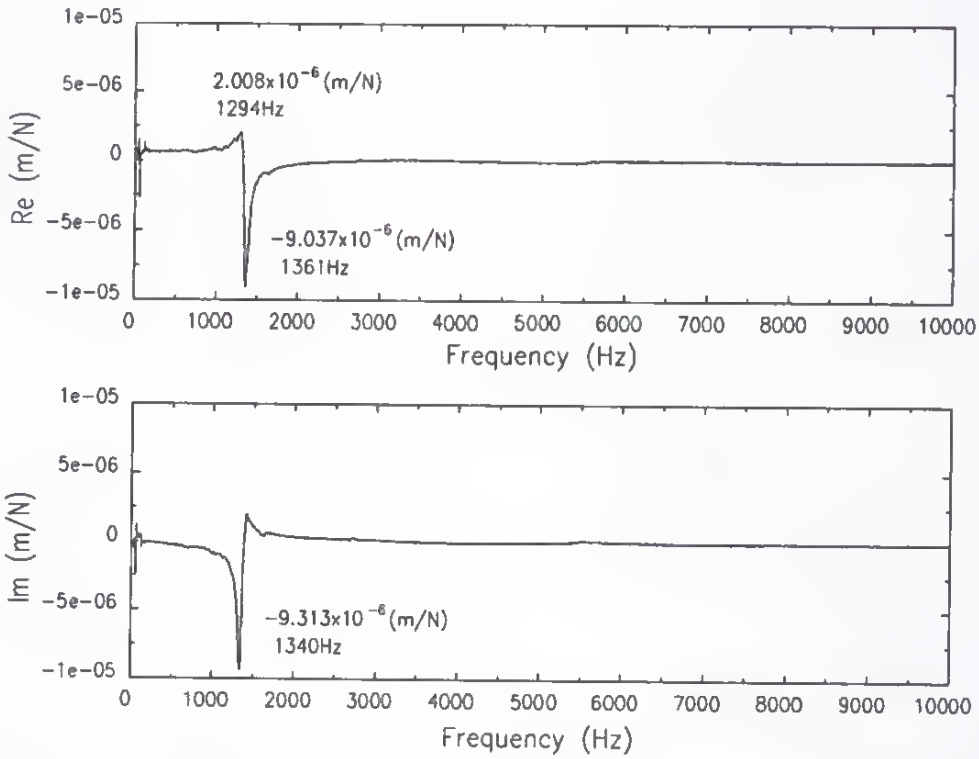

Figure 3.16 Transfer function of the solid carbide ball end mill SGS SER3LB1/2.

direction of the tool. The stability limit for slotting can be calculated from Equation (3.23) with H13 steel as the workpiece material.

$$b_{\lim} = -\frac{1}{2\times1\times4000(N/mm^2)\times0.342\times(-9.037\times10^{-3})(mm/N)} = 0.04\ mm\ (0.0015\ in) \tag{3.25}$$

with such a small stability limit, the cutting will easily fall into instability. The tools with such a higher flexibility can only be used in the finishing cutting on the hardened materials. A cutting test with a excessive depth of cut was conducted and the cutting sound signal was collected by a directional microphone. The spectrum of the signal is shown in Figure 3.17.

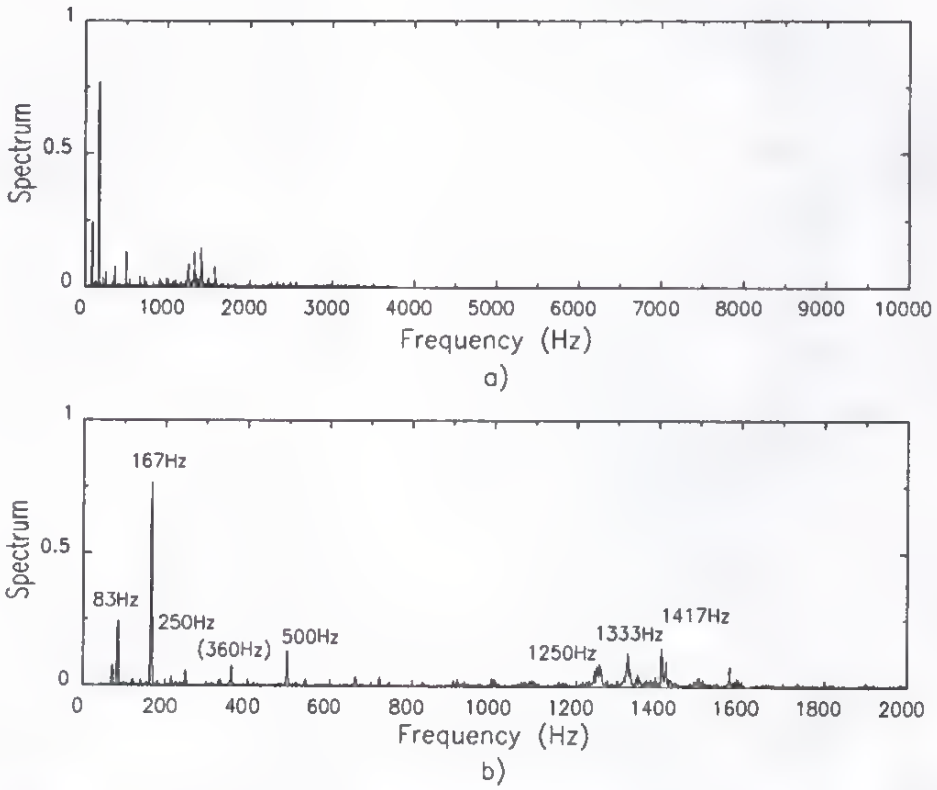

Figure 3.17 Spectrum of the sound signal in slotting with SGS SER3LB1/2 tool. (5000 rpm, 50 ipm, 1mm (0.04 in) depth). a) 0-10000 Hz; b) 0-2000 Hz.

It can be seen that a group of energy peaks appears at the frequency range around 1300 Hz. This frequency matches the natural frequency of the tool as shown in Figure 3.16. It indicates that chatter happens during the cutting process. Differing from the chatter signal seen in the flat end milling on aluminum workpieces, which usually has a single chatter frequency, the chatter signal in ball end milling on hardened materials is modulated by the tool run-out frequency as shown in Figure 3.17. Similar phenomenon was also observed in Nelson's research (1996). The modulation may be due to the strong once-per-revolution or twice-per-revolution force caused by the single or two-flute ball end cutters. The parameters of the solid carbide ball end mill was also input into the spindle analysis software SPA with the parameters of SETCO high speed spindle. The calculation results are shown in Table 3.2 and the first four mode shapes are shown in Figure 3.18.

Table 3.2 Calculation results of the tool-tool holder-spindle system (Valenite 50K1R10W3 ball end mill, SETCO high speed spindle).

Natural Frequency (Hz)	Modal Stiffness (N/m)	Modal Mass (Kg)	Modal Damping Coefficient (%)	
777.64	.45847E+08	.19204E+01	.750	
1193.69	.53823E+07	.95681E-01	.750	(Tool Mode)
1678.95	.87142E+07	.78305E-01	.750	
2182.45	.20571E+09	.10940E+01	.750	
2489.22	.13973E+12	.57122E+03	.750	
3804.33	.14076E+10	.24636E+01	.750	
5374.97	.20262E+10	.17765E+01	.750	
7203.52	.11306E+10	.55192E+00	.750	
8556.98	.96353E+08	.33332E-01	.750	
9265.47	.25093E+09	.74039E-01	.750	

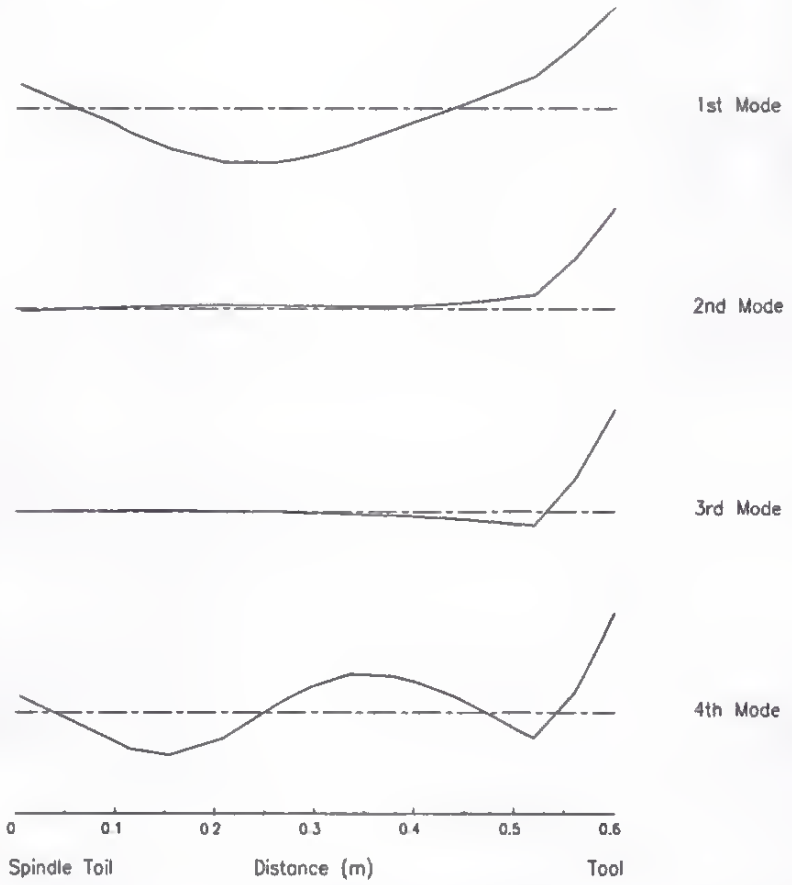

Figure 3.18 Modes shapes of the SGS SER3LB1/2 solid carbide ball end mill and SETCO high speed spindle.

From Table 3.2 it can be seen that the tool mode has the lowest stiffness with a low natural frequency. The flexibility can be also seen in Figure 3.18. The tool mode starts to dominate the mode shape of the system from the second mode. For the tools with lower stiffness, it is important to carefully select the cutting parameter, particularly the depth of the cut, to prevent chatter. Since the depth of cut increases with the inclined tools as shown in Figures 3.5, care must be taken when machining with low stiffness tools in the inclined manner.

Another situation where chatter is prone to happen is the transition point where the cutting transfers from the plane cutting to the inclined tool or inclined surface cutting manner. Although the calculation for either plane cutting or the inclined cutting part indicates that the cutting is stable, chatter may happen at the transition point, since the actual depth of cut in that area is much higher than either side of the directional changing point as shown in Figure 3.19. In an aluminium injection mold machining test, an 8 mm solid carbide ball end mill was used. The stability limit for the tool and workpiece combination was calculated as 3.5 mm. The removed layer thickness was set to 1 mm. The spindle speed was 15,000 rpm. In the plane cutting area, shown in Figure 3.19 as Position 1, the maximum depth of cut was equal to the removed layer thickness t, which was 1 mm. In Position 3, with a surface inclined angle of 68°, the depth was calculated from Equation (3.20) as 3.4 mm. However at Position 2, the transition point, the depth reached 5.9 mm. It exceeds the stability limit with a large

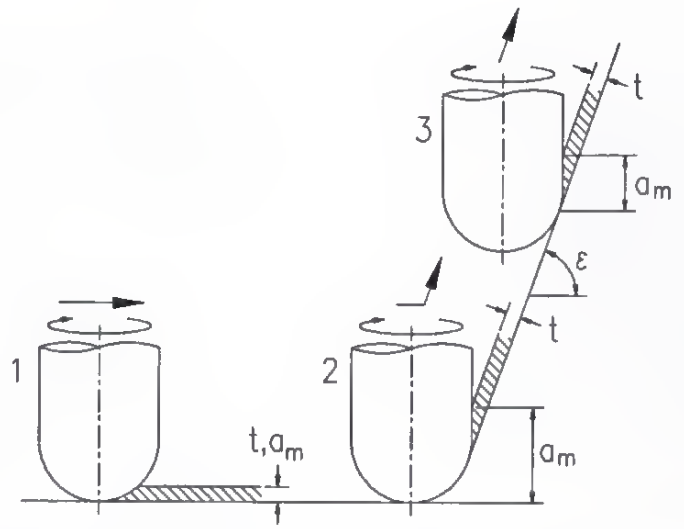

Figure 3.19 Depth of cut at the entry of the inclined surface cutting.

margin. During the cutting operation, chatter was detected every time when the cutting tool passed through that position while it was stable at other positions.

CHAPTER FOUR
OPEN ARCHITECTURE CONTROLLER AND ITS IMPLEMENTATION ON MILLING MACHINE

Background of Open Architecture Controller

The control and automation techniques for machine tools have been advanced greatly in the forty years since the first numerical control (NC) machine tool was built. The most important advance was the development of computer numerical control (CNC) in the 1970s. CNC has become popular in NC machine tools due to its flexibility and versatility. With the continued fast development of computer technologies, the computing speed and data sampling rate of controllers have increased dramatically, allowing CNC machine tools with higher accuracies and higher cutting speeds. In addition, the continuing price decreases of microprocessors and other devices have made CNC controllers more affordable. In recent years, most die and mold manufacturers are using CNC machine tools to machine their products, in part also due to the increasing accuracy and complexity requirements of the dies and molds.

Most contemporary commercial CNC controllers are "closed" systems. The concepts and designs of CNC controllers differ between manufacturers. Although most controllers offer adequate control strategies and friendly user interfaces, modifications are often desired by the user for various reasons. However, it is usually very complicated to modify a controller from general applications to a particular task. Sometimes, the modification turns

out to be impossible without help from the controller manufacturer. Updating an existing controller on a CNC machine tool is also often time consuming and costly. It might be easier to update the existing controller with a new or more advanced one made by the same manufacturer. However, it would generally be difficult to retrofit a CNC machine tool with a new controller made by another manufacturer.

The concept of an "open control system" was first proposed in Germany in 1970's (Pritschow et al, 1993), aiming to resolve the problems of "closed" systems. A consortium of machine tool and controller manufacturers and universities in Germany reached an agreement to build a common control system called "MPST" (Multi-Processor Control System). The work was continued until the late 1980's. However due to the limitations of the computer technology at that time, the system was not very successful. In 1992, led by Pritschow (Pritschow et al, 1993; Pritschow and Junghans, 1994), a large scale project "OSACA" (Open System Architecture for Controls within Automation Systems) was started. Supported by the European Community, leading machine tool and controller industries and universities in France, Germany, Italy, Spain and Switzerland participated. The main goal of the project was to define a hardware-independent reference architecture for CNC machine tool controllers and other control systems. A framework was proposed consisting of functional units, communication protocols and interfaces to operating systems, and data base systems. The first "vendor-neutral open control" prototype was planned to be presented in 1995.

Similar programs have been conducted in the United States. MAP (Manufacturing Automation Protocol) in the 1980s was the first program in US challenging the "closed"

control architecture. A uniform application interface to data base, file system and remote program invocation functionalities was developed. It followed the Open Systems Integration standard defined by ISO (International Standards Organization), and used other standards. Later, the NGC (Next Generation Machine / Workstation Controller) program conducted an extensive consultation with experts in the US manufacturing industry. It resulted in a specification for NGC with a wide range of requirements including hardware and software architectures, networking capabilities, and provisions for task planning, process control fault management and sensor interfaces. The controller system proposed by NGC consists of a workstation and a controller. While the controller is working on "real-time" computing such as on-line compensation, the workstation handles all other "non-real-time" events such as network communication and user interfacing. MOSAIC (Machine Open Standard Architecture Intelligent Controller) was another program conducted by researchers at New York University. A concept similar to NGC was implemented in a three-axis milling machine. A workstation equipped with standard UNIX operation system handled network communication and user interface. A real time controller provided the access to the machine tool. The workstation and the controller were connected by a real time VME bus. The further development of MOSAIC included the development of a real time operating system, the development of an Advanced Manufacturing Language (AML), and the integration of sensors in a milling implementation (Teltz, 1994).

In order to investigate the advances of an open architecture controller, a few open architecture controller platforms have been built by individual researchers. Considering their strong network communication ability and other features, workstations were still the most

popular computers for non-real-time computation in open architecture controllers. However, due to their low costs and increasing capabilities, personal computers (PCS) have become more attractive to many researchers. NIST (National Institute of Standards and Technology) used a commercial 486 DX2/50 computer in their open architecture shop-floor controller in its EMC (Enhanced Machine Controller) project (Yang, undated). There are several products commercially available for real time computation in command interpretation motion control. PMAC (Programmable Multi-Axis Controller), made by Delta Tau Data Systems, Inc., is one of them. NIST used a PMAC-PC in its shop floor controller. Teltz et al (1994) used a PMAC-VME in their OAC (Open Architecture Controller) hardware platform.

Open Architecture Controller in MTRC

Hardware Platform

In order to investigate the advantages of the open architecture controller and, more importantly, to integrate the advanced dynamic control techniques recently developed in the MTRC, (such as feedforward control, chatter control, and tool breakage detection) into a machine tool, an open architecture controller was built in the MTRC. The hardware platform of the open architecture controller was installed in a White-Sundstrand Series 20 Omini Machining Center. The machine was originally equipped with a Swinc CNC controller featuring a DEC (Digital Equipment Corporation) LSI-11 micro-computer with 31K words of 16 bit solid state RAM. The input data was read from a Remex photoelectric tape reader-spooler. The reading speed was 150 characters per second. In 1990, the machine was retrofitted with a Automation Intelligence FlexMate motion co-processor. The core of

FlexMate motion co-processor was an IBM 7552 industrial computer, featuring an Intel 80286 micro-processor with 10 MHZ clock speed and 512 KB of system memory. Due to the dated technology and the "closed" control architecture of the FlexMate controller, the expansion of its application to accommodate the new technologies developed in the MTRC was very difficult. Therefore, the FlexMate controller was replaced by the open architecture controller built in the MTRC.

The hardware platform of the open architecture controller built in the MTRC consists of three parts: a 486DX 33MHz Personal Computer, a Delta Tau PMAC-PC multi-axis controller, and the peripheral devices.

The reason for selecting a PC to handle non-real-time computation was mainly economical. However, the performance gap between PCS and workstations is becoming smaller due to the rapid development of computer technology. The computation speed and the memory capacity of a PC are already comparable to those in a workstation. With proper setup, a PC can easily connect to a network to handle data exchange. Another reason for selecting a PC is that most data acquisition and analyzing hardware and CAD/CAM software in the MTRC were PC oriented, so the further development of the open architecture controller would be easier if a PC was selected.

A PMAC-PC was selected as the real time motion controller for the open architecture controller in the MTRC after an investigation of the available machine controllers. The main reason for selecting the PMAC-PC was its hardware and software "openness". In addition, its 30 MHZ clock speed can ensure a short servo cycle time and a high block execution rate, allowing the machine tool to have a rapid dynamic response. The PMAC-PC was also

selected due to its flexibility to interface various input and output devices. The major features of PMAC-PC installed in MTRC are listed in Table 4.1.

Table 4.1 Specification of PMAC-PC

CPU	
Type:	Motorola DSP56001
Architecture:	24-bit Fixed Point
Clock:	29.4912 MHZ
MEMORY	
ROM:	128K x 8 EPROM firmware (master control program)
RAM:	348K bytes Static
	Active Memory: 128K x 24-bit words
	User program storage: 252K bytes
RAM Speed:	Zero wait state at 30 MHZ
PERFORMANCE	
Servo Cycle Time:	55 μsec per axis.
	(220 μsec for a three-axis machine with spindle controlled by PMAC)
Block Execution Rate:	Approximately 800 blocks/sec
Velocity Range:	0.0001 to 15,000,000 encoder counts/sec
Position Range:	±32 billion counts with automatic programmable rollover
Position Accuracy:	±1 count on A/B quadrature encoder input
	Sub-count interpolation with 5 additional bits (x32) is possible.
CAPABILITIES	
Position Feedbacks:	8 channels of A/B quadrature encoders
Analog Output (DAC):	8 channels ±10V, 16-bit resolution differential outputs
	300 μvolts/step, optically isolated
Serial Communication:	RS-232/RS-422 serial data port
Parallel Communication:	PC Bus communication

Figure 4.1 shows the block diagram of the PID position servo filter provided by PMAC. In addition to a basic PID filter with its proportional, derivative and integral gains,

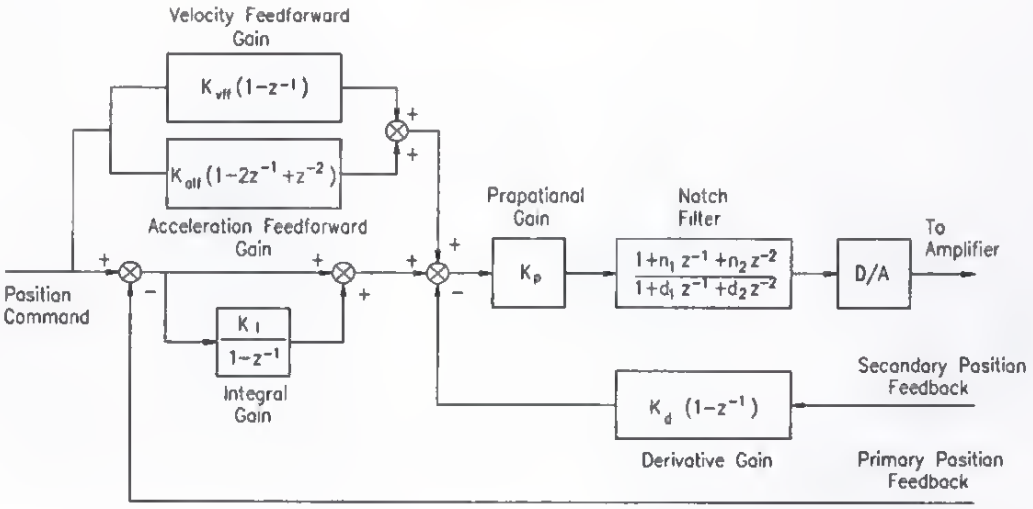

Figure 4.1 PMAC PID servo loop block diagram.

PMAC also provides a velocity and an acceleration feedforward gains in the servo loop. If a plant, a DC motor in most contemporary situations, can be simplified to a second order system, the velocity and acceleration feedforward gain can effectively reduce the position following error introduced by the system damping and the system inertia. For an ideal second order system, the error can be theoretically eliminated by adding the appropriate velocity and acceleration feedforward gain. A notch filter is also inserted in the servo loop. The filter would be most commonly used as an anti-resonance filter. However, by properly setting parameters n_1, n_2, d_1 and d_2, it can be also modified to be other compensation filters.

The PID servo filter in PMAC provides a reasonable efficient approach to control a plant with quasi-second order system characteristics. However, if the higher order components are not negligible in a plant, the simplification of the plant to a second order system might be inaccurate. In those cases, the velocity and acceleration feedforward gains in the PMAC servo filter might not offer effective compensation.

One of the advantages of PMAC controller is that the "openness" is extended to its servo loop closing algorithm. Instead of using the standard servo algorithm provided by PMAC, the users can write their own servo algorithm and implement it in PMAC. It gives the users a tremendous freedom to investigate their plant in detail, and then write an optimum servo algorithm to best compensate their system. A project is currently being conducted in the MTRC on the best feedforward control for high speed machining. The results can be integrated into the open architecture controller.

In addition to the PC bus, PMAC controller provide I/O ports to communicate with peripherals. The major I/O ports used in the MTRC PMAC controller are listed in Table 4.2.

Table 4.2 PMAC I/O Port List (selected)

JMACH	Quadrature encoder inputs, dedicated digital inputs including overtravel limits, home flags and amplifier fault, dedicated digital outputs for amplifier enable, analog DAC outputs.
JOPTO	General purpose digital inputs and outputs.
JTHW	Thumb wheel port for multiplexed or non-multiplexed uses.
JPAN	Control panel port for command inputs, motor or coordinate selector inputs, reset, handwheel inputs, wiper analog inputs, status outputs.

Four encoder input and DAC output channels are assigned to the machine axes. For the X, Y and Z axes, a quadrature rotary encoder with 2500 lines per revolution was installed as position feedback device respectively. The pitches of the ball screws for the axes are all 0.5 inch per revolution. A quadrature rotary encoder with 400 lines is attached to the spindle to improve its performance by running at a closed loop fashion, instead of its original design of open loop control. The assignments are listed in Table 4.3.

Table 4.3 Encoder input and DAC output channel assignment

Encoder input	DAC output	Axis	PMAC Assignment Command
Channel 1	Channel 1	X	&1#1->20000X
Channel 2	Channel 2	Y	&1#2->20000Y
Channel 3	Channel 3	Z	&1#3->20000Z
Channel 4	Channel 4	Spindle	&1#4->0

In Table 4.3, "&1#1->20000X" is a PMAC on-line command. It means that in the first coordinate system, motor #1 is assigned to the X axis, and each position unit in X axis (inch) is equivalent to 20000 encoder counts. Similar assignments are commanded to the Y and Z axes. Special assignment needs to be given to the spindle, as listed in Table 4.3, which will be discussed later in the software design section.

During the development of the open architecture controller, a major modification of the peripherals was made to accommodate the open architecture controller. The control logic circuits, the I/O interface, the operation panel were completely redesigned. Figure 4.2 shows the new main operation panel design.

The push buttons and the switches in the operation panel can be divided into two groups. One group is directly connected to the PMAC through its dedicated control panel port JPAN. Another group is connected to the machine logic control circuits. Some of the push buttons in the second group work together with the PLC programs to be discussed later. Some other push buttons and switches were also installed on the side of the machine for easy operation, including emergency stop, cycle start, spindle release for tool changing, chip

conveyors, and high pressure coolant. The functions of the push buttons and the switches are listed in Table 4.4.

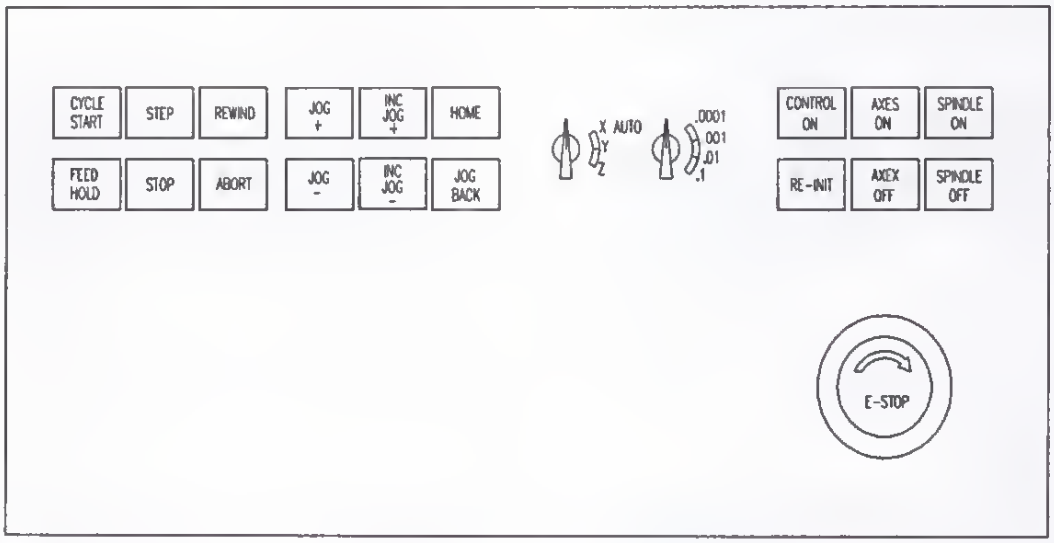

Figure 4.2 Operation Panel of MTRC motion controller.

Table 4.4 Operation panel push buttons and switches

---

(1) Push buttons and switches to PMAC

CYCLE START:

Start to continuously run a motion program from the location of the program counter.

FEED HOLD:

Suspend execution of the motion program immediately by overriding all axis speed to zero. The program can be resumed by pressing "CYCLE START" or "STEP" push button.

STEP:

Start a single-step execution of a motion program form the location of the program counter. It process all lines down to the next move command.

REWIND:

Reset the program counter to zero.

Table 4.4 continued

ABORT:

Abort the currently running program, all axes begin immediately to decelerate to a stop.

JOG+:

Jog an axis (depending on AXES SELECTING SWITCH) in the positive direction as long as the push button is pressed.

JOG-:

Jog an axis (depending on AXES SELECTING SWITCH) in the positive direction as long as the push button is pressed.

HOME:

Start an axis (depending on AXES SELECTING SWITCH) to move to its home position.

JOG BACK:

Jog an axis (depending on AXES SELECTING SWITCH) back to its most recent programmed position.

AXES SELECTING SWITCH:

Select an axis as current. It has three selections: X axis, Y axis and Z axis. The switch must be set at X axis before starting a motion program.

RE-INT:

Reinitialize PMAC controller.

(2) Push buttons and switches to logic control circuit

STOP:

Stop a program at the end of the currently executing move or the next move if that has already been calculated. The program counter is set to the next line, so the program can be resumed by pressing "CYCLE START" or "STEP" push button.

INC JOG+:

Incremental Jog. Jog an axis (depending on AXES SELECTING SWITCH) to a certain distance (depending on INC JOG STEP SELECTING SWITCH) from the current position in the positive direction.

INC JOG-:

Incremental Jog. Jog an axis (depending on AXES SELECTING SWITCH) to a certain distance (depending on INC JOG STEP SELECTING SWITCH) from the current position in the negative direction.

INC JOG STEP SELECTING SWITCH:

Incremental jog distance from the current position. It has four selections: 0.0001 in, 0.001 in, 0.01 in and 0.1 in.

CONTROL ON:

Turn on the power to logic control circuit.

Table 4.4 continued

AXES ON:
Turn on the power to all axes (X,Y and Z).
AXES OFF:
Turn off the power to all axes (X,Y and Z).
SPINDLE ON:
Turn on spindle power.
SPINDLE OFF:
Turn off spindle power.
E-STOP:
Emergency Stop. Power to all axes and spindle are disconnected.
COOLANT ON (machine side)
Turn on the high pressure coolant power.
COOLANT OFF (machine side)
Turn off the high pressure coolant power.
COLLET CLAMP (machine side)
Clamp cutting tool into collet.
COLLET UNCLAMP (machine side)
Unclamp cutting tool from collet.
CHIP CONVEYOR ON / OFF (machine side)
Turn on/off the chip conveyor.

In addition to the logic control circuits, which will be discussed later, some important digital signals are brought to PMAC, either for monitoring or safety protection. Those signals are input to PMAC through its three I/O ports, JMACH, JOPT and JTHW. Table 4.5 lists those signals and their application.

Machine Control Circuits

In order to accommodate the PMAC controller, the machine control circuits of the Sundstrand Milling Machine were redesigned. The complete circuit diagrams are shown in Appendix A and the functions of the major components are listed in Appendix B. Some examples of the control follow.

Table 4.5 Digital input signals to the PMAC

I/O Port	Symbol	Use
JMACH	+LIM1	X axis negative end of travel
	-LIM1	X axis positive end of travel
	+LIM2	Y axis negative end of travel
	-LIM2	Y axis positive end of travel
	+LIM3	Z axis negative end of travel
	-LIM3	Z axis positive end of travel
	HMFL1	X axis home position
	HMFL2	Y axis home position
	HMFL3	Z axis home position
	FAULT1-3	Axes overload
	FAULT4	Spindle overheat
JOPT	MI1	Power On
	MI2	Axes On
	MI3	Spindle On
	MI4	Spindle lubrication
	MI5	Way lubrication
	MI6	Air pressure
	MI7	Axes On
JTHW	DAT6	Control On
	DAT7	High Pressure Coolant On

Machine starting

The control circuit for machine starting is shown in Figure 4.3. To start the machine, the CONTROL ON push button needs to be pressed first. The numerical control emergency stop relay NCES is then energized and maintains the energized status even if the CONTROL ON push button is released afterwards. The CONTROL ON push button and NCES relay function as an "entrance gate" of the entire control circuit. One of the following events will

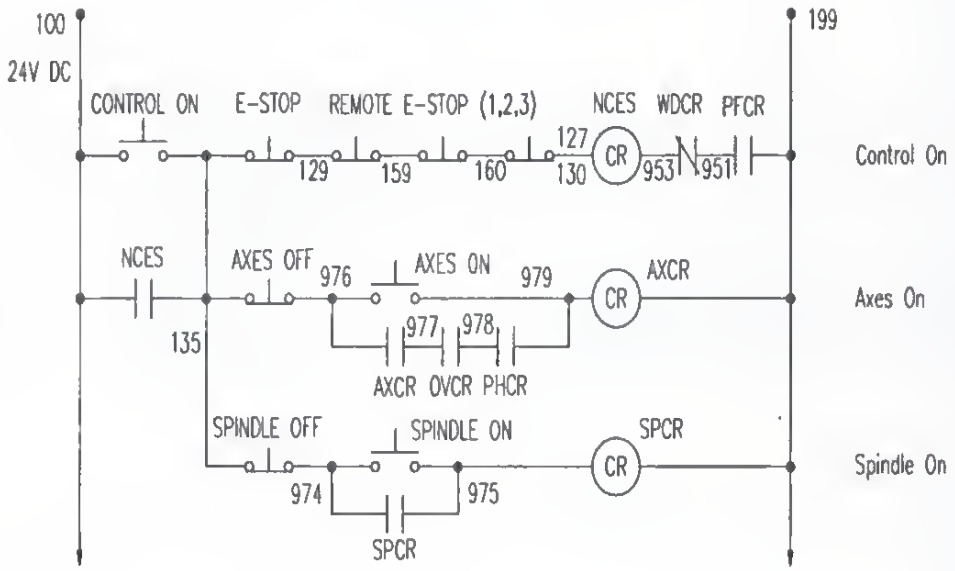

Figure 4.3 Machine starting circuit.

cause the NCES to release and turn off the control circuit to ensure the safety of the machine: the emergency stop push button E-STOP is pressed by the operator, computer power failure occurs (the computer power failure relay PFCR is triggered), or the PMAC is not working properly (the PMAC watch-dog relay WDCR is triggered). Besides the E-STOP push button on the main operation panel, three additional REMOTE E-STOP push buttons are installed in the front and side of the machine tool, so that the operator can easily reach an E-STOP button from most positions around the machine tool. Besides the E-STOP, two other important push buttons for a NC controller, CYCLE START and FEED HOLD (See Figure A.2 in Appendix A), also have additional setups in the front of the machine. After CONTROL ON is pressed and NCES is energized, the operator can press AXES ON and SPINDLE ON to power up the axes and the spindle drives. If a 3-phase power failure or axis

overload occurs, the power to the axes drive will be disconnected. The axes power and the spindle power can be disconnected individually by pressing AXES OFF and SPINDLE OFF, or together by pressing E-STOP.

High pressure coolant

The circuit for controlling the high pressure coolant pump is shown in Figure 4.4. The coolant can be controlled either manually or automatically depending on the high pressure coolant mode switch HP COOL MODE. In the manual mode, the coolant pump is turned on or off by HP COOL ON and HP COOL OFF push buttons installed on both sides of the machine. In the automatic mode, the coolant pump is controlled by a solid state relay O3SSR, which is in turn controlled by NC program commands. The circuit will be disconnected if the secondary control circuit relay MCR is released, which is synchronized with the NCES relay.

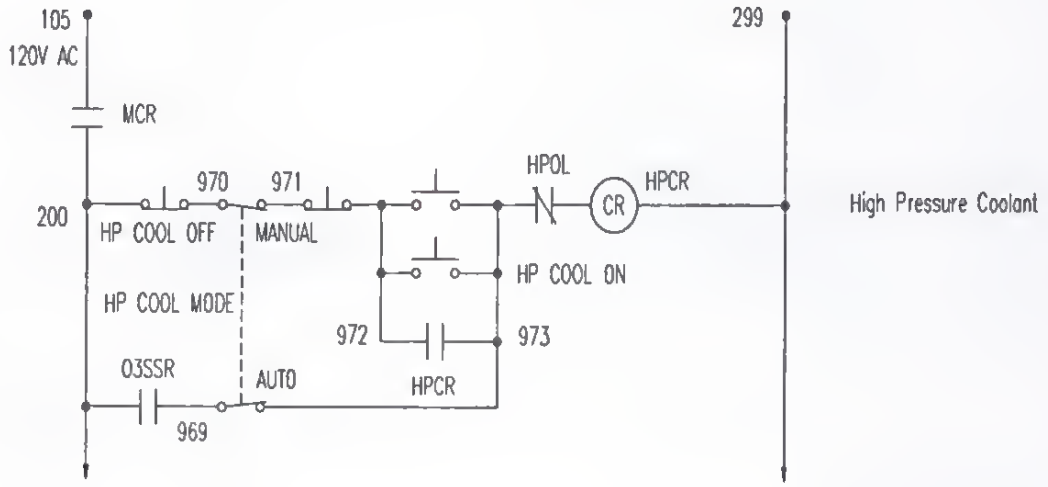

Figure 4.4 Circuit for controlling high pressure coolant pump.

Tool change

Figure 4.5 shows the circuit for controlling the pneumatic tool changing mechanism on the spindle. If the collet clamping switch 6SS is turned to CLAMP position, the collet clamp relay CLCR is energized and the tool changing mechanism clamps the tool holder so that the spindle is ready to rotate. If 6SS is switched to UNCLAMP position, the collet unclamp relay UCCR is energized and stays energized until the tool changing is completed and 6SS is switched back to CLAMP again. It is ensured by a pair of normally closed contacts from spindle-on relay SPCR that no tool changing is allowed when spindle is running. On the other hand, while tool changing is in process, the spindle is unable to start, since the spindle start relay 4CR is disconnected by the normally closed contacts of UCCR.

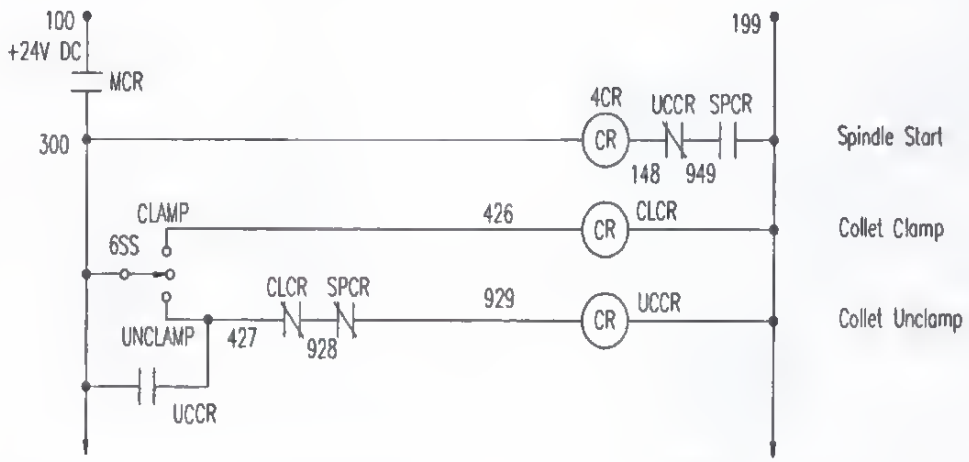

Figure 4.5 Circuit for tool changing.

PLC Programs

Due to its advantages in the areas of capability, accessibility, flexibility and modifiability, software PLC (Programmable Logic Control) has become more popular in CNC

machine tool controllers than the traditional hardware PLC. Software PLC is a special type of computer program which continuously scans through its inputs, and controls the outputs as a hardware PLC does. Unlike the motion control program in the CNC controller, the PLC program operates asynchronously to the motion sequences. The openness of the PMAC controller offers the possibility for user-written PLC programs. Appendix C lists five PLC programs written for the Sundstrand Milling Machine. Cooperating with hardware, the PLC programs perform various functions for machine operation and machine safety. The following are examples of PLC programs used on the White-Sundstrand Milling Machine.

Incremental jogging

Incremental jogging is a convenient function to jog an axis to a certain distance from its current position. However, this function is not furnished in the PMAC function library. In order to implement the incremental jogging function in the controller, a PLC program (PLC4) was written as listed in Appendix C.1. PLC4 is a typical software logic control program which performs the same function usually done by hardware PLC. The program continuously checks the status of the INC JOG+ and INC JOG- push buttons. Whenever one of the push buttons is pressed, the program check the current status of AXES SELECTING and STEP SELECTING switches. Based on the status of the input push buttons and selecting switches, the program issues a corresponding command to jog a certain axis a certain distance in the selected direction. Depending upon the hand operation of individual operators and the mechanical property of push buttons, the input signal from a push button is often not so "clean" due to the contact bounce. According to Bollinger and Duffie (1988), "contact bounce is the rapid, repeated opening and closing of switch contacts while the switch

position is changing". In order to ensure that each time when the operator presses an incremental jogging push button, the corresponding axis only moves one step, a "software debouncing" routine is included in the PLC program. Whenever an incremental jogging push button, INC JOG+ or INC JOG-, is pressed, the first "rising edge" of the input signal is accepted and the corresponding axis is commanded to move one step. When the operator releases the push button or the push button bounces itself, the first "falling edge" triggers a timer. In a certain time period set by the timer, the program ignores all following input signals from the contact bounce of the push button. The program will be allowed to accept another input signal only after the timer runs off. The timer was experimentally set to 0.9 second, so that the signal is well conditioned but the repeated jogging was not sluggish. The program also ensures one step motion when the push button is continuously pressed or even when the push button is stuck in its ON status due to mechanical failure.

Timer and counter

The PLC program PLC5 listed in Appendix C.2 contains three software timers to control the periodical pumping of the lubrication oil to the guide ways and ball screws on the machine. The three timers are: pumping timer, releasing timer and pause interval timer. The time span of the software timers can be easily adjusted by setting the corresponding time constant. In the current setup, the lubrication piston pump operates ten times in every five minutes. PLC6 in Appendix C.3 is a software counter to calculate the spindle speed by counting the encoder counts in each second for the display in the user interface.

Hot keys

PLC7 and PLC8 in Appendices C.4 and C.5 create two useful "hot keys" in the control panel, REWIND and STOP. REWIND key rewinds a program back to the beginning after running it. It saves the efforts to reload the same program again when a repeated operation is conducted. STOP key stops a program at the end of the current motion command. It can be used as a non-emergency stop to temporarily interrupt a program at the end of a motion, instead of halfway through the motion if the PMAC function key "FEED HOLD" or "ABORT" is used. The program can be resumed by "CYCLE START" or "STEP" from the next motion command.

Initial loop closing

PLC9 in Appendix C.6 is used to close the servo loop of each axis whenever AXES ON is pressed. It is a safety procedure to prevent the possible drifting of the axes in open loop status.

User Interface

In order to provide a user friendly operating system and a flexible software platform for further development of the open architecture controller, a DOS-driven user interface program was developed. The user interface uses PC bus and interrupt-based communication to conduct the data exchange between the host computer and PMAC controller. The flow chart of the user interface is shown in Figure 4.6. A "Tree" structure is used in the program. The program branches to various functions by function keys and then returns back to the "root" after completing the selected function. The "branches" are independent of each other. Modifying functions or adding new features in the future can be accomplished without

changing the program structure and unrelated functions. The user interface was written in the C language. Borland Graphic Library was used to build the display screen. The source code is about 3500 lines and the executable file takes about 110 KB memory space.

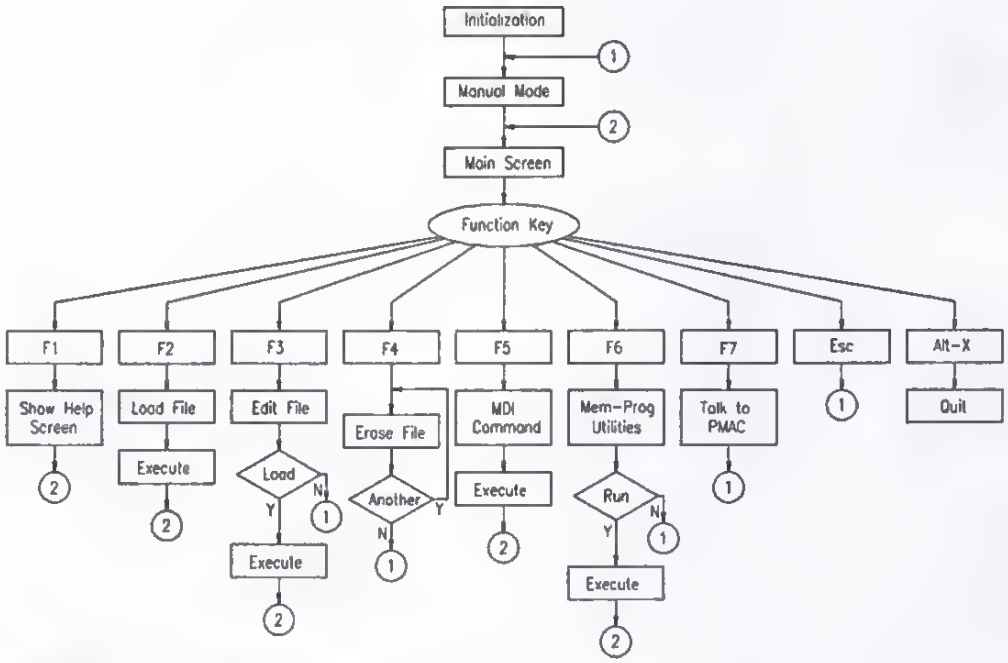

Figure 4.6 Flow chart of the user interface.

Display and operating system

The main display screen is shown in Figure 4.7. It consists of three sub-windows: position window, monitor window and program window. The position window displays the actual current position of X, Y and Z axis and the rotational speed of the spindle, the monitor window indicates the current machine status, and the program window shows the current motion program in the buffer. The function keys used in the operation are listed on the bottom of the display screen. The function keys and their specifications are listed in Table 4.6.

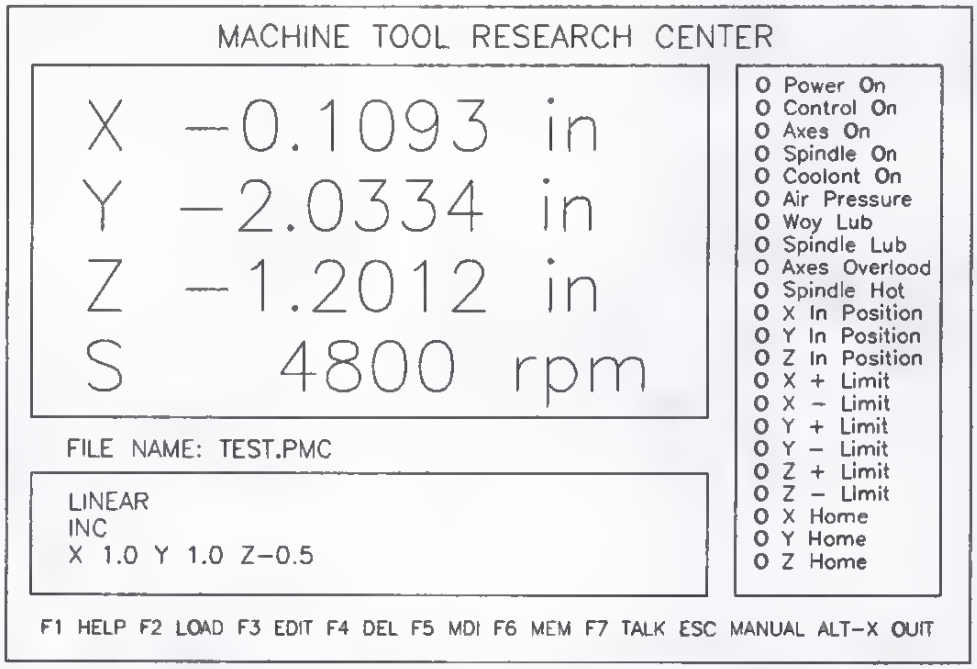

Figure 4.7 DISPLAY SCREEN OF THE USER INTERFACE.

Table 4.6 Function keys in user interface

Key	Use	Description
F1	HELP	Show help screen for the usage of the function keys
F2	LOAD	Load a motion program from a file
F3	EDIT	Edit a motion program from a file and then load it optionally.
F4	DEL	Delete a motion program file
F5	MDI	Manual Data Input
F6	MEM	PMAC memory program service
F7	TALK	Direct communication with PMAC
ESC	MANUAL	Manual mode
Alt-X	QUIT	Quit to DOS

The use of the keyboard is limited to switching the operation mode and manipulating the motion program files. After a motion program is downloaded into the controller,

"keyboard free" operation is realized, so that the operator can concentrate on the cutting process, since all the commands to the machine tool are issued from the operation panel.

Four operation modes are designed in the user interface: manual mode, program mode, MDI mode, and communication mode. The current operating mode is shown above the program window.

Manual mode. The user interface starts at the manual mode, which allows the operator to home or jog the axes through operation panel. After working on the other modes, pressing the ESC key will cause the user interface to return back to the manual mode.

Program mode. The program mode, or automatic mode, is turned on by pressing either F2, F3 or F6 key. If the F2 key is pressed, a list of the motion program files stored in a pre-assigned sub-directory in the disk drive are shown on the screen, the operator can select a motion program and load it into the controller from the list. When the program is ready, the file name will be displayed on the screen, and the operator can execute it from the operation panel by pressing "CYCLE START" or "STEP". The F3 key gives the operator a chance to modify the motion program before loading it into the controller. The F4 key is used to delete a motion program file from the source drive.

In addition to loading the program from the disk drive, programs stored in PMAC memory can also be loaded into the controller. More discussion about the two kinds of motion programs will be included later in the "File management" section. To make the operation on a PMAC memory program more convenient, a sub-menu called "Memory Program Utility Menu" was designed as shown in Figure 4.8.

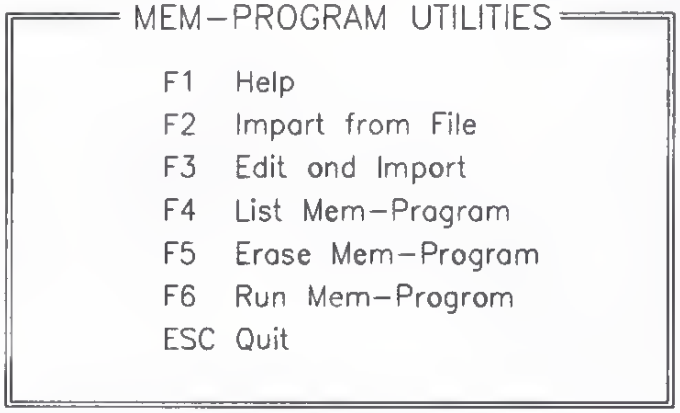

Figure 4.8 Memory program utility menu.

After the memory program utility is selected (F6 key in main screen), the utility menu is displayed on the screen. The operator can then use function keys to prepare a memory program, such as import the memory program from a file on disk drive (F2 key), or edit the file before import (F3 key), list a memory file (F4 key), or erase a memory file (F5 key). If the operator choose "Run Mem-Program" (F6 key) in the menu, the selected memory program will become current and ready to operate through the operating panel. There is also a help screen (F1 key) to help the operator understand the functions. ESC key will cause the user interface to switch back to the manual mode.

MDI mode. MDI (Manual Data Input) is a special operation mode on the machine controller. It allows the operator to command the machine by directly writing instructions into the controller memory, instead of downloading a pre-documented motion program. Unfortunately, the PMAC controller does not have this feature built in. A software version of this feature is implemented in the user interface. The software structure of the approach will be discussed later in the "File management" section. To work in MDI mode, the operator

only needs to press the F5 key to enter the MDI mode, then type in the instruction directly in the program window and execute it on the operation panel.

Communication mode. The user interface also provides an opportunity for researchers to directly communicate with the PMAC controller. By pressing F7 (TALK), a scratch board is shown on the screen, the researchers can type in any on-line command recognized by PMAC to obtain the information about the controller setup or perform some special operation. The user interface will return back to manual mode whenever ESC is pressed. It should be noted that in the communication mode, the controller is wide "open" to the user, an improper on-line command may change the setup of the controller and cause malfunction. Therefore the communication mode is not recommended for general operation.

Motion program management

Rotary buffer. In modern die and mold manufacturing, the part programs are usually generated by commercial CAD/CAM software. Due to the complexity of the geometry of the dies and molds, the part programs are often unavoidably lengthy. However, the memory space of a NC controller is usually limited. Particularly in PMAC, the user program storage is only 252K bytes. If expressed by sub-blocks, it has only 42k sub-blocks (a simple command like 'X1.0 Y1.0' takes two sub-blocks). Therefore, most times it is impossible to load a complete part program into the NC controller at one time. A common method is to decompose a part program into several shorter sub-programs, and then to load and run the sub-programs one after another. The drawbacks of this method are obvious. A more advanced method is to use rotary buffer. With this method, the controller reads the motion command from the rotary buffer and executes it. When the number of command lines in the

rotary buffer is less than a pre-defined value, new command lines will be downloaded from the motion program stored in the disk drive. Real-time program downloading is performed by interrupt requests while executing the motion commands. Besides the buffer size, two control parameters in the rotary buffer, Buffer Request On and Buffer Request Off, are important. Those two parameters control when the rotary buffer should start and stop reading the command lines from the motion program file. As shown in Figure 4.9, if the number of command lines behind the executing point in the rotary buffer is less than *m*, which is determined by Buffer Request On, the controller will request the loading of more command lines from the motion program file. The command loading will continue until it reaches a point where the number of command lines behind the executing point is larger than *n*, which is determined by Buffer Request Off. Therefore, the number of command lines contained in the rotary butter is always between *m* and *n*, except at the end of the program, where the number is less than *m*.

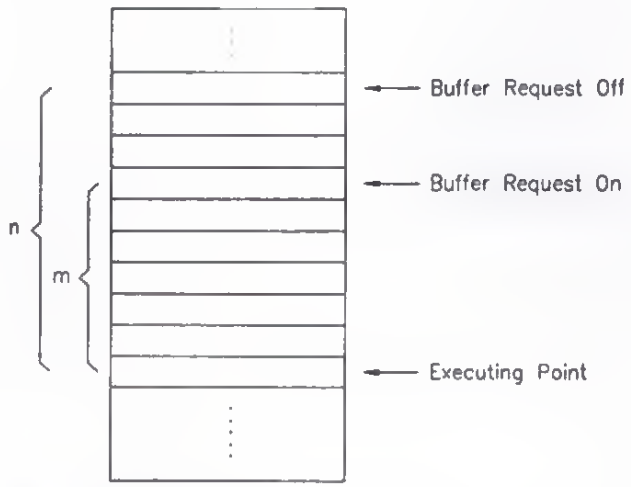

Figure 4.9 Rotary butter structure.

Program Filter. PMAC has its own motion program language. The unique language has both high level and low level computer language commands. The high level commands feature logical constructions such as while-loops, if-else-branches, and subroutines. They also include trigonometric, logarithmic and exponential functions. The language allows other motion programs to be called inside a program. At the low level, the PMAC contains basic direct motion commands such as linear and circular motion, feed rate specification, incremental and absolute motion modes, and cutter radius compensation. The combination of both high and low level languages provides PMAC programers with a useful toolbox which makes NC programming easier and more flexible. However, the PMAC language has not been recognized nor featured in commercial NC programming software packages at this time. In order to make the controller compatible with other NC program languages, a "program filter" is designed in the user interface. Before a NC program is loaded into the rotary buffer, it is checked line by line. If the program is not written with the PMAC language, the command lines are interpreted into PMAC language first. The "filtered" program is saved in another file. After all the command lines are the checked and interpreted if necessary, the rotary buffer starts to load and execute the commands from the "filtered" program file instead of the original file. By this method, incompatibilities are corrected before the program is loaded into the PMAC, so the execution of the program is smooth and continuous. In the current version, the "filter" only features the interpretation tools for the standard "G-Code" (RS-274). The interpretation for other NC programming languages could be easily realized by modifying the "filter". However, the real purpose of using a "program filter" is not only for the language interpretations. More advanced features can be implemented in the future,

such as constant cutting velocity in ball end milling of sculptured surface, in which the variation of the spindle speed depends on the sculpture radius.

Memory program. As mentioned above in "Program filter", PMAC has its own programming language. A few commands in PMAC language can only be used in a motion program stored in PMAC memory. Those are mainly logical commands such as while-loop and if-branch. In order to provide a complete access to all PMAC commands, a group of utility functions are written for the user to work on the memory programs. The user can import, edit, and run a memory program by using function keys. When a program is imported into the PMAC memory, a program number needs to be assigned to the program, since PMAC can only recognize program numbers in its memory programs. When the user runs a memory program, the program number needs to be called instead of a program file name.

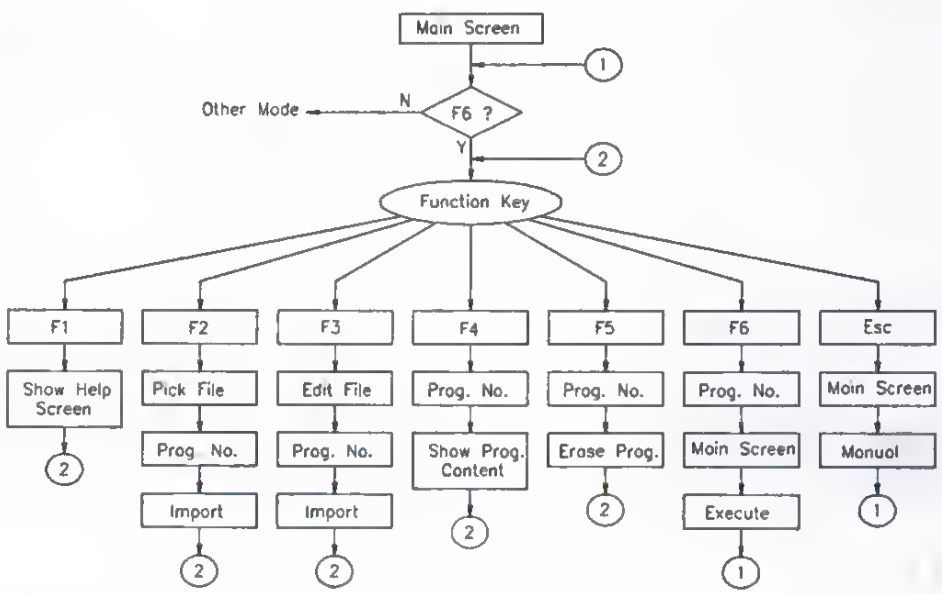

Figure 4.10 Flow chart of the memory program utilities.

The flow chart of the utility is shown in Figure 4.10. Similar to the main program, the utility is also "tree-structured". The utility functions branch from and return back to the "root".

Program rewind. In some circumstance, the operator needs to repeatedly run the same program. However, PMAC does not have the feature to restart a program from its beginning. Therefore, a rewind utility is implemented in the user interface. In fact, rewinding a program is a combined effort from the hardware, the user interface and the PMAC PLC program. The rewinding command is issued by the "Rewind" push button on the operation panel. When a rewinding signal is received by the user interface, it reinitializes the rotary buffer and rewinds the program, while PLC moves the buffer pointer to the beginning. The flow chart of the program rewinding is shown in Figure 4.11. In the memory program mode, rewinding is relatively simple. The user interface only needs to quit the current program and call the same program number again, while the PLC program moves the pointer back to the beginning.

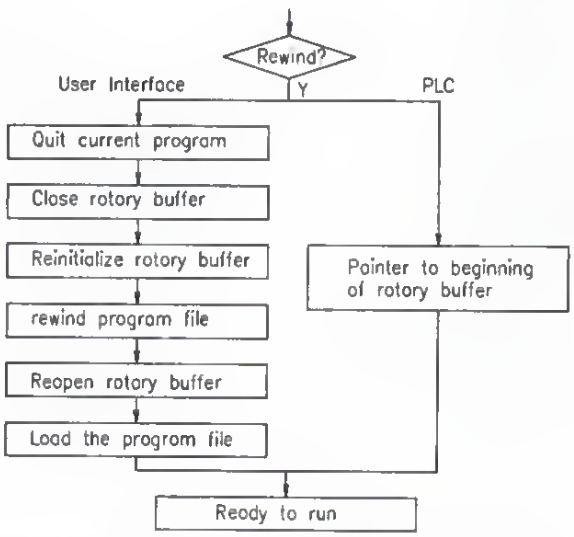

Figure 4.11 Program rewinding in rotary buffer.

MDI. Manual Data Input (MDI) is a special operation mode to command the machine by directly writing an instruction into the controller memory. This feature is particularly useful in laboratory testings. MDI in this controller is implemented in the user interface due to the lack of a MDI feature in the PMAC. The flow chart of the MDI mode is shown in Figure 4.12. The F5 key is used here to toggle the MDI Mode. When MDI mode is turned on, the user can type in a command line, which will be echoed on the program window on the main screen. When the command line is completed with the Enter Key, the command will be sent to a specified program file. The file with a single line command is then loaded into the rotary buffer and ready to be executed. After the command is executed by pressing "CYCLE START" or "STEP" key in the operation panel, MDI mode is turned off, and the program returns back to the manual mode and is ready to receive further commands, which could be another MDI command if F5 is pressed again. Strictly speaking, this software implementation is not a real MDI, since in fact the command line is temporarily stored in a pre-defined file and then being loaded, instead of directly writing into the controller memory. However, difference will not be noticed by the operator.

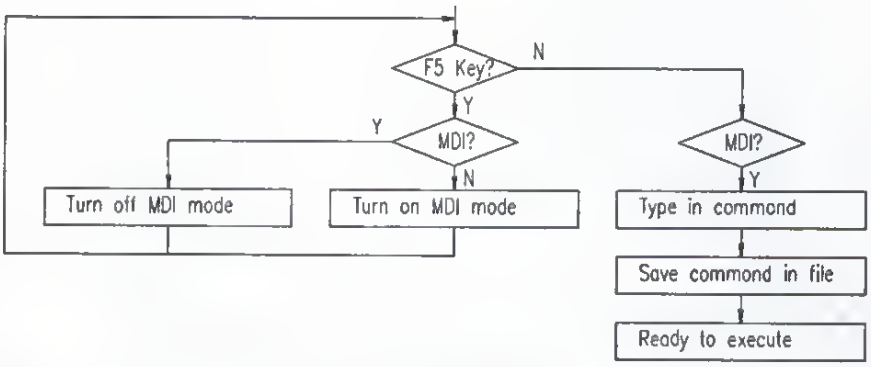

Figure 4.12 MDI mode flow chart.

After the open architecture controller was implemented in the White-Sundstrand Milling Machine, a large portion of the cutting experiments for the hardened die and mold machining has been completed on this machine. In addition, several other machining tasks and research projects have been conducted on this machine, such as the machining of parts for MTRC five-axis machine and the laser ball bar measurements. The performance of the controller and the user interface has been satisfactory.

CHAPTER FIVE
PRACTICE OF HIGH PRESSURE COOLANT

Function of Cutting Fluids

The functions of cutting fluids have been discussed in the literature (Dieter, 1976; Schey, 1987; Kalpakjian, 1992). It is generally accepted that cutting fluids can:

1. Cool the cutting area.
2. Lubricate the interface between the tool and the workpiece.
3. Flush chips.
4. Protect the workpiece surface from corrosion.

As one of the fundamental functions, cutting fluids are extensively used to reduce the heat generated in the cutting process to increase the tool life. Merchant (1950a) gave a mathematical expression between the temperature and the tool life of the form

$$T\,\theta_i^n = C \tag{5.1}$$

where T is the tool life, θ_i is the temperature at tool-chip interface, C and n are constants depending on the materials of the tool and the workpiece. Based on the research by Merchant, about 25% of the heat generated from the metal cutting process is estimated to be from friction between the cutting tool and the chip, which also contributes to the inefficience in metal cutting.

Another major function of cutting fluids is to work as lubricants to reduce the friction at the tool-chip interface. It was shown by Merchant (1950b) that a 10% of the reduction of the friction coefficient by using proper cutting fluids will not only result in an 8.2% drop in the heat evolved from the chip friction, but also will cause a 5.5% drop in the heat evolved from the deformation of the metal in the shear zone. Merchant (1950b) indicated that cutting fluids do not work well as a lubricant to reduce the friction at the tool-chip interface. During the cutting process, the chip always closely follows the surface of the tool, and the contact between the chip and the tool is in the form of a great number of small bridges. Cutting fluids can only gain access to the tool-chip interface by capillarity action. It has been also proved that due to the extremely high pressure and high temperature at the tool-chip interface, a continuous hydrodynamic load-supporting film cannot exist to separate the tool and the chip (Bisshopp et al, 1950). Experimental evidence has shown that the lubrication at the tool-chip interface is realized by chemical reaction between cutting fluids and the newly formed chip surface under the high pressure and high temperature at the interface, which has been known as "mechanical activation" (Shaw, 1948). Merchant (1950a) has also confirmed that a solid material with low shear resistance is formed by the chemical reaction between the tool and the chip material to prevent metal-to-metal contact. As sliding occurs, only the shear strength of this solid material needs to be overcome rather than the bridges formed by the tool and chip material. The effect of lubrication by cutting fluids depends highly on the cutting conditions. Effectively at low cutting speed, the reduction of friction attenuates with increasing cutting speed. Merchant (1950b) pointed out that the lubrication ability of cutting fluids declines toward zero after 30 meters per minute. The reason is that with high cutting speed, the

contact time for any element on the chip with the tool surface is too short to permit penetration of the cutting fluid as well as the following chemical reaction.

The cutting temperature increases with increased cutting speed. The cutting fluid plays a more important role as a coolant rather than a lubricant at high cutting speeds, such as in most turning or milling operations. Often a cutting fluid is simply called a coolant in metal machining, especially for water-based cutting fluids.

Although it is generally accepted that applying cutting fluids may increase tool life, positive results are not always guaranteed for intermittent cutting operations, such as milling. Kalpakjian (1992) pointed out that cutting fluids would lead to the thermal crack on the cutting teeth due to the extended temperature amplitude range. On the other hand, cutting fluids might cause curlier chips, which in turn causes the concentrating of the stress and heat on the tip of the cutting edge so that the tool life is reduced. Koenig et al (1990) reported the reduced tool life both on carbide and CBN tools when cutting fluids were applied in milling operations.

High Pressure Coolant

The traditional and still the most common method of applying coolant is "flooding". With a low pressure and a considerable flow rate, the coolant "floods" over the entire cutting area. Mainly due to the difficulty for the coolant to reach the tool-chip and tool-workpiece interfaces, the cooling and lubricating efficiency may be poor in some operations. Many attempts have been made to improve the effectiveness of cutting fluids in metal machining. One of the successful attempts in this area is the high pressure jet coolant system. Its main

idea is to point a high pressure coolant stream directly to the cutting edge of the tool. Pigott and Colwell (1952) built such a system called "Hi-Jet" on a lathe, and directed the coolant stream to the clearance edge of the tool. Using mineral oil as cutting fluid with a pressure up to 2.8 MPa, the tool life could be extended to more than 10 times than that with normal flood cooling. Similar experiments were conducted by Nagpal and Sharma (1973). They used four different cutting fluids in a "Hi-Jet" system with a pressure up to 3.4 MPa. They found that when "Hi-Jet" was applied, the tool-chip interface temperature dropped to half of that with normal flood cooling. Instead of leading the coolant to the clearance edge, some researchers also tried to direct the cutting fluid to the rake edge. Since it is extremely difficult to lead the coolant reaching the tool-chip interface, some researchers were using specially modified hollowed tools to lead the coolant to the interface. Sharma et al (1971) used tools with a hole of 0.25 mm diameter on the rake face, and injected high pressure coolant (69 MPa) directly to the tool-chip interface. It was found that the tool-chip friction dropped to 40 percent of that with dry cutting. Similar experiments were conducted by Wertheim et al (1992) on grooving tools with lower pressure at 2.7 MPa. Tool life is increased to 4 times of that with flood cooling. Some researchers also tried to use regular cutting tools and feed a high pressure coolant stream along the rake face. Such a system was built and tested by Mazurkiewicz et al (1989). In order to penetrate to the tool-chip interface, an ultra high pressure of up to 280 MPa was applied on the coolant jet. The friction coefficient was reduced to 40 to 50 percent of that with dry cutting or regular cooling method. Figure 5.1 summarizes the approaches made by above mentioned researchers.

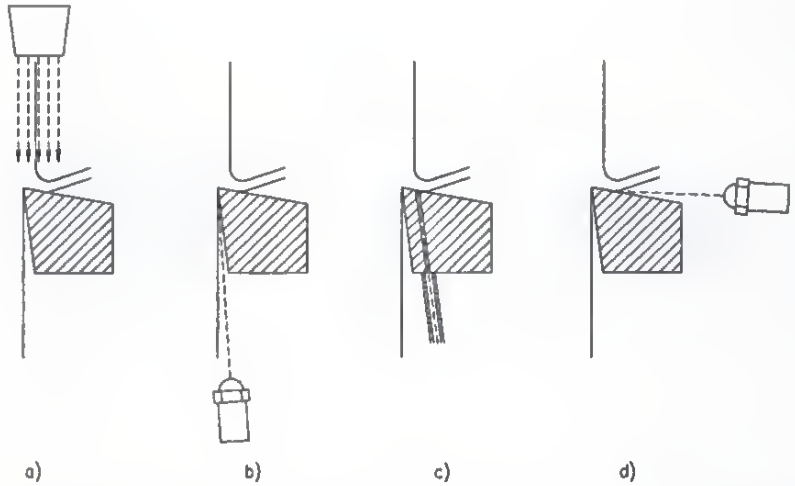

Figure 5.1 a) Flood coolant; b) High pressure coolant jet by Pigott and by Nagpal; c) By Sharma and by Wertheim; d) By Mazurkiewicz.

The key point for the high pressure coolant jet system is that the coolant stream must be precisely directed to the cutting edge by the nozzle or through the internal channel in the cutting tool. The need for the precise direction may explain the reason that the above mentioned experiments were exclusively conducted on lathes for turning procedures.

Recently Kovacevic et al (1995) applied the high pressure coolant jet technique to face milling. The up to 380 MPa high pressure coolant was guided into a specially made face milling cutter through a rotary swivel with a maximum speed of 2000 rpm. The high pressure coolant was directed to sapphire orifices behind each cutting insert in the cutter. A through hole of up to 0.45 mm diameter was drilled by EDM on the inserts. The travel speed of the coolant could reach 300 m/sec. Decreased cutting force and reduced flank wear on the cutting inserts were observed. Due to the less tool wear, the surface finish was also improved.

Mitsui Seiki (1992) introduced a commercial high pressure coolant system on milling machines. The coolant was sprayed on to the cutting area externally, rather than guided into the tool cutting edge through internal channels. The difference from the regular flood coolant is its relatively high pressure (up to 6.9 MPa) and high flow rate (60 L/min). The advantage of the system is that no special cutting tools are required. Good results were obtained with commercial solid carbide tools.

Experimental Setup

In order to investigate the influence of high pressure coolant on the machining of hardened die and mold steel, an experimental setup was built at the Machine Tool Research Center (MTRC). Figure 5.2 shows the hydraulic circuit diagram of the setup. The coolant is supplied from tank T through filter F by pump P, which is driven by motor M. The coolant jets out through the nozzles N. To ensure the system working properly, a pressure regulating valve R, a bypassing valve B, and a pressure gage G were installed in the system to insure proper performance.

The pump used in the experiments was an industrial diaphragm pump from Wanner Engineering, Inc. The model H25XFCNHFEC pump delivers 54.5 L/min (14.4 gpm) at 700 rpm rotational speed and 6.9 MPa (1000 psi) pressure. A 7.36 Kw (10 HP) 3-phase AC motor was used to drive the pump.

Two zero-degree spray angle nozzles with 28.4 L/min (7.5 gpm) capacity at 6.9 MPa (1000 psi) were used in the coolant system. With adjustable joints, the nozzles were able to be pointed to the tool tip for various cutting tools. Unlike most spray nozzles, the model

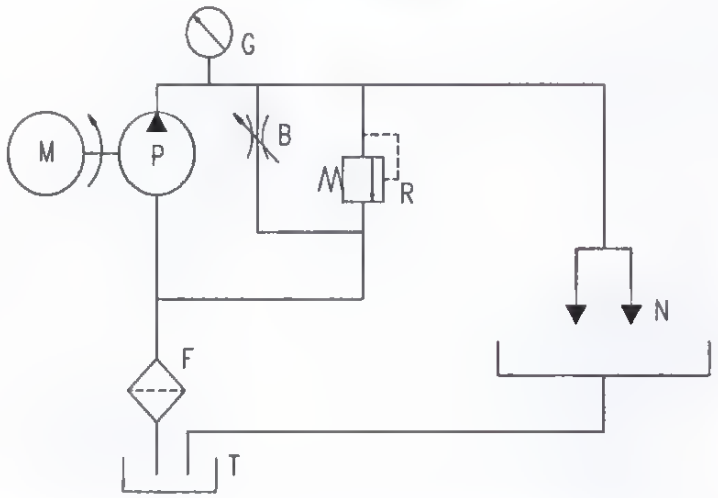

Figure 5.2 Circuit diagram of the high pressure coolant system.

1/4MEG-0015 nozzles, made by Spraying Systems, Co., feature an internal guide vane to stabilizes liquid turbulence to provide maximum spray stream integrity and impact. With zero spray angle, the flow speed at the nozzle outlet V_{fl} can be calculated from the flow rate passing through the nozzle Q_{fl} and the nozzle orifice area A_{or} if it is assumed that there is no flow contraction through the nozzle

$$V_{fl} = \frac{Q_{fl}}{A_{or}} \tag{5.2}$$

Assuming the maximum flow is evenly distributed into two nozzles, then Q_{fl} is 27.3 L/min (7.2 gpm) for each nozzle. The nozzle orifice area A_{or} was calculated from the nozzle orifice diameter, which was measured as 2.25 mm (0.0895 in). The flow speed at the nozzle outlet then can be calculated as 114 m/sec (375 feet per second or 256 mph).

The blast force of the stream from each nozzle F_{fl} can be obtained from

$$F_{fl} = \rho_{fl} Q_{fl} V_{fl} \quad \textbf{(5.3)}$$

where ρ_{fl} is the density of the cutting fluid. Since the cutting fluid is a weak solution of the concentrated coolant fluid in water, ρ_{fl} can be approximated to be the density of water. With above obtained Q_{fl} and V_{fl}, the force can be calculated to be 52 N (11.7 lb_f) from each nozzle.

The coolant used in the experiments was Mistic Mist Concentrate made by Aetna MFG Co. It is a synthetic fluid which contains no hazardous ingredients per OSHA's hazard communication rule. Rust inhibitors are present to protect the workpiece and the machine tool. Biocide additives are also included to prevent bacteria and odor. In these experiments, it was diluted with tap water at a ratio of 1:30.

The high pressure coolant system was installed on a Series 20 Omnimil Machining Center. The machine tool was modified to machine workpieces with large dimensions. The table was enlarged from 432 x 432 mm (17 x 17 in) to 762 x 1524 mm (30 x 60 in). The table longitudinal stroke (X axis) was extended from 610 mm (24 in) to 1220 mm (48 in). The spindle head vertical stroke (Y axis) was extended from 508 mm (20 in) to 635 mm (25 in). An enclosure was designed and installed on the machine tool to accommodate the application of the high pressure coolant.

Experiments with High Pressure Coolant

Preliminary cutting tests were conducted with the installed high pressure coolant system. The cutting tool is a Kennametal KIPR075RP25 end mill. The nominal diameter is

19.05 mm (0.75 in). Two carbide circular inserts RPGB2515 with KC850 coating of diameter of 7.94 mm (5/16 in) are installed on the tool. Figure 5.3 shows the tool dimensions.

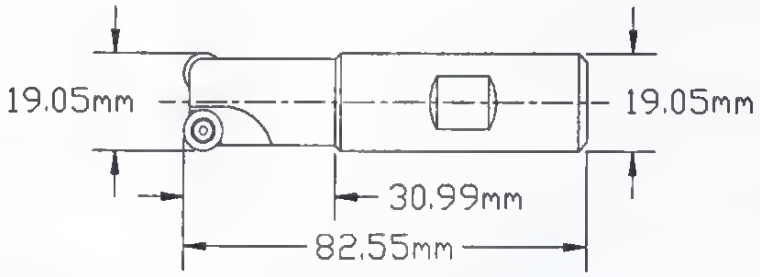

Figure 5.3 Cutting tool used in the experiments with coolant.

Three cutting conditions were compared: cutting with high pressure coolant (HP), cutting with regular flood coolant (FL) and dry cutting (DY). The flood coolant was delivered by a 23HI sump pump made by Little Giant Pump Company with 6.4 L/min (1.7 gpm) flow rate. The flow rate was sufficient to cover the entire cutting area. The workpiece material was H13 steel pre-hardened to HRC 47-49. For plane cutting, the removed layer thickness varied from 0.25 mm to 1 mm (0.010 in to 0.040 in). The radial feed was 0.5 mm (0.020 in). The spindle speed was 5000 rpm. The feed rate was 1.27 m/min (50 in/min). The feed per tooth was 0.127 mm (0.005 in). Cutting force were measured during the cutting process with a KISLER 9067 Dynamometer. For each cutting condition (HP, FL and DY), a group of new inserts were installed. After the same cutting length was completed, the tool wear was measured under a Titan Zoomatic TM-II measuring microscope.

The cutting forces for the normal direction and the axial direction for the three conditions are shown in Figures 5.4 and 5.5.

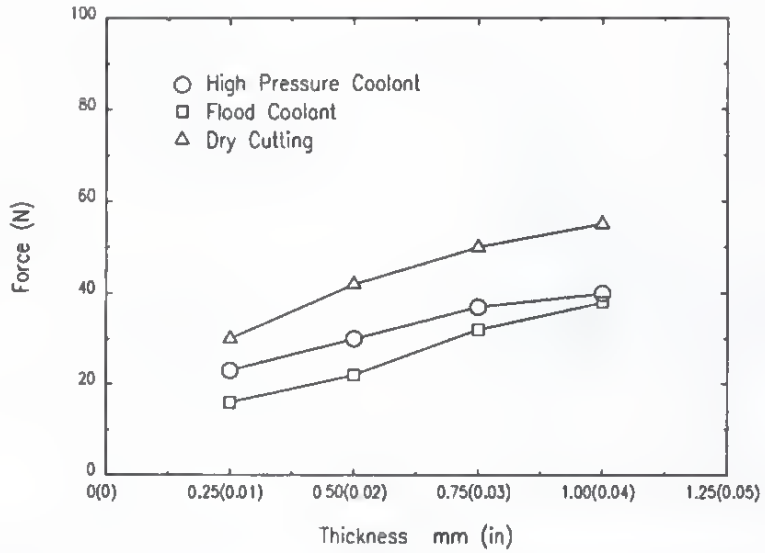

Figure 5.5 The normal cutting force with coolant. (5000 rpm, 50 ipm, carbide inserts, H13 steel).

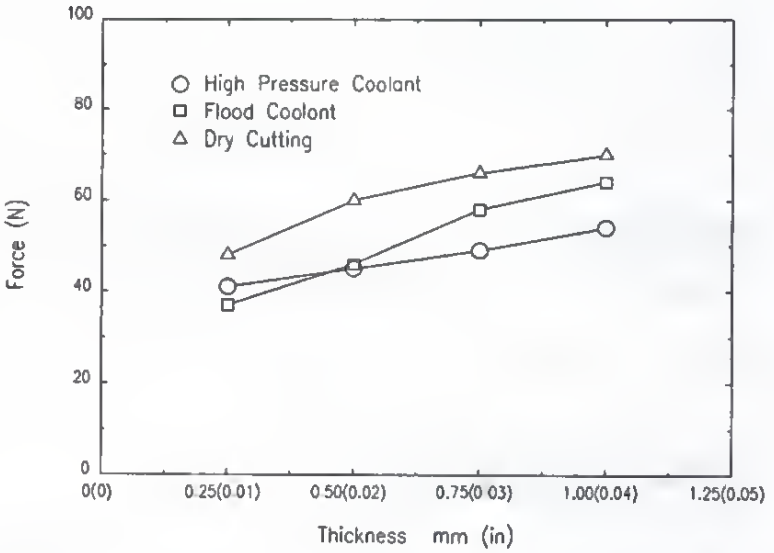

Figure 5.4 The axial cutting force with coolant. (5000 rpm, 50 ipm, carbide inserts, H13 steel).

It can be seen that the cutting forces on both directions decreased when coolant was applied, either high pressure coolant or flood coolant. Although the difference of the cutting force

between the high pressure and the flood coolant was not significant in the experimental cutting range, the force increasing rate with the high pressure coolant was lower than that with flood coolant. The reason may be the higher cooling efficiency of the high pressure coolant. Due to the mechanical strength limit of the insert, the removed layer thickness was less than 1 mm (0.040 in). Figures 5.4 and 5.5 indicate that for a larger depth of cut or higher metal removal rate, the cutting force for the flood coolant can go higher.

A problem with the application of coolant in the hardened steel machining was the chipping on the tool cutting edge. Figure 5.6 shows the tool wear measured on the flank face in three conditions (HP, FL and DY) after same cutting length. The observation under the microscope showed that tool wear with coolant applied was mainly due to the chipping instead of being "worn" by the friction. Chipping became more visible in ball end milling

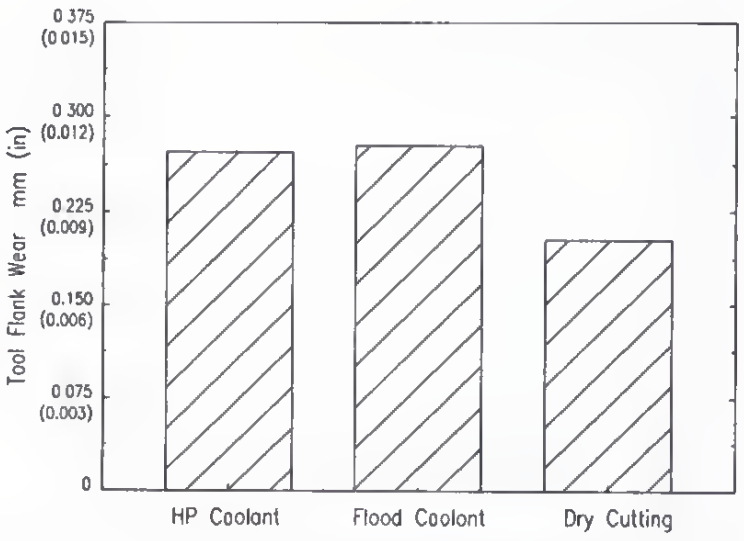

Figure 5.6 Tool wear in cutting with coolant. (5000 rpm, 50 ipm, 18.75 mm bull nose end mill, carbide inserts, H13 steel).

where the cutting speed was low at the tip of the ball nose cutter. Figure 5.7 shows the tool wear in a slotting cutting test with the ball end mill. The milling cutter used was a Valenite 50K1R10W3 ball end mill with V1N coated carbide inserts. The high tool wear on the high pressure coolant case was found to be major chipping from observations under the microscope. The reason for the chipping was mainly due to the thermal cycle subjected by the cutting edge in milling operations with coolant applied externally. Relied on capillarity action, coolant had limited access to the tool-chip interface. The temperature in the tool-chip interface was still high when coolant was applied outside of the interface. When the cutting edge was disengaged from the cutting, it was immediately quenched by the coolant. The significant temperature difference caused high internal stress in the cutting edge so that it was easily being chipped.

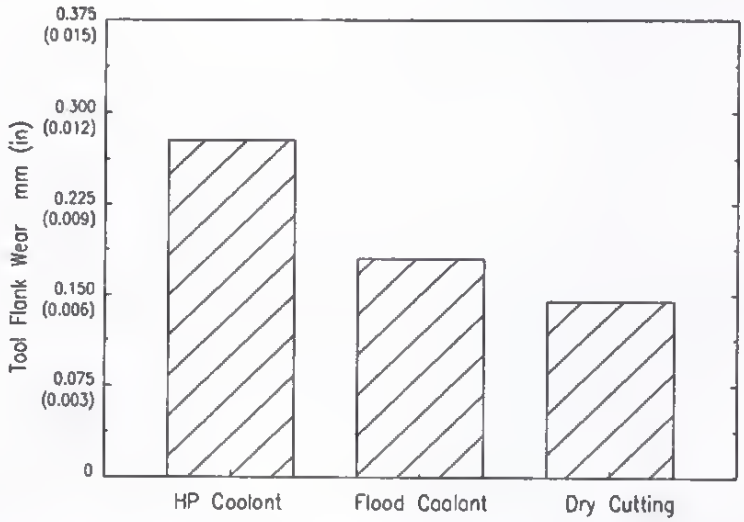

Figure 5.7 Tool wear in cutting with coolant. (4800 rpm, 10 ipm, 12.5 mm ball end mill, carbide inserts, H13 steel).

It can be concluded that the high pressure coolant can significantly decrease the cutting temperature in the cutting area. The cutting force can be reduced by applying coolant during the cutting process. The advantage of high pressure coolant in the cutting force reducing becomes more obvious in higher metal removal rate situations due to its high cooling ability. Another advantage for using the high pressure coolant is its strong chip removal capability. It was observed in the experiments that no chips were left in the cutting area when high pressure coolant was applied. This feature will be particularly beneficial for a vertical milling machine or a five-axis machine. The application of the high pressure coolant can be also expanded to the machining of other workpiece materials, such as aluminium. Especially in the high speed machining of thin wall aluminium workpieces, the cutting heat is accumulated in the thin wall part due to the limited cross section area for the heat conduction to the other parts of the workpiece. The heat accumulation causes built-up-edge on the cutting tool. With the assistance of high pressure coolant, this problem could be hopefully solved easily by carrying away the heat from the thin wall area. The problem found in the cutting experiments was that chipping is prone to occur on the carbide cutting edge when cutting hardened carbon tool steels with coolant applied.

CHAPTER SIX
ACCOMPLISHMENTS AND FUTURE WORK

Accomplishments

Cutting method and machine tool issues for die and mold machining were investigated. The analytical solution for calculating the instant depth of cut in multi-path ball end milling has been derived. The solutions can be used for locating the engaged cutting zone on the cutting edge in ball end milling, predicting the cutting force, and extending the chatter theory into ball end milling. It was found that the "step-up" path increment mode created the best cutting condition for three-axis ball end milling. The cutting geometry of the inclined ball end milling was discussed. By using this method, the cutting with "zero speed zone" at the tip of ball end mills can be avoided, and the engaged cutting zone on the cutting edge is shifted to the higher speed region. Experimental cutting tests with ball end milling were conducted. The cutting force with various cutting parameters was measured. It was found that the axial cutting force decreased if the "step-up" increment mode or the inclined ball end milling was applied. These cutting methods can create a favorable cutting condition for the high speed milling operation. Lesser requirements for axial stiffness will be needed for high speed spindles if those methods are applied. Finite element analyses on the SETCO Phase I high speed spindle were conducted with two different ball end mills. For a insert type ball end mill with high stiffness, the calculation showed that the major vibration modes were the spindle modes, while for a solid ball end mill with low stiffness the tool mode dominated. The cutting

experiments followed the calculation results. No chatter was detected when the ball end mill with high stiffness was used, while chatter signals at the tool natural frequency appeared on the sound signal spectrum when the low stiffness tool was used. A high pressure high flow rate coolant system with the maximum capacity of 6.9 MPa (1000 psi) and maximum flow rate of 54.5 L/min (14.4 gpm) was built and installed in a White-Sundstrand Series 20 milling machining center. Comparison cutting experiments with high pressure coolant, flood coolant and dry cutting were conducted. The high pressure coolant greatly reduced the cutting temperature. The cutting force was reduced when coolant was applied. Chipping became the major cause of the tool wear for cutting hardened steel with coolant. An open architecture CNC controller based on a PMAC motion control board was developed and installed in the White-Sundstrand milling machine. The control circuits of the milling machine were redesigned. A user interface software was developed for the controller. The modified milling machine with the open architecture controller has been used for several machining tasks. The performance was satisfactory.

Future Work

More experimental cutting tests should be conducted. A greater variety of die and mold workpiece materials and hardnesses should be tested, so that the results and conclusions obtained from this project have more general significance. A few typical dies and molds designed and used in the industry should be machined to explore the potential problems which did not occur in the simple path cutting tests.

The effect of the high pressure coolant on die and mold machining should be investigated in more detail. The high pressure coolant technique should not be limited to hardened steel machining. Its application can be extended to other machining tasks and other workpiece materials such as aluminium.

The interface of the open architecture controller with other computer facilities should be established. The direct downloading of part programs from commercial CAD and CAM software to the controller should be realized. The techniques developed in MTRC, such as chatter recognition and cutter breakage detection, should be implemented in the open architecture controller.

APPENDIX A
CIRCUIT DIAGRAMS OF MACHINE LOGIC CONTROL

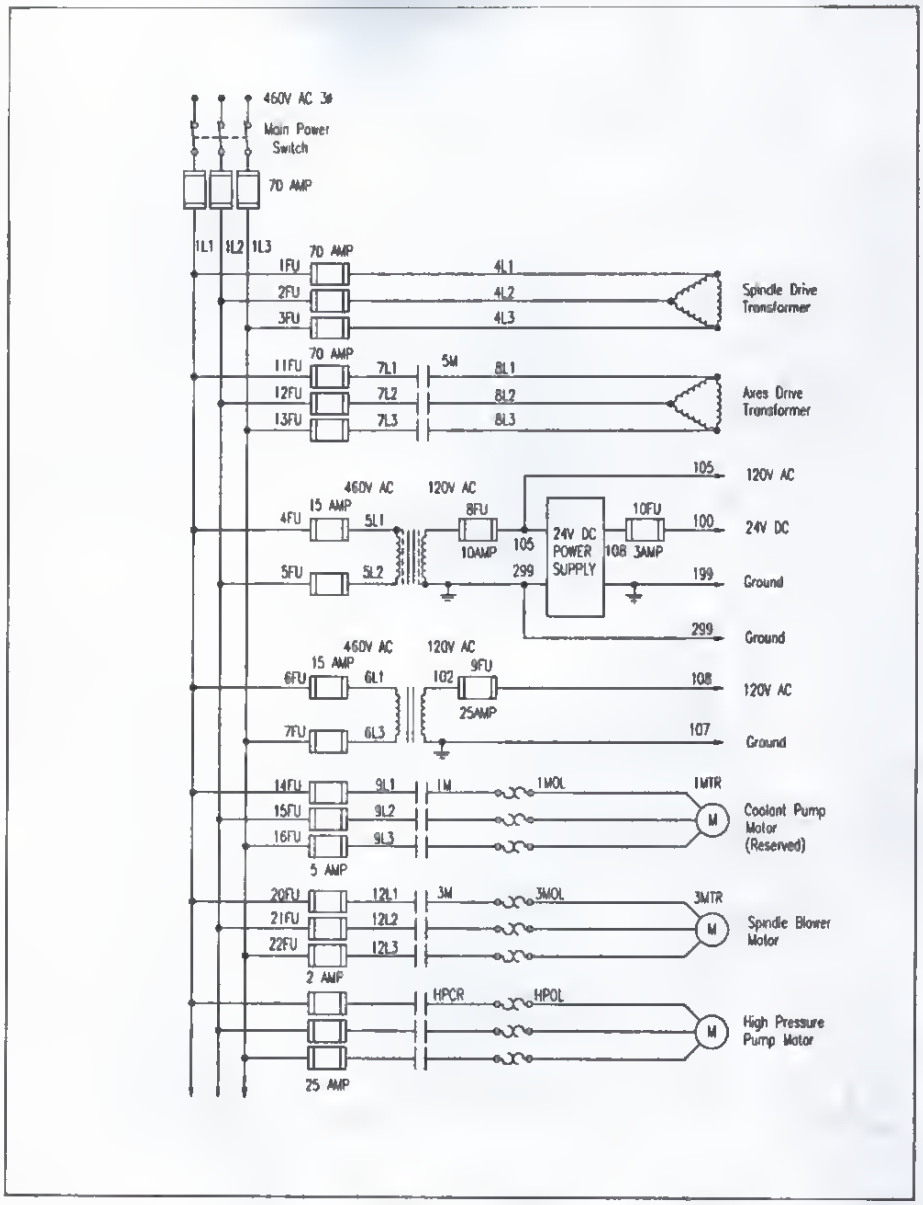

Figure A.1 Three phase AC power circuits.

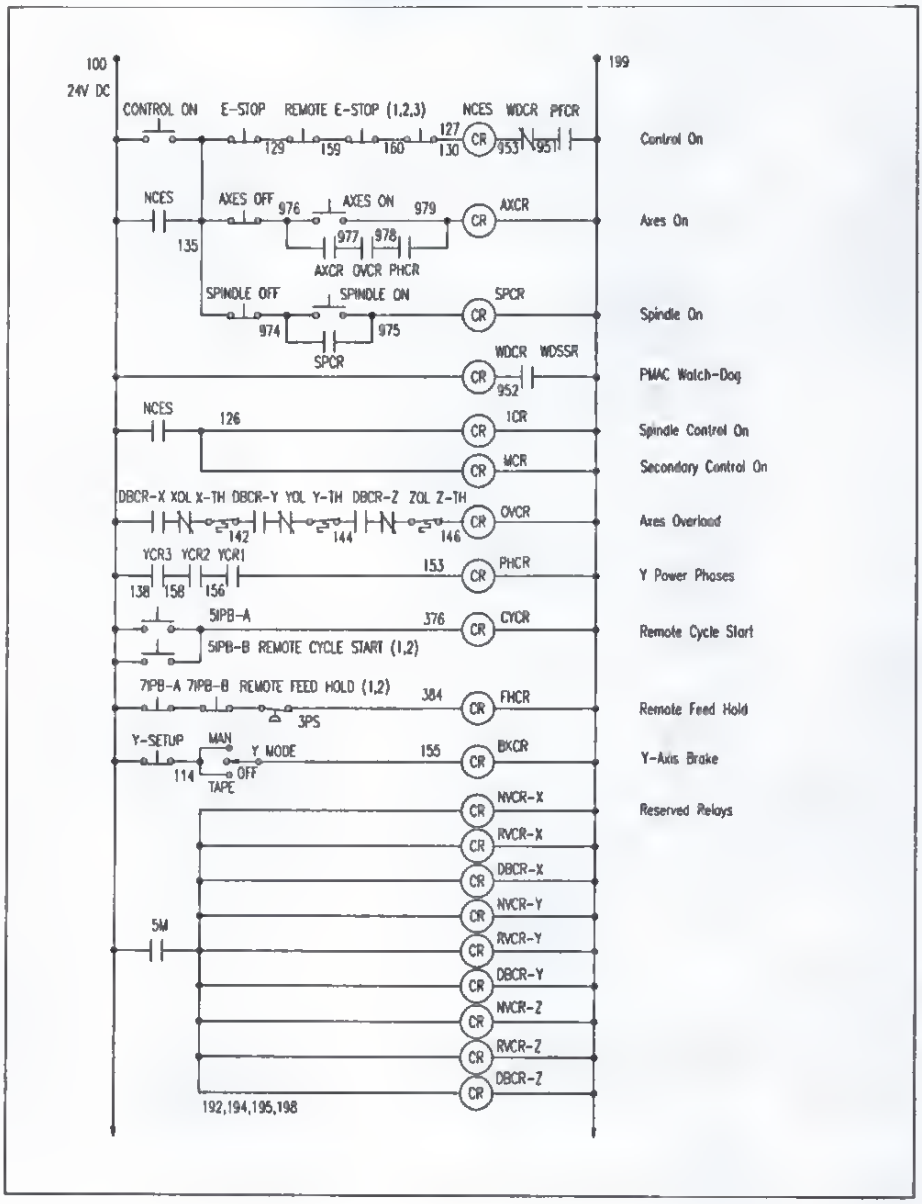

Figure A.2 Circuit diagram of machine logic control curcuit (1).

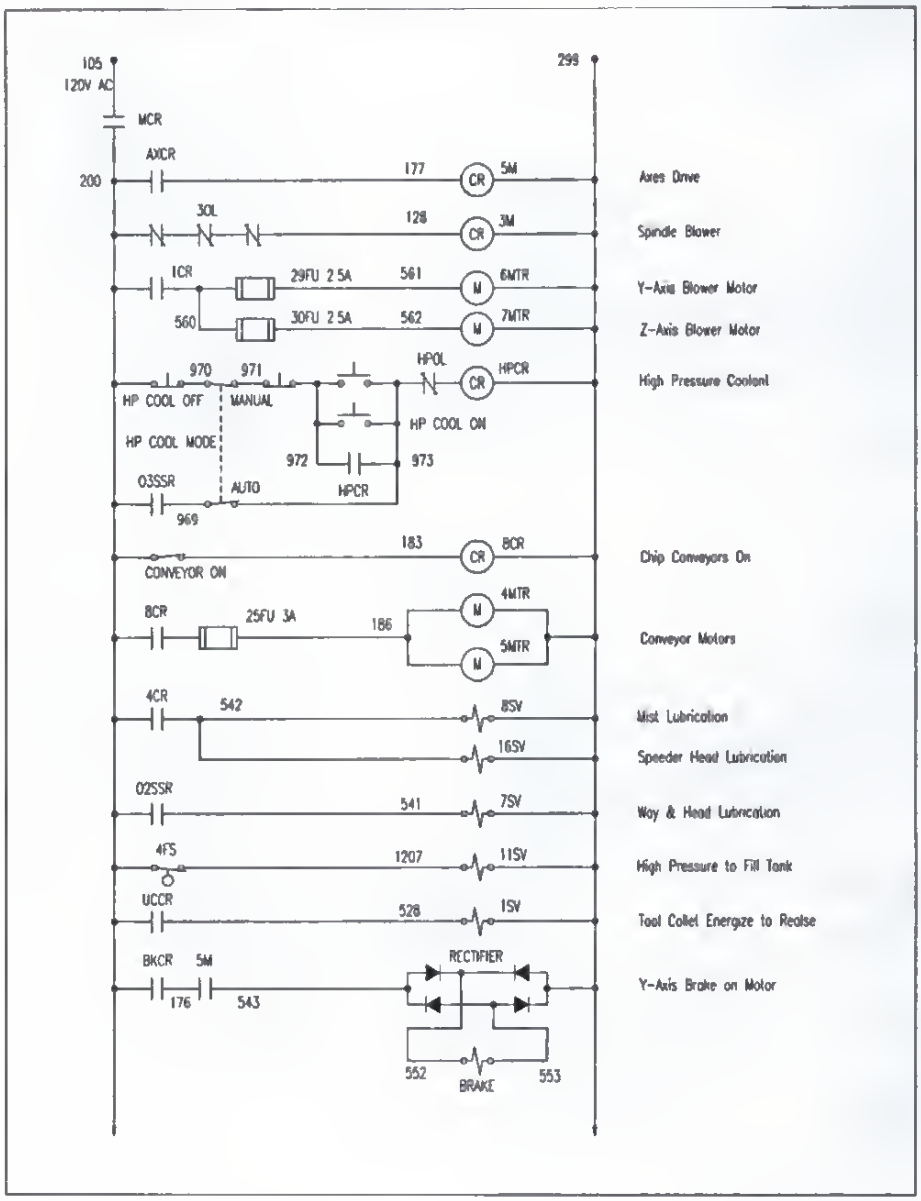

Figure A.3 Circuit diagram of machine logic control curcuit (2).

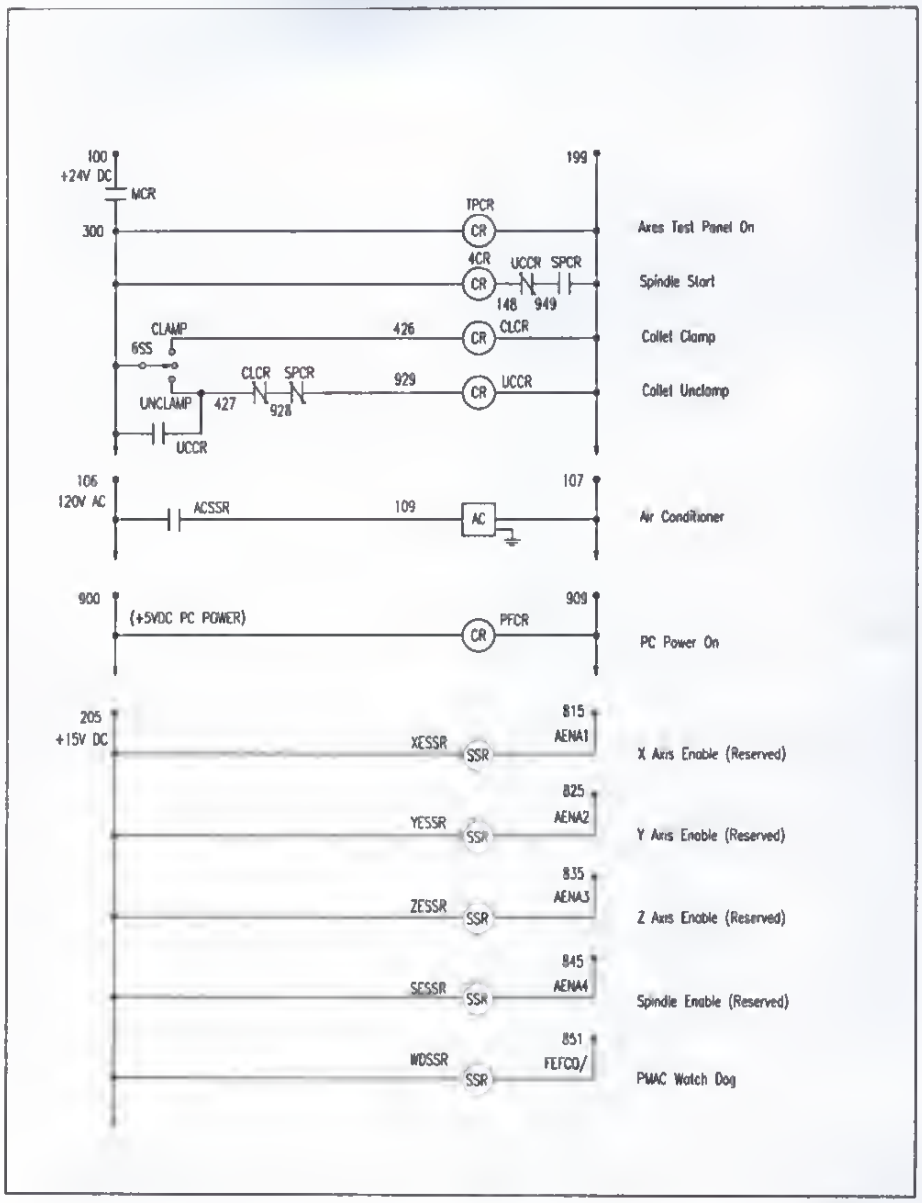

Figure A.4 Circuit diagram of machine logic control curcuit (3).

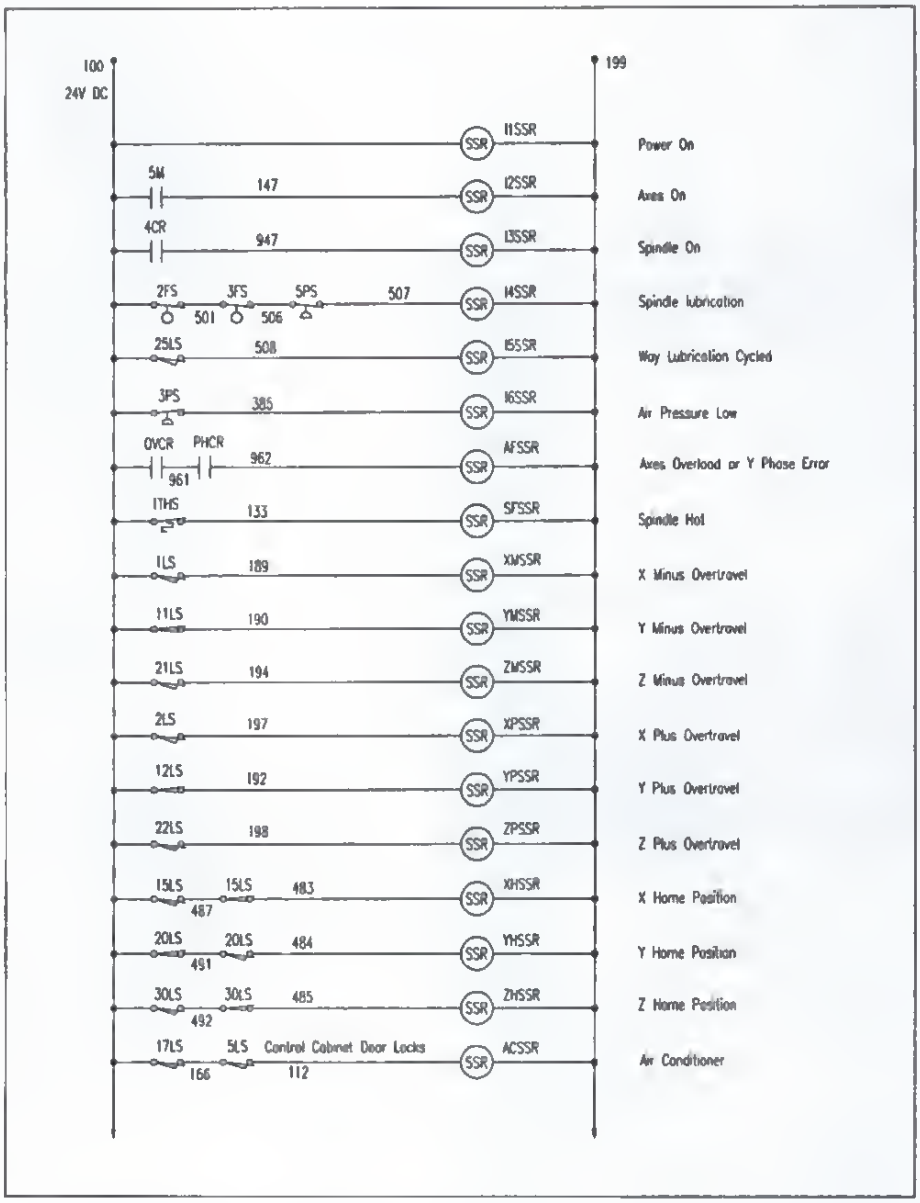

Figure A.5 Circuit diagram of machine logic control curcuit (4).

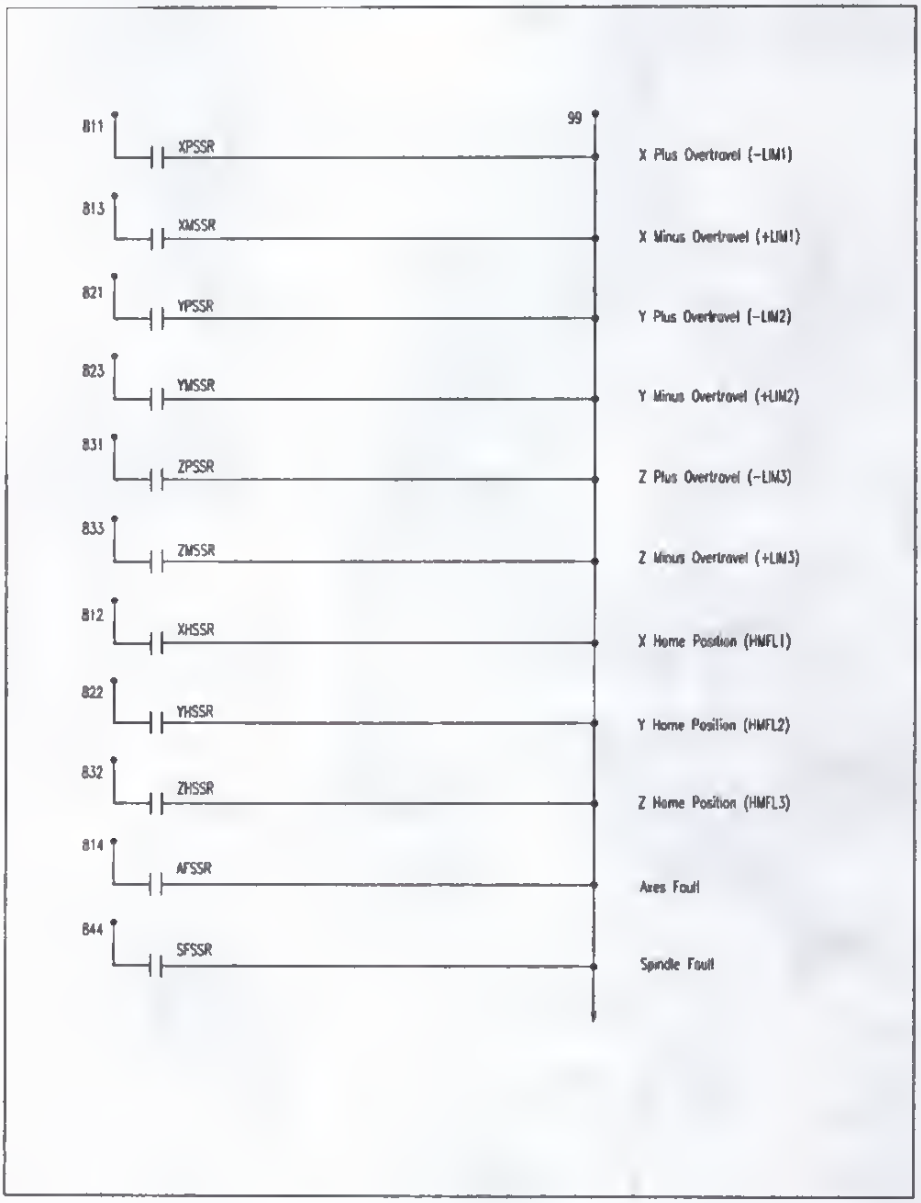

Figure A.6 Circuit diagram of machine logic control curcuit (5).

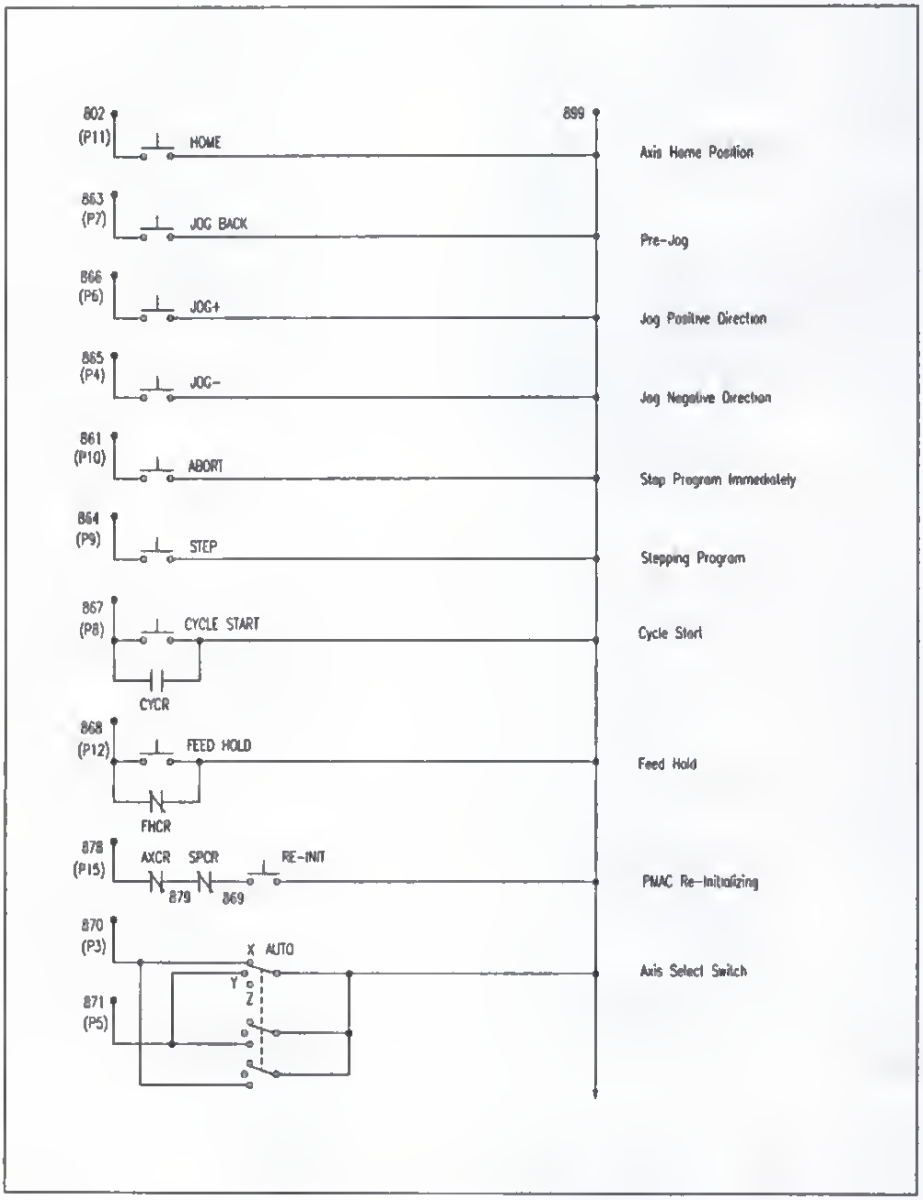

Figure A.7 Circuit diagram of machine logic control curcuit (6).

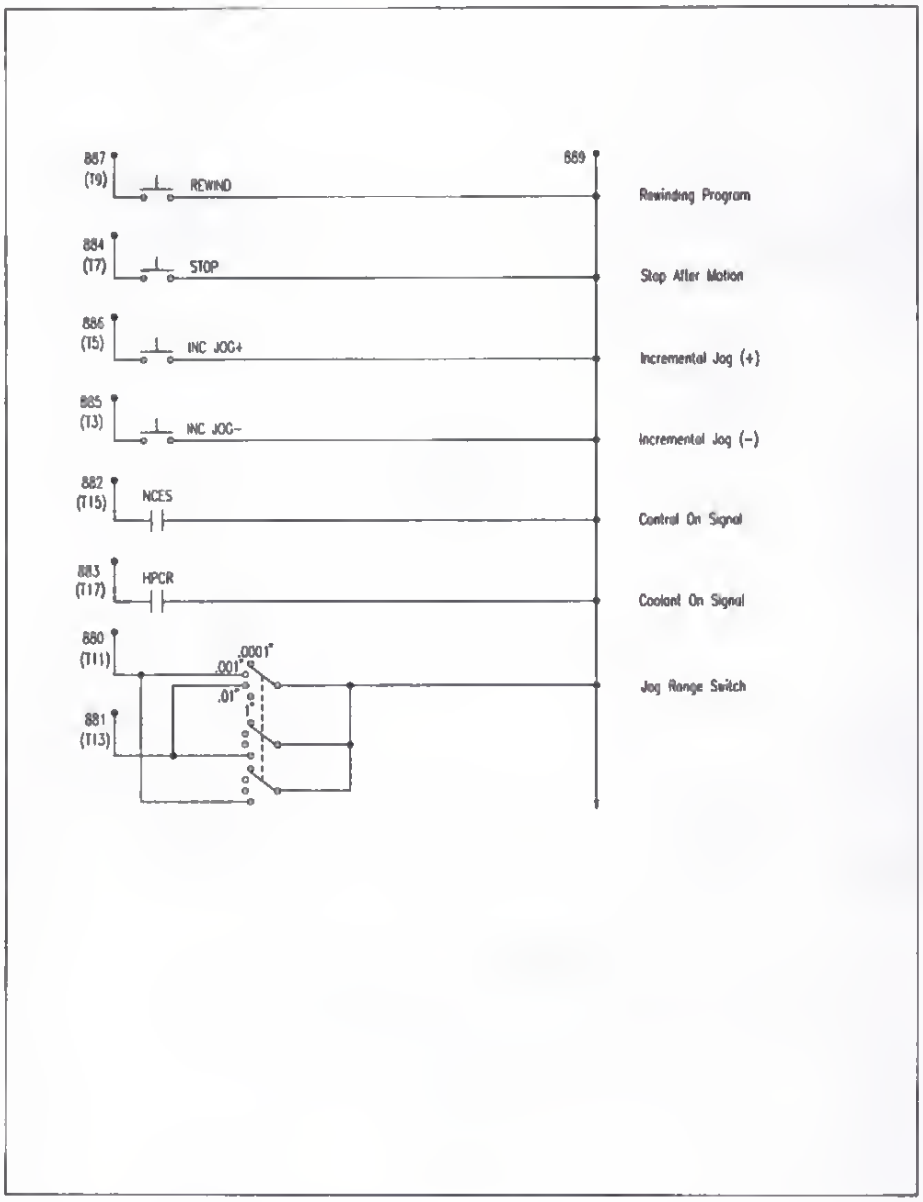

Figure A.8 Circuit diagram of machine logic control curcuit (7).

APPENDIX B
FUNCTION OF MAJOR COMPONENTS IN CONTROL CIRCUIT

Component	Symbol	Fig.	Function
Spindle Drive Transformer		A.1	Supplying power to spindle drive.
Axes Drive Transformer		A.1	Supplying power to axes drives.
120V AC (1)		A.1	AC control power supply
24V DC		A.1	DC control power supply
120V AC (2)		A.1	AC power supply for air conditioner
Flood Coolant Pump Motor	1MTR	A.1	(Reserved)
Spindle Blower Motor	3MTR	A.1	Cooling and lubricating the spindle.
High Pressure Pump Motor		A.1	High pressure coolant pump.
Control On Relay	NCES	A.2	Turning on/off control power.
Axes On Relay	AXCR	A.2	Turning on/off axes power contactor.
Spindle On Relay	SPCR	A.2	Turning on/off axes power.
PMAC Watch-Dog Relay	WDCR	A.2	Converting normally-open contacts (NO) of Watch-Dog SSR to nomally closed contacts (NC) used in NCES.
Spindle Control On Relay	1CR	A.2	Turning on the spindle control power. It is also used to control Y and Z axis blowers.
Secondary Control On Relay	MCR	A.2	Turing on 120V AC control power.
Axes Overload Relay	OVCR	A.2	Detecting axis overload and disconnecting AXCR.
Y Power Phase Relay	PHCR	A.2	Detecting phase failure in Y axis power and disconnecting AXCR.
Remote Cycle Start Relay	CYCR	A.2	Transmit remote cycle start push button signal to PMAC I/O port.

Component	Symbol	Fig.	Function
Remote Feed Hold Relay	FHCR	A.2	Transmit remote feed hold push button signal to PMAC I/O port. Also triggered by air pressure switch 3PS when air pressure is too low.
Y Axis Break Relay	BKCR	A.2	Braking Y axis when Y MODE in OFF or Y-SETUP is pressed.
Reserved Relays		A.2	Reserved for future use.
Axes Drive Contactor	5M	A.3	Turning on/off axes drive power.
Spindle Blower Contactor	3M	A.3	Turning on/off spindle blower.
Y-Axis Blower Motor	6MTR	A.3	Air blower motor for cooling Y axis.
Z-Axis Blower Motor	7MTR	A.3	Air blower motor for cooling Z axis.
High Pressure Coolant Contactor	HPCR	A.3	Turning on/off high pressure coolant pump motor.
Chip Conveyors On Contactor	8CR	A.3	Turning on/off chip conveyor motors.
Chip Conveyor Motors	4,5MTR	A.3	Driving chip conveyors.
Mist Lubrication Valve	8SV	A.3	Turning on/off mist lubrication.
Speeder Head Lubrication Valve	16SV	A.3	Turning on/off speeder lubrication.
Way and Head Lubrication Valve	7SV	A.3	Turning on/off way and head lubrication.
High Pressure Tank Filling Valve	11SV	A.3	Filling lubrication tank.
Tool Collet Release Valve	1SV	A.3	Unclamp collet for tool changing.
Y-Axis Brake		A.3	Brake Y axis if it is not active.
Axes Test Panel Relay	TPCR	A.4	Turning on axes drive test panel.
Spindle Start Relay	4CR	A.4	Starting spindle.
Collet Clamp Relay	CLCR	A.4	Clamping tool collet.
Collet Unclamp Relay	UCCR	A.4	Unclamping collet for tool changing.
Air Conditioner		A.4	Air conditioner for electrical cabinet.

Component	Symbol	Fig.	Function
PC Power On Relay	PFCR	A.4	Disconnect control circuit (NCES) if PC power fails.
X Axis Enable SSR (Solid State Relay)	XESSR	A.4	Enable X axis power amplifier (Reserved).
Y Axis Enable SSR	YESSR	A.4	Enable Y axis power amplifier (Reserved).
Z Axis Enable SSR	ZESSR	A.4	Enable Z axis power amplifier (Reserved).
Spidle Enable SSR	XESSR	A.4	Enable spindle drive (Reserved).
PMAC Watch-Dog SSR	WDSSR	A.4	Detecting PMAC software malfunction and disconnect control power.
Power On SSR	11SSR	A.5	On when machine powered.
Axes On SSR	12SSR	A.5	On when axes power (5M) is on.
Spindle On SSR	13SSR	A.5	On when spindle is on.
Spindle Lubrication SSR	14SSR	A.5	On when spindle lubrication is working.
Way Lubrication Cycled SSR	15SSR	A.5	On when way lubrication is working.
Air Pressure Low SSR	16SSR	A.5	On when air pressure is low.
Axes Overload or Y Phase Error SSR	AFSSR	A.5	On when axes are not overload and has no phase-losing accident.
Spindle Hot SSR	SFSSR	A.5	On when spindle is not hot.
X Minus Overtravel SSR	XMSSR	A.5	On when X hits minus overtravel limit switch.
Y Minus Overtravel SSR	YMSSR	A.5	On when Y hits minus overtravel limit switch.
Z Minus Overtravel SSR	ZMSSR	A.5	On when Z hits minus overtravel limit switch.
X Plus Overtravel SSR	XPSSR	A.5	On when X hits plus overtravel limit switch.
Y Plus Overtravel SSR	YPSSR	A.5	On when Y hits plus overtravel limit switch.
Z Plus Overtravel SSR	ZPSSR	A.5	On when Z hits plus overtravel limit switch.
X Home Position SSR	XHSSR	A.5	On when X not hit home position limit switch.
Y Home Position SSR	YHSSR	A.5	On when Y not hit home position limit switch.

Component	Symbol	Fig.	Function
Z Home Position SSR	ZHSSR	A.5	On when Z not hit home position limit switch.
Air Conditioner SSR	ACSSR	A.5	On when control cabinet door is closed.
X Plus Overtravel Signal		A.6	Signal when X hits plus overtravel limit switch.
X Minus Overtravel Signal		A.6	Signal when X hits minus overtravel limit switch.
Y Plus Overtravel Signal		A.6	Signal when Y hits plus overtravel limit switch.
Y Minus Overtravel Signal		A.6	Signal when Y hits minus overtravel limit switch.
Z Plus Overtravel Signal		A.6	Signal when Z hits plus overtravel limit switch.
Z Minus Overtravel Signal		A.6	Signal when Z hits minus overtravel limit switch.
X Home Position Signal		A.6	Signal when X not hit home position limit switch.
Y Home Position Signal		A.6	Signal when Y not hit home position limit switch.
Z Home Position Signal		A.6	Signal when Z not hit home position limit switch.
Axes Fault signal		A.6	Signal when axes not overload and no phase -losing accident.
Spindle Fault Signal		A.6	Signal when spindle is not hot.
Axis Home Position PB (Push button)	HOME	A.7	Homing axes.
Pre-Jog PB	JOG BACK	A.7	Jog to previous programed or jogged position.
Jog Positive Position PB	JOG+	A.7	Jog to positive direction.
Jog Negative Position PB	JOG-	A.7	Jog to negative direction.
Stop Program Immediately PB	ABORT	A.7	Stop the motion program immediately.
Stepping Program PB	STEP	A.7	Step through the motion program.
Cycle Start PB	CYCLE START	A.7	Start motion program.
Feed Hold PB	FEED HOLD	A.7	Feed hold during the execution of a program.

Component	Symbol	Fig.	Function
PMAC Re-Initializing PB	RE-INT	A.7	Reinitialize PMAC controller. Access only when axes and spindle stop.
Axis Select Switch		A.7	Selecting axis for jogging or homing.
Rewinding Program PB	REWIND	A.8	Point to the starting of the program.
Stop After Motion PB	STOP	A.8	Stop a program after the next motion.
Incremental Jog (+) PB	INC JOG+	A.8	Incremental jogging in positive direction.
Incremental Jog (-) PB	INC JOG-	A.8	Incremental jogging in negative direction.
Control On Signal		A.8	Signal for Control On (NCES).
Coolant On Signal		A.8	Signal for High Pressure Coolant On (HPCR).
Jog Range Switch		A.8	Selecting incremental jogging distance.

APPENDIX C
PLC PROGRAMS

C.1 PLC PROGRAM No.4

```
;PLC 4   Implement "Inc. Jog" keys
DELETE GATHER DELETE TRACE

CLOSE

M0->X:$0,24                    ;Servo cycle counter
M91->*                         ;"Latching" or "Rising edge" bits
M92->*
M93->X:$07F2,24                     ;Free 24-bit registers
M94->X:$07F3,24
M95->X:$07F4,24
M96->X:$07F5,24

M28->y:$ffc0,16,1              ; Motor select bit 0
M29->y:$ffc0,17,1              ; Motor select bit 1

OPEN PLC 4
CLEAR

IF(M50=0)                  ;If "Inc. Jog -" pressed

     IF(M91=0)             ;If "Rising edge" flag ready

          IF(M28=0 AND M29=1)       ;X axis

               IF(M54=1 AND M55=1)  ;If switch on 0.0001
                    CMD"#1J:-2"     ;Incremental jog 2 counts, negative
               ENDIF

               IF (M54=0 AND M55=1)      ;If switch on 0.001
                    CMD"#1J:-20"
               ENDIF

               IF (M54=1 AND M55=0)      ;If switch on 0.01
                    CMD"#1J:-200"
               ENDIF

               IF (M54=0 AND M55=0)      ;If switch on 0.1
                    CMD"#1J:-2000"
               ENDIF

          ENDIF
```

```
          IF(M28=1 AND M29=0)        ;Y axis

               IF(M54=1 AND M55=1)   ;If switch on 0.0001
                     CMD"#2J:-2"     ;Incremental jog 2 counts, negative
               ENDIF

               IF (M54=0 AND M55=1)        ;If switch on 0.001
                     CMD"#2J:-20"
               ENDIF

               IF (M54=1 AND M55=0)        ;If switch on 0.01
                     CMD"#2J:-200"
               ENDIF

               IF (M54=0 AND M55=0)        ;If switch on 0.1
                     CMD"#2J:-2000"
               ENDIF

          ENDIF

          IF(M28=0 AND M29=0)        ;Z axis

               IF(M54=1 AND M55=1)   ;If switch on 0.0001
                     CMD"#3J:-2"     ;Incremental jog 2 counts, negative
               ENDIF

               IF (M54=0 AND M55=1)        ;If switch on 0.001
                     CMD"#3J:-20"
               ENDIF

               IF (M54=1 AND M55=0)        ;If switch on 0.01
                     CMD"#3J:-200"
               ENDIF

               IF (M54=0 AND M55=0)        ;If switch on 0.1
                     CMD"#3J:-2000"
               ENDIF

          ENDIF

          M91=1                    ;Set "Rising edge" prohibited

     ENDIF

ELSE                          ;If "Inc. Jog -" key not pressed

     IF (M91=1)                    ;If "Rising edge" high
          M93=M0                   ;Set up starting time
          M94=M0-M93               ;Get elapsed time
          WHILE(M94<2000)               ;Wait <0.9sec (1sec=2262)
               M94=M0-M93          ;Get elapsed time
          ENDWHILE
          M91=0                    ;Make "Rising edge" ready again
     ENDIF

ENDIF
```

```
IF(M51=0)                ;If "Inc. Jog +" pressed

     IF(M92=0)           ;If "Rising edge" flag ready

          IF(M28=0 AND M29=1)       ;X axis

               IF(M54=1 AND M55=1)  ;If switch on 0.0001
                    CMD"#1J:2"      ;Incremental jog 2 counts, negative
               ENDIF

               IF (M54=0 AND M55=1)      ;If switch on 0.001
                    CMD"#1J:20"
               ENDIF

               IF (M54=1 AND M55=0)      ;If switch on 0.01
                    CMD"#1J:200"
               ENDIF

               IF (M54=0 AND M55=0)      ;If switch on 0.1
                    CMD"#1J:2000"
               ENDIF

          ENDIF

          IF(M28=1 AND M29=0)       ;Y axis

               IF(M54=1 AND M55=1)  ;If switch on 0.0001
                    CMD"#2J:2"      ;Incremental jog 2 counts, negative
               ENDIF

               IF (M54=0 AND M55=1)      ;If switch on 0.001
                    CMD"#2J:20"
               ENDIF

               IF (M54=1 AND M55=0)      ;If switch on 0.01
                    CMD"#2J:200"
               ENDIF

               IF (M54=0 AND M55=0)      ;If switch on 0.1
                    CMD"#2J:2000"
               ENDIF

          ENDIF

          IF(M28=0 AND M29=0)       ;Z axis

               IF(M54=1 AND M55=1)  ;If switch on 0.0001
                    CMD"#3J:2"      ;Incremental jog 2 counts, negative
               ENDIF

               IF (M54=0 AND M55=1)      ;If switch on 0.001
                    CMD"#3J:20"
               ENDIF

               IF (M54=1 AND M55=0)      ;If switch on 0.01
                    CMD"#3J:200"
               ENDIF
```

```
                IF (M54=0 AND M55=0)      ;If switch on 0.1
                    CMD"#3J:2000"
                ENDIF

            ENDIF

            M92=1                ;Set "Rising edge" prohibited

        ENDIF

ELSE                        ;If "Inc. Jog +" key not pressed

        IF (M92=1)                ;If "Rising edge" high
            M95=M0                ;Set up starting time
            M96=M0-M95            ;Get elapsed time
            WHILE(M96<2000)           ;Wait 0.9sec (1sec=2262)
                M96=M0-M95        ;Get elapsed time
            ENDWHILE
            M92=0                 ;Make "Rising edge" ready again
        ENDIF
ENDIF

CLOSE
```

C.2 PLC PROGRAM No.5

```
; PLC 5   Pumping Oil to guideway periodically

;
CLOSE
DELETE GATHER DELETE TRACE

M0->X:$0,24                         ; servo counter register
M85->X:$07F0,24                     ; Free 24-bit register
M86->X:$07F1,24

OPEN PLC 5 CLEAR

IF (M11=1)                          ; only if axes on is pressed

     M85=M0                         ; set m85 as old time to main counter
     M86=M0-M85                     ; find diff in counter and m85
     P80=0                          ; reset flag for # of pumps
     WHILE(P80<10)                  ; loop to pump 10 times
          m2=1                      ; PUMPING
          WHILE(M86<4500)               ; loop to wait 2 sec while pumping
               M86=M0-M85
          ENDW
          m2=0                      ; No longer pumping
          M85=M0                    ; set m85(old time) to current count
          M86=M0-M85                ; reset counter to curret time
          WHILE(M86<4500)               ; Loop for while not pumping
               M86=M0-M85
          ENDW
          M85=M0                    ; set m85(old time) to current count
          M86=M0-M85                ; restet counter
          P80=P80+1                 ; add on to number of pumps
     ENDW

     M85=M0                         ; set m85(old time) to counter
     M86=M0-M85                     ; reset counter
     WHILE(M86<678600)     ; 5 min(1357200 for 10 min),until next cycle
          M86=M0-M85
          IF (M11=0)                ; if axes off is pressed then the
               M86=678601 ; 5 min+1,(1357201 for 10 min),loop terminated
          ENDIF
     ENDW
ENDIF
CLOSE
```

C.3 PLC PROGRAM No.6

```
; PLC 6   GET VELOCITY OF SPINDLE
;
CLOSE
DELETE GATHER DELETE TRACE

M0->X:$0,24                      ; servo counter register
M65->X:$07F2,24                  ; Free 24-bit registers
M66->X:$07F3,24
M60->D:$07F4                     ; Free double registers
M61->D:$07F5

OPEN PLC 6 CLEAR

M65=M0                       ; Set m65 as old time to main counter
M66=M0-M65                   ; Find diff in counter and m65
M60=M462                     ; Initial position
WHILE(M66<2259)              ; Count 1 sec
     M66=M0-M65
ENDW
M60=M462-M60                 ; Get current position diff
;M61=0.0919134*M60/M66       ; Get velocity.
M61=(M60/480)*60/(M66/2259)/(96*32)
M61=0.0919134*M60/M66*2      ; Display is half of actual
CLOSE
```

C.4 PLC PROGRAM No.7

```
;PLC 7 Make a "Rewind" key
DELETE GATHER DELETE TRACE

CLOSE

OPEN PLC 7
CLEAR

IF (M53=0)              ; If "Rewind" pressed
     CMD"B"             ; Rewind to begining of current file
ENDIF

CLOSE
```

C.5 PLC PROGRAM No.8

```
;PLC 8 Make a "Stop" key
DELETE GATHER DELETE TRACE

CLOSE

OPEN PLC 8
CLEAR

IF (M52=0)              ; If "Stop" pressed
     CMD"Q"             ; Quit the program at the end of next motion
ENDIF

CLOSE
```

C.6 PLC PROGRAM No.9

```
;PLC 9  Closing the loops when "Axes On" is pressed
DELETE GATHER DELETE TRACE

CLOSE

M0->X:$0,24                    ; servo counter register
M97->X:$07F2,24                ; Free 24-bit registers
M98->X:$07F3,24
M59->*

OPEN PLC 9
CLEAR

IF (M12=1)             ; If "Axes On" pressed and AXCR energiezed
     if(M59=0)         ; Make a "rising edge" trigger
          M97=M0               ; Set m97 as old time to main counter
          M98=M0-M97           ; Find diff in counter and m97
          WHILE(M98<226)       ; Count 0.1 sec
               M98=M0-M97
          ENDW
          CMD"#1J/"
          CMD"#2J/"
          CMD"#3J/"
          CMD"#4J/"
          CMD"#5J/"            ; Closing the loops
          M59=1
     ENDIF
ELSE
     IF(M59=1)
          M59=0
     ENDIF
ENDIF
CLOSE
```

REFERENCES

Altintas, Y., and Lee, P., A general Mechanics and Dynamics Model for Helical End Mills, Annals of CIRP, Vol. 45, 1/1996, pp. 59-64.

ASM, Dies and Die Materials for Hot Forging, Metals Handbook, 9th Edition, Vol. 14. Metals Park, Ohio, 1989.

Bisshopp, K. E., Lype, E. F., and Raynor S., 1950, The Role of Cutting Fluid as a Lubricant, Lubrication Engineering, 4/1950, pp. 70-74.

Bollinger, J., and Duffie, N., Computer Control of Machines and Processes, Addison-Wesley Publishing Co., Reading, MA., 1988.

Department of Commerce, U.S. Industrial Outlook 1993, United States Department of Commerce, 1993, pp. 16.5-16.6.

Dieter, G. E., Mechanical Metallurgy, 2nd ed. New York: McGraw-Hill Book Co., 1976.

Feng, H., and C. Menq, The Prediction of Cutting Forces in the Ball-end Milling Process - I. Model Formulation and Model Building Procedure, International Journal of Machine Tools and Manufacture, Vol. 34. No. 5. 1994, pp. 697-710.

Feng, H., and C. Menq, The Prediction of Cutting Forces in the Ball-end Milling Process - II. Cut Geometry Analysis and Model Verification, International Journal of Machine Tools and Manufacture, Vol. 34. No. 5. 1994, pp. 711-719.

Hosoi, T., and T. Hoshi, Cutting Actions of Ball End Mill with a Spiral Edge, Annals of the CIRP, Vol. 25. 1/1977, pp. 49-53.

Kalpakjian, S., Manufacturing Engineering and Technology, 2nd ed. Addison-Wesley Publishing Co., Reading, MA., 1992.

Koenig, W., and Bieker, R., NC-Fraesbearbeitung vergueteter Stahlhohformen, Industrie-Anzeiger, Vol. 28, 1989, pp. 23-26.

Koenig, W., Klinger, M., and Link, R., Machining Hard Materials with Geometrically Defined Cutting Edges-Field of Applications and Limitations, Annals of CIRP, Vol. 39, 1/1990, pp. 61-64.

Koenig, W., and Koenig, M., CBN erfolgreich eingesetzt, Industrie-Anzeiger, Vol. 37, 1991, pp. 28-30.

Koenig, W., Komanduri, R., and Schenecady, D., Machining of Hard Materials, Annals of CIRP, Vol. 33, 1/1984, pp 417-427.

Kovacevic, R., Cherukuthota. C., and Mohan. R., Improving Milling Performance with High Pressure Waterjet Assisted Cooling Lubrication, Journal of Engineering for Industry, Vol. 117, 8/1995, pp. 331-339.

Mazurkiewicz, M., Kubala, Z., and Chow, J., Metal Machining with High-Pressure Water-Jet Cooling Assistance - A New Possibility, ASME Journal of Engineering for Industry, Vol. 111, 2/1989, pp. 7-12.

Merchant, M. E., 1950a, Fundamentals of Cutting Fluid Action, Lubrication Engineering, 10/1950, pp. 163-167, 181.

Merchant, M. E., 1950b, The Action of Cutting Fluids in Machinery, Iron and Steel Engineer, 11/1950, pp. 101-108.

Mitsui Seiki, High Jet Center HJH63A. Unpublished Product Literature (in Japanese). 1992

Nagpal, B. K., and Sharma, C. S., Cutting Fluids Performance, ASME Journal of Engineering for Industry, Vol. 95, 2/1973, pp. 881-889.

Nelson, J. S., Tool Wear in Milling Hardened Die Steel, Masters thesis, University of Florida, 1996

Pigott, R. J. S., and Colwell, A. T., Hi-Jet System for Increasing Tool Life, SAE Quarterly Transactions. Vol. 6, 7/1952, pp. 547-566.

Pritschow, G., and Junghans, G., Open System Controls - A Challenge for the Future of the Machine Tool Industry, Annals of the CIRP, Vol. 42/1/1993, pp. 449-452.

Pritschow, G., and Junghans, G., Open System Controls, a Challenge for the Future of the Machine Tool Industry, Proceedings of 6th IMEC, Osaka, Japan, 11/1994, pp. 223-236.

Roubik, J. R. 1952, Carbide Steel Milling with Cutting Fluids - A Progress Report," Lubrication Engineering, 10/1952, pp. 235-261.

Schey, J. A., Introduction to Manufacturing Processes, Second Edition. New York: McGraw-Hill Book Company, 1987

Schueller, J. K., Tlusty, J., and Xu, L., Machining Hardened Materials for Die and Mold Manufacturing, MTRC Report, No. MTRC/31/93, 6/1993.

Sharma, C. S., Rice, W. B., and Salmon, R., Some Effects of Injecting Cutting Fluids Directly into the Chip-Tool Interface, ASME Journal of Engineering for Industry, Vol. 93, 5/1971, pp. 441-444.

Shaw, M. C., 1948, Mechanical Activation - A Newly Developed Chemical Process, Journal of Applied Mechanics, 3/1948, pp. 37-44.

Sim, C., and Yang, M., The Prediction of the Cutting Force in Ball-end Milling with a Flexible Cutter, International Journal of Machine Tools and Manufacture, Vol. 33, No. 2, 1993, pp. 267-284.

Smith, S., and Tlusty, J., Update on High-Speed Milling Dynamics, Journal of Engineering for Industry, Vol. 112, 5/1990, pp. 142-149.

Smith, S., and Tlusty, J., An Overview of Modeling and Simulation of the Milling Process, Journal of Engineering for Industry, Vol. 113, 5/1991, pp. 169-175.

Smith, S., and Tlusty, J., Stabilizing Chatter by Automatic Spindle Speed Regulation, Annals of the CIRP, Vol. 41, 1/1992, pp. 433-436.

Smith, S., and Tlusty, J., Efficient Simulation Programs for Chatter in Milling, Annals of the CIRP, Vol. 42, 1/1993, pp. 463-466.

Teltz, R., Urbasik, K., and Elbestawi, M. A., Intelligent, Open Architecture Control for Machining Systems, Manufacturing Science and Engineering, PED-Vol. 68-2, 11/1994, pp. 851-867.

Tlusty, J., Dynamics of High-Speed Milling, Journal of Engineering for Industry, Vol. 108, 5/1986, pp. 59-67.

Wertheim, R., Rotberg, J., and Ber, A., Influence of High-Pressure Flushing through the Rake Face of the Cutting Tool, Annals of the CIRP, Vol. 41, 1/1992, pp. 101-106.

Yang, C., Shop-Floor Controller Software Overview, Unpublished Internal Report of National Institute of Standards and Technology, undated.

Yang, M. and Park, H., The Prediction of Cutting Force in Ball-end Milling, International Journal of Machine Tools and Manufacture, Vol. 31, No. 1, 1991, pp. 45-54.

Yucesan G. and Altintas Y., Mechanics of Ball End Milling Process, Manufacturing Science and Engineering, PED-Vol. 64, American Society of Mechanical Engineers, 1993, pp. 543-551.

Yucesan G. and Altintas Y., Prediction of Ball End Milling Forces, Journal of Engineering for Industry, Vol. 118, 2/1996, pp. 95-103.

BIOGRAPHICAL SKETCH

The author was born in 1953 in Shanghai, China, and grew up in Beijing, China. After receiving his B.S. degree in Mechanical Engineering in 1982 he worked in the automobile industry for seven years. He came to the United States in 1989 to pursue advanced degrees. He received his M.S. degree in Mechanical Engineering in 1991 at the University of Florida. He is currently working on his Ph.D. degree in Mechanical Engineering in the Machine Tool Research Center at the University of Florida.

I certify that I have read this study and that in my opinion it conforms to acceptable standards of scholarly presentation and is fully adequate, in scope and quality, as a dissertation for the degree of Doctor of Philosophy.

John K. Schueller, Chairman
Associate Professor of
Mechanical Engineering

I certify that I have read this study and that in my opinion it conforms to acceptable standards of scholarly presentation and is fully adequate, in scope and quality, as a dissertation for the degree of Doctor of Philosophy.

Jiri Tlusty, Cochairman
Graduate Research Professor of
Mechanical Engineering

I certify that I have read this study and that in my opinion it conforms to acceptable standards of scholarly presentation and is fully adequate, in scope and quality, as a dissertation for the degree of Doctor of Philosophy.

Kevin Scott Smith
Associate Professor of
Mechanical Engineering

I certify that I have read this study and that in my opinion it conforms to acceptable standards of scholarly presentation and is fully adequate, in scope and quality, as a dissertation for the degree of Doctor of Philosophy.

John C. Ziegert
Associate Professor of
Mechanical Engineering

I certify that I have read this study and that in my opinion it conforms to acceptable standards of scholarly presentation and is fully adequate, in scope and quality, as a dissertation for the degree of Doctor of Philosophy.

Sherman X. Bai
Assistant Professor of
Industrial and Systems Engineering

This dissertation was submitted to the Graduate Faculty of the College of Engineering and to the Graduate School and was accepted as partial fulfillment of the requirements for the degree of Doctor of Philosophy.

December 1996

Winfred M. Phillips
Dean, College of Engineering

Karen A. Holbrook
Dean, Graduate School